The Structure of Sperm Autoantigenic Protein (SPA17): An R2D2 Protein Critical to Cilia and Implicated in Oncogenesis

Heather Raquel Dahlin

A dissertation

submitted in partial fulfillment of the

requirements for the degree of

Doctor of Philosophy

University of Washington

2021

Reading Committee:

John D. Scott, Chair

Ning Zheng

Linda Wordeman

Program Authorized to Offer Degree:

Pharmacology

University of Washington

Abstract

Structure of SPA17:
An R2D2 Protein Critical to Cilia and Implicated in Oncogenesis

Heather Raquel Dahlin

Chair of the Supervisory Committee:
John D. Scott, Ph.D., Edwin G. Krebs- Speights Professor of Cell Signaling and Cancer Biology
Pharmacology

A-Kinase Anchoring proteins (AKAPs) localize the activity of cyclic AMP (cAMP)-Dependent Protein Kinase (PKA) through interaction of an amphipathic helix that binds to a conserved RIIα docking and dimerization (R2D2) domain on the N-terminus of PKA. Genome analysis indicates that at least thirteen other RIIα superfamily proteins exist in humans, which are not coupled to cyclic nucleotide binding domains and are largely localized to cilia and flagella. The newly reported R2D2 proteins exist in two lineages differing by their similarity to Type I or Type II PKA. Moreover, R2D2 domains bind to AKAPs and can contain extra regulatory sequences conferring novel functions and binding specificity. Here we detail the structure of one such domain comprising the N-terminus of Sperm Autoantigenic Protein 17 (SPA17) resolved to 1.72 Å. The structure of core hydrophobic sites for dimerization and AKAP binding are highly conserved between PKA and SPA17. Additional flanking sequences outside of the core R2D2 domain occlude the AKAP binding site and reduce the affinity for AKAP helices in the absence of heterodimerization with another R2D2 protein, ROPN1L.

TABLE OF CONTENTS

LIST OF FIGURES

LIST OF TABLES

ACKNOWLEDGEMENTS

I would like to acknowledge my mother Liane Leedom, M.D. for providing mentorship during my project. I also need to thank Rad2Cool aka Derrek Allen Jones III for supporting me during the writing of my thesis. My service dog Voltaire, and my African Grey Athena and cockatiels Pikachu and Pichu were also instrumental during my PhD and the writing of this thesis for their love and support. Thomas Hinds assisted with Octet and SEC-MALS experiments and protocols. Ning Zheng was instrumental for the design of the listed experiments and this work would not have been completed without his assistance. Peter Hsu PhD and Domnita Rusnac PhD from the Zheng lab assisted in x-ray data collection. John Scott financially supported this project and supported my salary with the Pharmacological Sciences Training Program.

DEDICATION

My work is dedicated to those on whose shoulders I stand beginning with John M. Leedom, M.D., my great, great, grandfather who graduated from medical school in 1879. My grandfather John M. Leedom, M.D., Hastings Professor of Medicine, Chief of Infectious Disease, LAC/USC Medical Center until 2007, and my mother Liane Leedom, M.D. psychiatrist, and Associate Professor of Counseling at the University of Bridgeport. All valued science as a means of understanding the wonders of life and ending the suffering of humankind. With their accomplishments, love, and support, I am the first of my family to obtain a Ph.D.

Chapter 1. THE PKA-R PROTOTYPE

1.1 PKA-R AND AKAP INTERACTIONS: A PROTOTYPE FOR MODULARITY

When Walsh, Perkins, and Krebs (1968) first discovered and purified a rabbit skeletal muscle protein kinase that catalyzes cyclic AMP-dependent phosphorylation of casein and protamine, they did not know this protein would later serve as a prototype for an entire superfamily of eukaryotic protein kinases. Although it was originally named phosphorylase kinase, kinase (after its substrate), this protein is now known as protein kinase A (PKA) (Taylor et al., 2012). In the fifty-two years since its discovery, detailed studies of the structure and function of PKA have enabled it to achieve prototype status (Taylor et al., 2012). PKA catalyzes transfer of the γ-phosphate group of adenosine 5′-triphosphate (ATP) to serine and threonine residues on substrates; as such it is a serine/threonine kinase with varied substrates depending on PKA cellular localization (Turnham & Scott, 2016).

Structural analyses reveal that the PKA holoenzyme exists as a tetramer comprised of a regulatory (R) subunit dimer and two catalytic (C) subunits (Turnham & Scott, 2016). The catalytic activity of PKA is confined to the C subunits that are kept inactive through association with the R subunits. Isoforms of R subunits include the RI subunits (termed RIα and RIβ) and the two RII subunits (termed RIIα and RIIβ). These combine with C subunits to form tetrameric protein complexes known as the type I and type II PKA holoenzymes (Turnham & Scott, 2016). RI and RII subunits are composed of a docking and dimerization (DD) domain joined to a cyclic nucleotide binding (CNB) domain by a short 'hinge' segment (Li et al., 2000). This segment contains an inhibitor site that blocks the active site of the C subunit in the holoenzyme. RII subunits function as both substrates and inhibitors and differ from RI in not requiring ATP to form holoenzyme. Importantly the tetrameric holoenzyme isoforms are differently targeted and localized to specific subcellular compartments through protein-protein interactions between the R subunit dimer and A-kinase anchoring proteins (AKAPs) (Scott & McCartney, 1994).

Early research demonstrated that distinct pools of cAMP and PKA activity exist: the type I holoenzyme associated with the cytosol, and the type II holoenzyme associated with the particulate fraction. Theurkauf and Vallee (1982) identified the first AKAP, Microtubule Associated Protein 2 (MAP2), through isolation of microtubules and characterization of associated

cAMP regulated kinase activity. AKAPs are now known to direct R subunits, and therefore PKA to various subcellular compartments (Scott & McCartney, 1994). Lohnmann and colleagues (1984) developed a far-Western technique called the RII overlay to identify putative AKAP proteins whereby the type II regulatory subunit of PKA (RII) is biotinylated and overlaid onto a membrane containing separated cell lysates. Once thought to solely bind PKA, it is now recognized that AKAPs and the R subunit X-type four helix bundles that bind them are modular protein folds (Gold et al., 2006) that target and regulate myriad catalysts (Table 1.1).

There are R subunit homologous proteins that do not associate with the catalytic subunit of PKA, but anchor and regulate other catalysts. Newell et al. (2008) described four mammalian proteins, ASP/ROPN1L, ROPN1, SP17/SPA17, and CABYR that contain a highly conserved dimerization/docking domain that is homologous to the dimerization/docking domain of RII. These "R2D2 proteins" contain hydrophobic regions that presumably bind the amphipathic helix of AKAPs in a manner similar to RII. Search of the NCBI bioinformatic database using sequence analysis indicates there are at least thirteen proteins in humans in the RIIα superfamily (Table 1.1). It is therefore likely there are yet unspecified amphipathic helices (AKAPs) that bind to and target these macromolecules to sites of action. Moreover, there are AKAPs identified by RII overlay that do not bind PKA in all contexts, or in a physiologically relevant context; RSP3 is an example (Newell et al., 2008). These AKAPs may be the partners of R2D2 proteins.

PKA-RII thus represents a prototype for the way proteins containing the dimerization/docking domain bind AKAPs to regulate and target catalysts to the subcellular organelles where they function. Genes for the PKA Catalytic subunit isoforms are on chromosomes 1 and 19 in humans whereas genes for the Regulatory subunit isoforms are on 3, 7 and 17 (Stelzer et al., 2016). In contrast, R2D2 protein regulators and effectors are modules of a single protein and are each products of a single gene (albeit with exons and introns). It is tempting to speculate that the PKA holoenzyme is the more derived structure and that R2D2 proteins are more ancient (see Chapter 2). This work is the first to present the structure of the RIIα domain in an R2D2 protein, and specifically reports the structure of the R2D2 protein SPA17. By solving the structure, similarities and differences between this R2D2 protein and the PKA-RII prototype can be explored. The next section will review structural studies of PKA's RII subunits to demonstrate the role of crystallographic and NMR methods in such studies. Properties of the R2D2 proteins are

addressed further in Chapter 2, following a discussion of the ciliary structure in which these proteins primarily reside.

Table 1.1. Human R2D2 Proteins

Protein Name	Abbreviation	Catalytic Domain
Ropporin 1	ROPN1, ROPN1a	?
Ropporin 1B	ROPN1B	?
Ropporin 1-Like	ROPN1L	?
Calcium Binding Tyrosine Phosphorylation Regulated Protein	CABYR	EF-Hand, PxxP
Sperm Autogenic Protein 17	SPA17	IQ Domain
Tubulin Polyglutamylase Subunit 1	TPGS1	Armadillo
EF-Hand Calcium Binding Protein 10	EFCAB10	EF-Hand
RIIA Domain Containing Protein 1	RIIAD1	Probably N/A
Adenylate Kinase 5 (AK5)	AK5	P Loop NTH
Adenylate Kinase 8 (AK8)	AK8	P Look NTH
F-box and Leucine Rich Repeat Protein 13	FBXL13	F-Box/ LRR
Vestibule-1 Protein (C8ORF34)	VEST1	?
Ciliogenesis Associated TTC17 Interacting Protein (CATIP)	CATIP	?

1.2 Determining Structure: X-Ray Crystallography of R Subunit Structures

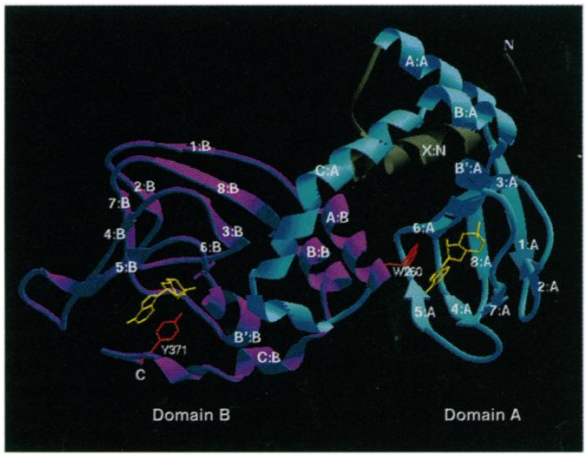

Figure 1.1. Structure of 1-91 deletion mutant of RIα.

B Domain (magenta), A Domain (Cyan), cAMP (yellow) (Su et al., 1995).

Crystalizing R subunits poses greater technical challenges as opposed to C subunits and so the structure-function relations of R isoenzymes were elucidated later than those of the C isoenzymes. Structure-function relations of R subunits are complex, due to the interaction of Rs to form dimers, association with cAMP and C subunits, and association with AKAPs. Domains of the R subunits must accomplish each of these functions. Table 1.2 lists extant X-Ray crystallographic studies of the PKA RII isoforms. The present discussion focuses primarily on RII structure as the R2D2 proteins are homologous to this structure. Su et al., (1995) first crystalized and determined the structure of RIα and its association with cAMP to 2.8 Å resolution. The R1α subunit consists of 2 modules A and B. In each of these, a network of hydrogen bonds between cAMP and RIα buries the cyclic phosphate and ribose between two beta sheet strands. This portion of the R subunit is known as the beta barrel. An aromatic ring lies outside the beta barrel and each adenosine stacks against this ring (Figure 1.1). Based on the model developed by Su et al., Diller et al. (2001) solved the structure of RIIβ (Figure 1.2). RII β barrels also bind phosphate of cAMP through hydrogen bonds. A conserved α helix flanks each β barrel and connects the barrel to functionally- specific sequences. RIIβ dimers cooperatively bind cAMP such that the two cAMP binding sites are not equivalent. cAMP of the inner site is trapped in a hydrophobic core leading to relatively high affinity (cAMP affinity for the outer site is much lower). Hence RIIβ has two different domain interface surfaces with a hinge like region between them. The differences between RI and RII isoforms result in functional differences and potentially allow for preferential targeting of RII by inhibitors.

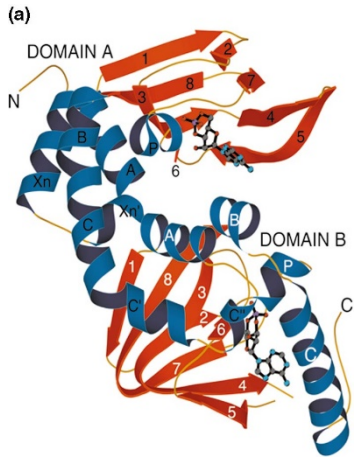

Figure 1.2. Structure of RIIβ CTD.
β Barrels (red), α Helices (Blue), cAMP (grey) (Diller et al., 2001).

Zhang et al. (2012) determined the structure and allosteric relationships of the RIIβ2:C2 tetrameric holoenzyme. Their model explains allosteric activation by cAMP. The two RIIβ subunits are anchored together by their β4-β5 loops. These "dock onto the carboxyl-terminal tail of the adjacent C subunit, thereby forcing the C subunit into a fully closed conformation in the absence of nucleotide" (Zhang et al., 2012, p. 712). Furthermore, the quaternary structure of the RIIβ tetramer is significantly different from that of the RIα tetramer, confirming previous studies demonstrating differing functional roles for the two classes of regulatory subunits.

An additional critical piece of the structural puzzle is the interaction of the R subunits with AKAPs. Work on this problem began with solution NMR spectroscopy methods (Newlon et al., 1997, 1999, 2001). The RII N-terminal region is a "well packed, antiparallel, dimeric, X-type four-helix bundle with C2 symmetry" (Newlon et al., 2001, p. 1651). This region contains the dimerization motif and extended hydrophobic face that binds AKAPs with high affinity, and so was named the dimerization and docking DD domain (Newlon et al., 2001). AKAPs then must possess a domain that interacts with the RII extended hydrophobic face. This domain which is a defining characteristic of AKAPs, consists of polar and hydrophobic residues on opposite sides of a helix that is therefore amphipathic (Carr et al., 1991). Solution NMR methods examining interactions between RIIβ and Ht31(493–515) and AKAP79(392–413) revealed that the DD domain contains a hydrophobic groove that accommodates one AKAP per RIIα DD (Newlon et al., 2001). X-Ray crystallographic imaging of the DD domain of rat RIIα bound to a 22-residue peptide from the PKA binding domain of D-AKAP2 also showed the hydrophobic grove (Kinderman et al., 2006). The crystal structure shows how RIIα binds numerous AKAPs with high affinity. As the structure is dimeric, the N terminus of one protomer is tightly bound to the AKAP while the other is disordered and so there are two potential docking modes (Kinderman et al., 2006). Gould et al. (2006) developed SuperAKAP-IS, a peptide that is 10,000-fold more selective

for the RII isoform relative to RI. Crystal structures of the docking and dimerization (DD) domain of the RIIα both in the apo state and in complex with this high-affinity anchoring peptide AKAP-IS were examined with high resolution. AKAP aliphatic residues that mediate RII interaction are highly conserved. Hydrophobic residues interact at the RII interface while polar residues confer R subunit specificity.

X-Ray crystallographic methods played a central role in determining the structure of the tetrameric PKA holoenzyme (for review see Taylor and Kornev (2017)). Structural information obtained relates directly to functional differences between isomers. In addition to elucidating molecular structure as related to PKA function, crystallography has been used to identify pharmacologic targets for PKA isomers (Brown et al., 2013). Plasmodium falciparum PKA-R structure has been studied to inform antimalarials targeting the parasite only (Littler et al., 2016). The structure of oncogenic J-PKAcα has been studied to assist with the development of targets for tumors containing this moiety. In summary, molecular structural imaging through NMR spectroscopy and X-Ray crystallography enables detailed determination of tertiary and quaternary structure of important cellular proteins and is the rationale for using these methods herein. Structural data regarding R2D2 proteins is lacking. These proteins along with AKAPs are abundant in cilia and flagella. The following sections discuss RII proteins and AKAPs important to the structure and function of cilia and flagella. RII proteins, AKAPs, and cilia derived structures are present throughout the eukaryotic tree as these are fundamental to mechanisms enabling intracellular signaling and differentiation and therefore the evolution of multicellular organisms.

Table 1.2. PKA-R Structures Solved through X-Ray Crystallography

Seminal Structural Studies of RI that Informed Studies of RII			
Reference	Identifier	Structure Resolved	Findings and Functional Significance
(Su et al., 1995)	1RGS	1-91 deletion mutant of RIα; Determined to 2.8 Å	1. A network of hydrogen bonds between cAMP and RIα buries the cyclic phosphate and ribose between two beta sheet strands linked by a short alpha helix (the beta barrel). 2. An aromatic ring lies outside the beta barrel. Each adenine stacks against this ring.
(Kim et al., 2005) (Kim et al., 2007)	3FHI 2QCS	PKA catalytic subunit bound to a deletion mutant of a regulatory subunit (RIα).	1. Catalytic subunit— Tyr247 in the G helix and Trp196 in the phosphorylated activation loop are anchor points that bind RIa. 2. Tyr247in the G helix and Trp196 in the phosphorylated activation loop competes with cAMP for the phosphate binding cassette in RIα.
(Ilouz et al., 2012)	4D1N	Crystal structure of RIβ dimer bound to two full-length C-subunits including ATP and two Mg+2 ions, PKA holoenzyme structure determined to 3.7-Å	1. The holoenzyme is dimers of dimers with twofold symmetry. 2. The geometry of the symmetry is unique for each holoenzyme.
(Brown et al., 2013)	4JVA	Crystal structures of both RIα and RIIβ bound to HE33 determined to 2.95 Å.	1. The RIIβ structure includes a hydrophobic pocket in which HE33 is buried. 2. RIα interacts with HE33 differently than RIIβ. 3. cAMP analogues can selectively target RIα or RIIβ due to differences in the conformation of binding domains.

Structural Studies of RII Isozymes			
Reference	Identifier	Structure Resolved	Findings and Functional Significance
(Diller et al., 2001)	1CX4	RIIβ; Determined to 2.45 Å	1. β barrels bind phosphate of cAMP through hydrogen bonds. 2. A conserved α- helix flanks each barrel and connects the barrel to functionally- specific sequences. 3. RIIβ dimers cooperatively bind cAMP such that the two cAMP binding sites are not equivalent. cAMP of the inner site is trapped in a hydrophobic core. cAMP affinity for the outer site is much lower.
(Gold et al., 2006)	2IZY 21ZX	DD domain of the RIIα both in the apo state and in complex with the high-affinity anchoring peptide AKAP-IS determined to 2.2 Å.	1. RII contains hydrophobic interface forms shallow grove on the surface of DD domain. 2. Developed SuperAKAP-IS, a peptide that is 10,000-fold more selective for the RII isoform relative to RI 3. AKAP-IS folds into an amphipathic alpha helix that binds to hydrophobic interface.
(Kinderman et al., 2006)	2HWN	DD domain of rat RIIα bound to a 22- residue peptide from the AKB domain of D-AKAP2 to 1.6 Å.	1. Identified structural differences between RIα and RIIβ that contribute to the functional and localization differences between these.
(Wu et al., 2007)	2QVS	RIIα holoenzyme compared to the RIα holoenzyme toβ 2.5 Å.	1. Determined the mechanism of C inhibition by R for both RI and RII. 2. Mechanism for holoenzyme activation by cAMP. 3. RIIα conformation changes dramatically upon C binding.
(Brown et al., 2009)	31DB 31DC	(108-268) RIIβ:C holoenzyme (102-265)RIIβ:C holoenzyme to 1.52 Å	1. Explored changes in RIIβ that occur with C binding and holoenzyme formation. 2. Linker region of RIIα and RIIβ differ.
(Zhang et al., 2012)	3TNP 3TNQ	The crystal structure of the tetrameric RIIβ2:C2 holoenzyme determined to 2.3 Å.	1. Isoform specific quaternary structures form even though tertiary structures are similar. 2. β4-β5 loop in the R subunit determines specificity for docking between the two heterodimers.
Reference	Identifier	Structure Resolved	Findings and Functional Significance

(Brown et al., 2013)	4JVA	Crystal structures of both RIα and RIIβ bound to HE33 determined to 2.95 Å.	1. The RIIβ structure includes a hydrophobic pocket in which HE33 is buried. 2. RIα interacts with HE33 differently than RIIβ. 3. cAMP analogues can selectively target RIα or RIIβ due to differences in the conformation of binding domains.
(Zhang, Ye, et al., 2015)	4X6Q	RIα:myrC and RIIβ2:myrC2	1. N-terminal myristylation site in the myrC serves as a flexible ‘‘switch’’ enabling membrane anchoring of RII, but not RI, holoenzymes.
(Zhang, Knape, et al., 2015)	4WBB	$RII\beta^{P}{}_2$:C_2:$(Ca_2ADP)_2$ holoenzyme to 2.8Å	1. Autophosphorylation/dephosphorylation of the RIIβ subunit, cAMP, and metal ions, contribute to the dynamics of PKA signaling.
(Götz et al., 2016)	4ZP3	AKAP18:PKA-RIIα to 2–2.5 Å	1. Three hydrophilic anchor points in AKAP18β outside the core PKA-binding domain mediate DD domain binding. 2. RI subunit binding by AKAPs mediated by a different set of anchor points.
Select Crystallographic Studies that Inform Drug Design			
(Littler et al., 2016)		Co-crystallized *Plasmodium falciparum* PKA-R with 7-CN-7-C-Ino.	1. 7-cyano-7-deazainosine, an anti-malarial drug, binds to R. 2. PfPKA-R is similar to RII, both have long C helix that buries CBD2 nucleotides, twice the length of RI.
(Cao et al., 2019)		Crystal structures of the chimeric fusion RIα2:J-PKAcα2 holoenzyme formed by oncogenic J-PKAcα and the subunit RIα and the wild type determined to 3.66 Å.	1. Chimera holoenzyme molecule consists of an RIα homodimer and two chimeric J-PKAcα subunits. 2. The J addition does not change the structure.

Chapter 2. RII AND AKAPS FUNCTION IN CILIA AND FLAGELLA

2.1 THE CILIUM

The cilium is a humble microtubule-based organelle whose influence on multicellular evolution is often overlooked. The putative single celled ancestor to all animals resides in the Choanoflagellate clade. As its name implies, this organism relies upon a cilia-like organelle for locomotion and therefore predator avoidance and feeding. Reliance on the cilia for these critical functions is problematic because the centriole is a single microtubule organizing center; both the cilium and the mitotic spindle apparatus required for cell division arise from the centriole. Cells with a functional cilium cannot divide, and the cilium is required for predator avoidance (Grosberg & Strathmann, 2007). The codependence of the cilium and spindle apparatus upon a single centriole led Margulis (1981, p. 272) to propose that "the failure to solve the problem of simultaneous division and motility on the single-cell level may have led, in several groups, to the origin of eukaryotic multicellularity." According to theory, cellular differentiation arose as organisms came to possess cell lines specialized for division or locomotion (Grosberg & Strathmann, 2007).

Differentiated epithelial and mesenchymal cells that apparently lack cilia still retain a structure called the primary cilium. Polycystic kidney disease is among the many disorders caused by genetic mutations that impact this structure (Satir & Christensen, 2007). Primary cilium respond to mechanical stimuli or ligands; in the kidney, primary cilium transduce calcium signals. In many cell types, the primary cilium is the source of information regarding the cell's environment and so it is referred to as a "cybernetic probe" or a "cellular global positioning device" (Satir & Christensen, 2007). Environmental information transduced by the cilium activates the hedgehog and Wnt signaling systems that mediate differentiation. The structure of primary cilium leads to the left right asymmetry critical to patterning in embryogenesis (Shinohara et al., 2015). Therefore, the cilium and related structures create not only spatial order (through complex structures) but also temporal order through signaling. In summary, cycling of second messengers and proteins in and out of the cilia, and ciliary growth and regression are integral to cell polarity, differentiation, and the cell cycle.

Motile cilia and flagella have a characteristic 9 + 2 axonemal architecture with a central pair of microtubules and nine outer doublet microtubules in most species (Carvalho-Santos et al., 2011;

Osinka et al., 2019). Linking the outer doublets to the central apparatus are the radial spokes, where a diverse family of scaffolds, A-Kinase Anchoring proteins (AKAPs), form the core organizing center of the "cybernetic probe"— the chemosensing and mechanosignaling apparatus (Yang et al., 2006). Hence, AKAPs proteins discovered through association with PKA are structural proteins of the cilium.

The AKAP binding site, an amphipathic helix with a conserved core of hydrophobic amino acids, was first identified in a microtubule associated protein (MAP) (Carr et al., 1991) and AKAPs are abundant in all animals with cilia. The central component of the radial spoke is a dimeric AKAP designated Radial Spoke Protein 3 (RSP3) in unicellular species or Radial Spoke Protein Homolog 3 (RSPH3) in higher organisms (Figure 2.2). This AKAP binds many different proteins within the Docking and Dimerization (DD) domain of cAMP-dependent Protein Kinase (PKA) regulatory type-II (RII) subunit superfamily (Yang et al., 2006). Moreover, the fibrous sheath which surrounds the axoneme in mammalian sperm is almost entirely composed of AKAPs and RII-like proteins
(Eddy et al., 2003).

Fundamentally, understanding chemomechanical signal transduction in cilia and flagella offers critical insight into how AKAPs and RII-like proteins ensure local signals are received and transmitted with high spatiotemporal fidelity. Recent high profile studies report that AKAPs function as 'signaling islands,' constraining PKA action within domains of action on the double digit nanometer scale (Langeberg & Scott, 2015). This work proposes that AKAPs constrain other RII-like proteins and respective catalysts to sites of action within cilia and flagella. All RII-type modules binding AKAPs appear to act as a bridge between the insoluble and soluble compartments, nucleating local order, constraining small molecule second messengers, and coordinating mechanical transitions. Despite the critical importance of the radial spokes and sperm fibrous sheath in information flow through signal transduction, their structure and mode of action are not well understood.

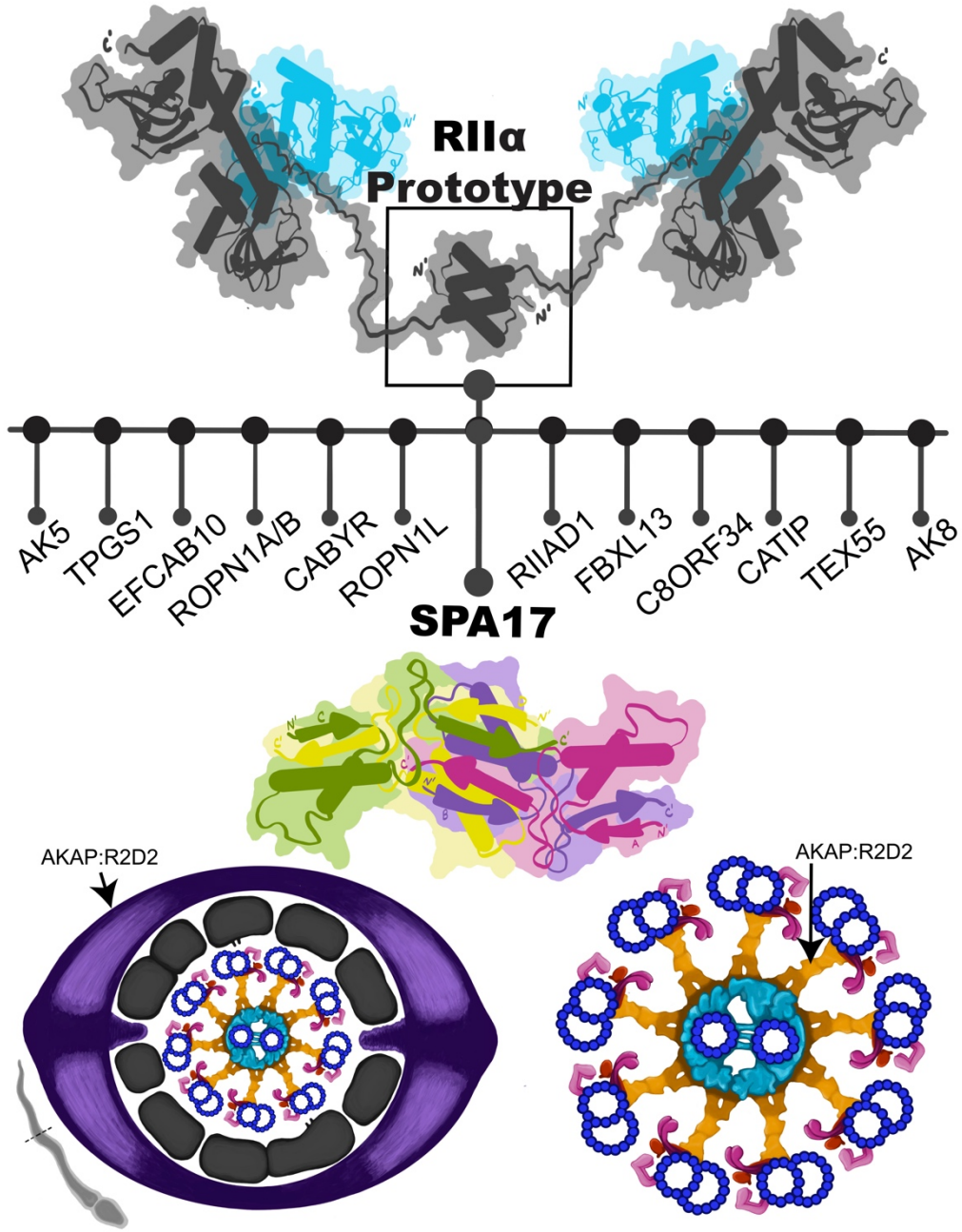

Figure 2.1. SPA17 and the RII superfamily.

The docking and dimerization domain of RII I. s a modular domain comprising its own superfamily. These members are upregulated in sperm and ciliated epithelium. AKAPs and R2D2 proteins form the core structure of the radial spoke and sperm fibrous sheath.

2.2 CILIA AND FLAGELLA

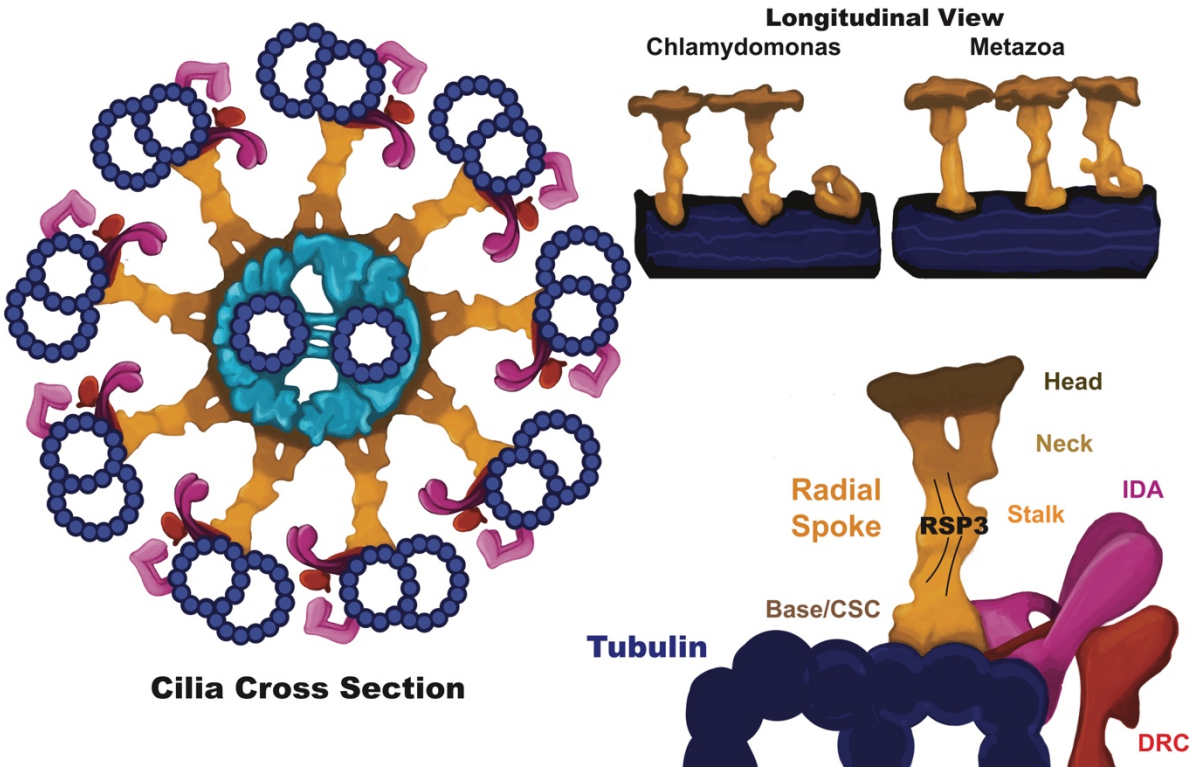

Figure 2.2. Cilia cross section detailing 9 + 2 organization and radial spokes. Top right. Longitudinal view of the radial spoke comparing *Chlamydomonas* and Metazoa. Bottom right. Location of RSP3 in the radial spoke and relationship of the radial spoke to central pair. In the cross-section, microtubules are navy, central pair apparatus is light blue, outer dynein arms are light pink, inner dynein arms (IDA) are dark pink, dynein regulatory complex (DRC) is red and radial spokes are orange.

Many protozoans and sperm utilize swimming as their predominant form of locomotion, reaching speeds of up to 1mm/s (Lodish et al., 2000). Cilia and flagella provide the propulsive force necessary for movement. Even multicellular metazoans still have ciliary based locomotion and cilia display a diverse architecture and specialization in this clade (Dutcher, 2020; Osinka et al., 2019). Organisms like snails have a foot covered with specialized cilia which move mucus between the animal and a surface, providing flow to allow the snail to slide relative to that surface. The structure of all cilia is surprisingly similar as described in the last section. The axoneme is the central component of the cilia, comprised of microtubule doublets formed by an A protomer with

13 protofilaments and an adjoining B protomer with 10 protofilaments. A special polymer of tubulin unique to the axoneme builds the filaments (Figure 2.3).

Cilia and flagella beat by the relative sliding of microtubule filaments, like muscle contraction is generated by the relative sliding of actin and myosin filaments. All doublet microtubules have their plus end at the tip of the axoneme and sliding is propagated along the entire length such that bending can proceed without dampening (Osinka et al., 2019). Dynein arms are the force generating proteins responsible for this movement. Inner and outer arm dyneins are arranged in a clockwise circle firmly attached to the A tubule and reaching towards an adjacent B tubule. Each dynein is a large multimeric protein with heavy, light, and regulatory chains that use the hydrolysis of ATP to drive bending. Bending is produced when a microtubule doublet slides, and the opposite doublet is rigid and resists sliding. The action of inner arm dyneins is controlled by the central pair apparatus and radial spokes which act in a coordinated manner to regulate relaxation and rigidity of opposite protomers (Osinka et al., 2019).

The radial spoke is a large macromolecular complex comprised of at least 23 proteins (Table 2.3). These proteins function as a chemomechanical transducers to regulate ATP hydrolysis by inner arm dyneins, but despite numerous structural and biochemical studies, exact mechanism of transduction remains elusive. Calcium is known to be integral to this mechanism, as at the base of the spoke nested between the spoke and inner arm dynein, rests the calmodulin and spoke associated complex (CSC) necessary for ciliary bending. The central stalk of this structure is formed by dimeric radial spoke protein 3 (RSP3), which contains two amphipathic helices for binding RII and DPY-30 domains. Triplets of radial spokes are arranged in a helical pattern along the length of the axoneme and each triplet has a unique composition and structure as demonstrated by cryo-electron tomography. *Chlamydomonas* only has two fully formed spokes while the third spoke resembles a vestigial structure. Thus, data on the composition of the spokes in higher organisms is lacking (Dutcher, 2020; Yang et al., 2006).

Table 2.3. Radial spoke proteins, their putative human homologs, domains, and location.

Chlamydamonas RSP	Putative Human Homolog	Domain	Location
RSP1	Meichroacidin/TSGA2	MORN	Head
RSP2	?	DPY-30 & GAF	Neck
RSP3	RSHL2/ RSPH3	AKAP	Stalk
RSP4	RSHL3 or RSHL1	?	Head
RSP5	?	Aldo-keto reductase	Stalk
RSP6	RSHL3 or RSHL1	?	Head
RSP7	SPA17?	RIIα & EF Hand	Stalk
RSP8	?	Armadillo	Stalk
RSP9	C6orf206	?	Head
RSP10	TSGA2	MORN	Head
RSP11	ROPN1L	RIIα & ?	Stalk
RSP12	PPIL6	Peptidl-prolyl isomerase	Stalk
RSP13	?	?	Stalk
RSP14	?	Armadillo	Stalk
RSP15	?	Leucine-rich repeat	Neck
RSP16	TSARG6	DnaJ	Stalk
RSP17	?	GAF	Stalk
RSP18	?	?	Stalk
RSP19	Multiple	?	Stalk
RSP20	Calmodulin	EF Hand	Stalk
RSP21	?	?	Stalk
RSP22	Dlc2	LC8	Stalk
RSP23	NME5	NDK/IQ motif	Neck
CaM-IP2	FAP91	AKAP & AAT-I	CSC
CaM-IP3	FAP61	Pyridine disulfide oxidoreductase	CSC
CaM-IP4	FAP251	WD repeat	CSC

Cilia exist in two major forms, motile and primary (Figure 2.3). Motile cilia and flagella have a 9+2 architecture in which movement is coordinated by the central pair and radial spoke complexes. Primary cilia exist on almost all cell types in the quiescent stage, and do not contain the central pair apparatus or radial spoke macromolecular complexes and therefore have a 9+0

architecture. Motile cilia are present on respiratory epithelium, fallopian tube epithelium and ependymal cells, and function to move mucosal secretions. Further, cilia evolved diverse roles in Metazoa and are key to sensory signaling (Figure 2.3). Modified cilia called kinocilia (9+2) in the inner ear sense balance, and retinal cilia (9+0) give rod and cone their distinctive shape and house photoreceptors. It is therefore not surprising that animals carry a wide variety of anchoring domains and scaffold partners which evolved to serve these complex functions dependent upon a high degree of organization.

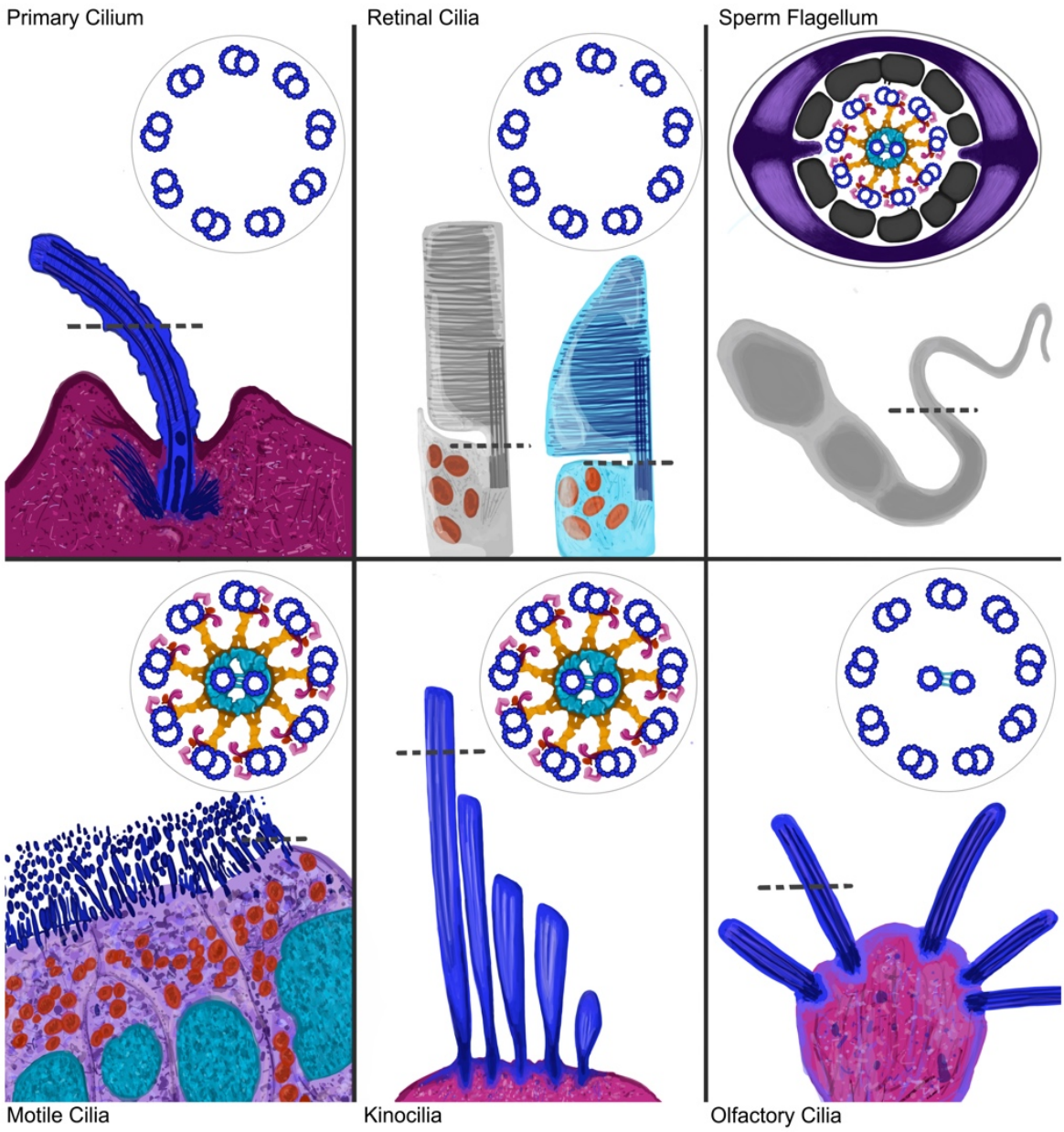

Figure 2.3. Cell types containing axonemes and their cross-sections.

Note that primary cilia and derived structures lack radial spokes and the central pair. In the cross-section, microtubules are navy, central pair apparatus is light blue, outer dynein arms are light pink, inner dynein arms are dark pink, DRC is red, and radial spokes are orange.

2.3 AKAPs: Structural Proteins of the Radial Spoke

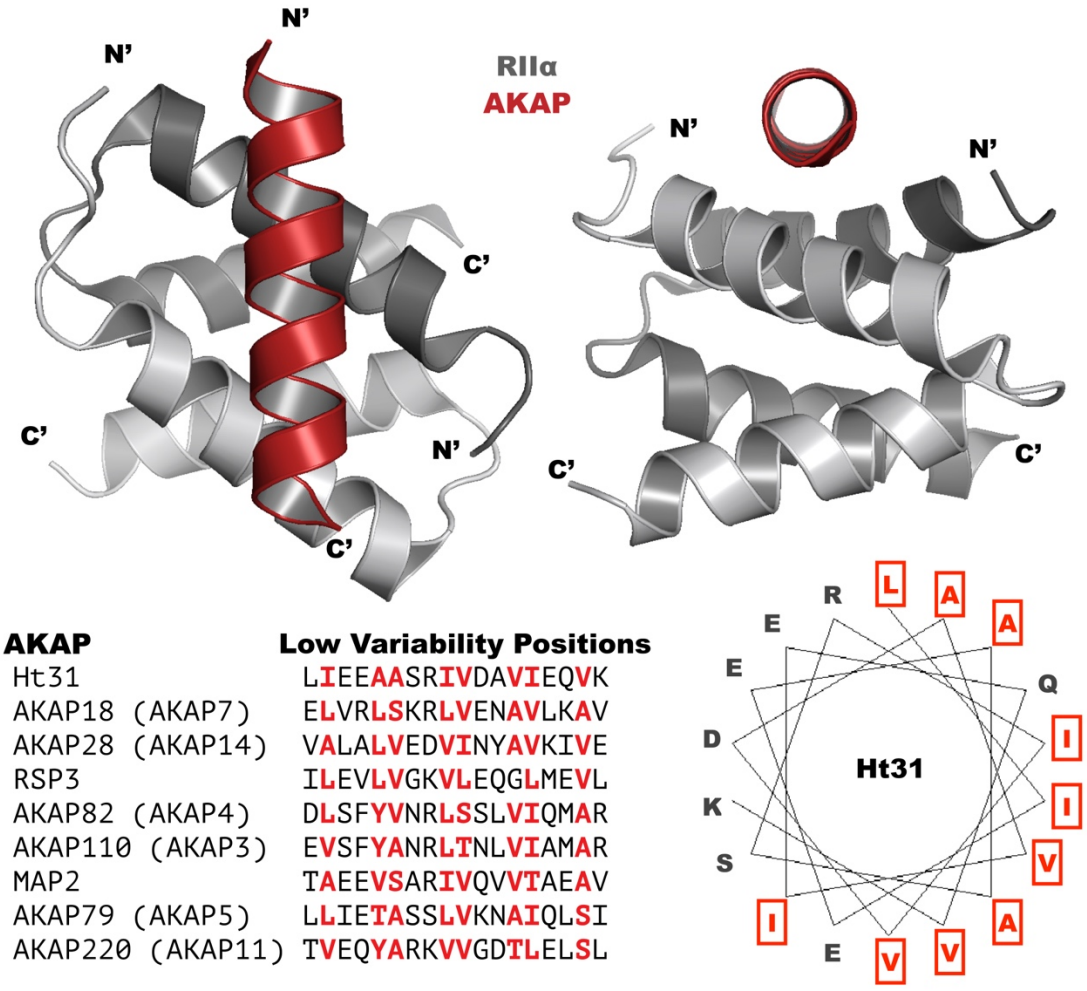

Figure 2.4. Low Variability Positions of AKAPs.

PDB ID: 2IZX

AKAPs are a diverse family of proteins with about 50 members united by their ability to bind PKA. In a recent review, Gray and Klussman (2020) ponder the diversity of AKAPs in the context of the limited number of PKA regulatory subunit isoforms RIα (RIa), RIβ (RIb), RIIα (RIIa), and RIIβ (RIIb). AKAPs all contain an amphipathic α-helix with regularly spaced hydrophobic residues. The amphipathic helix has a signature motif —conserved positioning of hydrophobic amino acid residues —*H*xx*HH*xx*HH*xx*HH*xx*HH* (H indicates the position of hydrophobic amino acid residues) (Hundsrucker et al., 2010) (Figure 2.4). Many AKAPs have been identified with a

far-Western technique called the RII overlay whereby the type II regulatory subunit of PKA (RII) is biotinylated and overlaid onto a membrane containing separated cell lysates which is then probed with streptavidin HRP to visualize AKAPs at specific molecular weights (Carr et al., 1991; Lohmann et al., 1984). Therefore, many AKAPs are named for their molecular weight in the literature e.g. dAKAP1 is also known as sAKAP84. There are AKAPs known to be localized to most subcellular structures including microtubules, mitochondria, outer membrane, peroxisomes, and cilia. RSP3 was identified as an AKAP by RII overlay and a number of papers have been published on PKA and cyclic nucleotide regulation of ciliary beating at the radial spoke, however no proteomic or biochemical studies have identified PKA as a component of this structure.

The radial spoke of Chlamydomonas can be separated from other axonemal structures by salt extraction and centrifugation. The composition of the radial spoke was interrogated by genetic mutations in which cells lack all or part of the radial spoke, but PKA has never been associated with the radial spoke in these studies (Yang et al., 2006). This observation and the existence of R2D2 proteins with alternative catalysts (Table 1.1), support the hypothesis that the importance of AKAPs extends far beyond PKA. Furthermore, the association between AKAPs and PKA may be the more derived function, because a diversity of R2D2 proteins are present in all clades of eukaryotes (see Table 2.4 and Figure 2.9).

2.4 RIIALPHA CLAN: X-TYPE FOUR HELIX BUNDLES

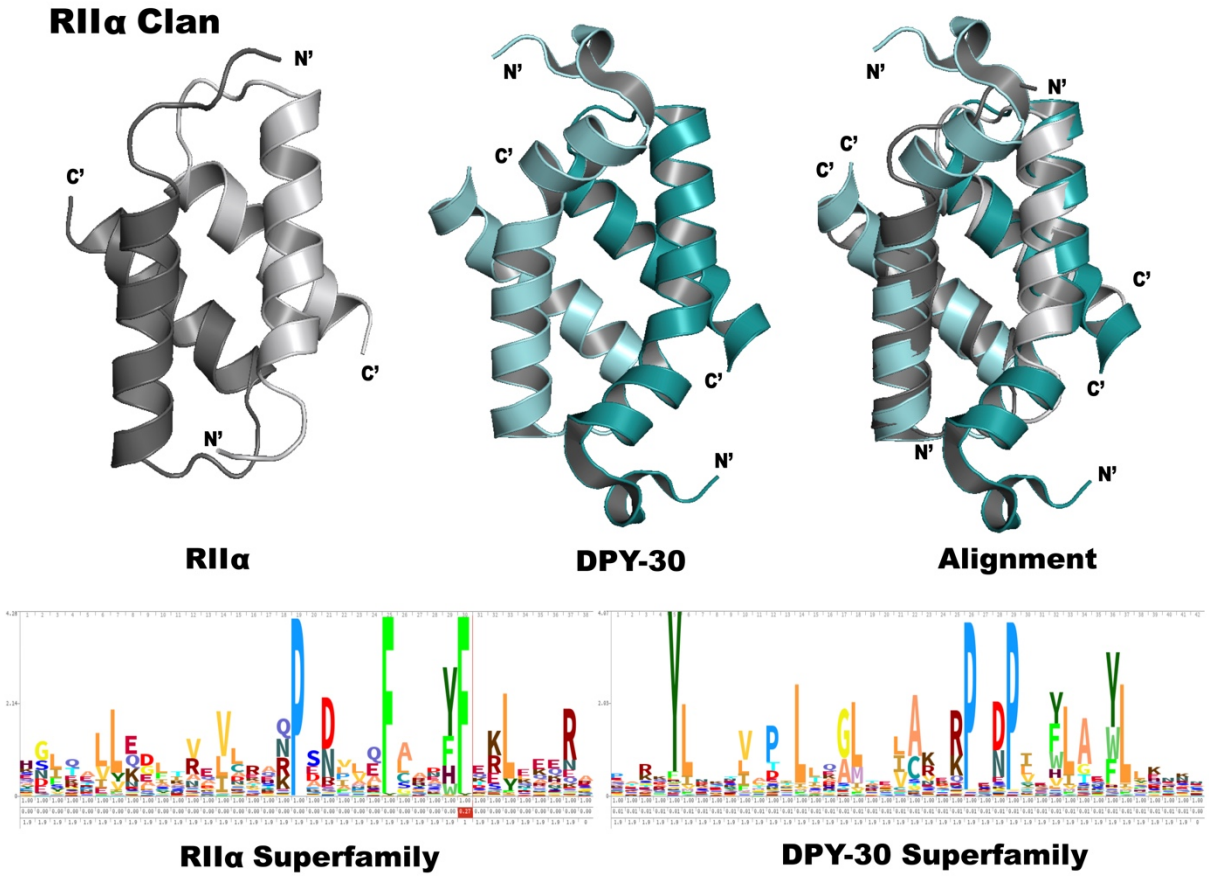

Figure 2.5 Structures and HMM logo of RIIa clan members.
RMSD = 2.6 Å, PBD ID: 2IZX, 3G36

X-type four helix bundles characterize the RIIα Clan which is composed of two superfamilies, RIIα and DPY-30 (Figure 2.4) (Finn et al., 2014). (Note the RIIα Superfamily includes both isoforms of RI and RII.) Proteins of the RIIα Clan possess the DD domain. Monomers contain two alpha helices. Dimerization is enabled as alpha helices of monomers associate in an antiparallel arrangement. Following dimerization, the holoenzyme X-type four helix bundles contain a hydrophobic groove for docking amphipathic helices. The RIIα domain was originally discovered and identified in the type II regulatory subunit of PKA by examining cyclic nucleotide activity associated with the particulate fraction. Subsequently, numerous AKAPs have been identified,

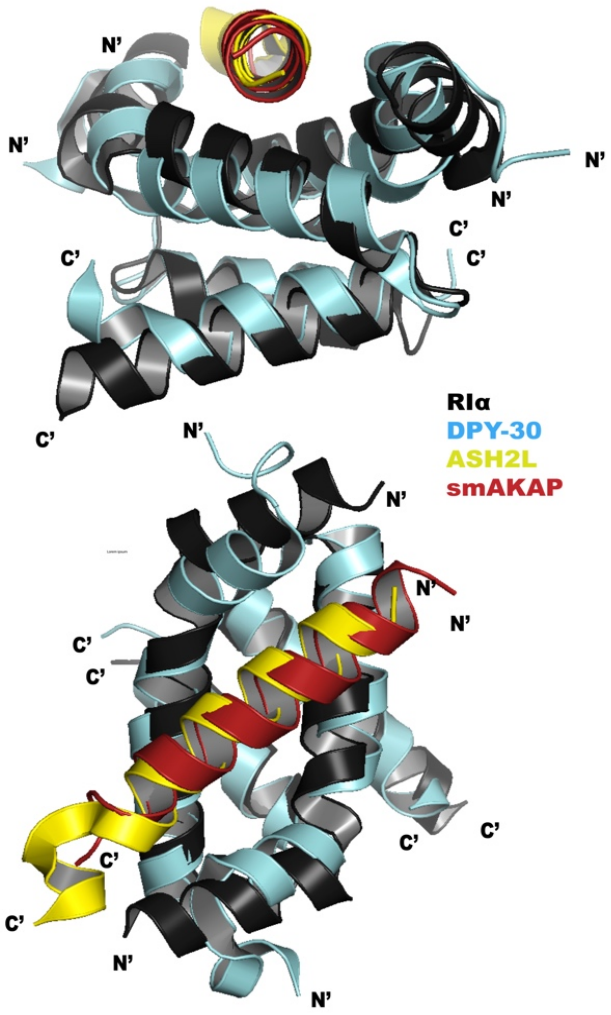

Figure 2.6. Alignment of RIα bound to smAKAP and DPY-30 bound to ASH2L.
RMSD = 2.9 Å; PBD IDs: 5HVZ, 4RIQ

which spatiotemporally regulate the activity of PKA holoenzymes, generating signaling islands which constrain cAMP-dependent phosphorylation to specific locations. It is apparent that numerous proteins other than AKAPs possess the amphipathic helix capable of interaction with RIIα Clan DD domains. As stated in Chapter 1 the PKA-R/AKAP model serves as a prototype for understanding this entire class of protein-protein interactions. The RIIα domain is not unique to PKA, and growing evidence presented here suggests this ancient domain diversified and was coopted into a wide array of signaling circuits (Table 1.1, Figure 2.5).

DPY-30 and ASH2L reside in the nucleus and are a part of the H3K4 methyltransferase catalytic module (Hsu et al., 2018). DPY-30 was originally identified in Caenorhabditis elegans as a regulator of X-chromosome dosage compensation (Hsu & Meyer, 1994). Methylation of histone H3 at Lys4 (H3K4) is a post-translational modification of chromatin that signals active transcription. DPY-30 functions as a regulatory subunit which participates in positive heterotypic allosteric regulation of methyltransferase enzymes, and knockdown of DPY-30 in a variety of organisms causes a widespread loss of H3K4 methylation (Haddad et al., 2018). The regulation of transferase activity is strictly regulated by the 44-residue RIIa Clan helical domain which binds to the last 30 residues of ASH2L (South et al., 2010; Tremblay et al., 2014).

In 2009, the DPY-30 domain was crystallized and its relation to the RIIα domain became evident (Wang et al., 2009). The two structures are superimposable and the AKAPs that dock into the helical groove on RII and DPY-30 dimers are amphipathic helices that share core hydrophobic binding residues (Figure 2.6). Amphipathic helices on AKAPs can even be promiscuous, as the helices on AKAP8 and RSP3 can bind both DPY-30 and RII domains. DPY-30 and RIIα differ primarily in their N-terminal regions, much like RI and RII. The N-terminal region is proposed to be a major determinant of specificity with both RI and DPY-30 containing extended N-terminal helices. RII contains strands with conserved hydrophobic residues for high affinity AKAP interactions. Another method by which specificity may be determined is localization. It is largely accepted that the nucleus excludes PKA, because the dimeric R-subunit is too large to pass into the nucleus (Yapo et al., 2018). It is not known how RSP3 complexes are assembled with promiscuous DPY-30 and RIIα binding helices. The radial spoke is also assembled in the cytosol and thus assembly must take place in the presence of the R subunit.

```
dAKAP2      ELAWKIAKMIVSDVMQQA
smAKAP      EYAHRLSQDILCDVMQQW
ASH2L       AVVEHTLADVLYHVETEV
```

Figure 2.7. Alignment of dAKAP2, smAKAP and ASH2L amphipathic helices.

2.5 RIIA SUPERFAMILY AND R2D2 PROTEINS

Beyond the initial split between the RIIa and DPY-30 superfamilies, the RIIa superfamily exhibits intrafamilial diversity, particularly within the Metazoan clade. R2D2 proteins were first identified

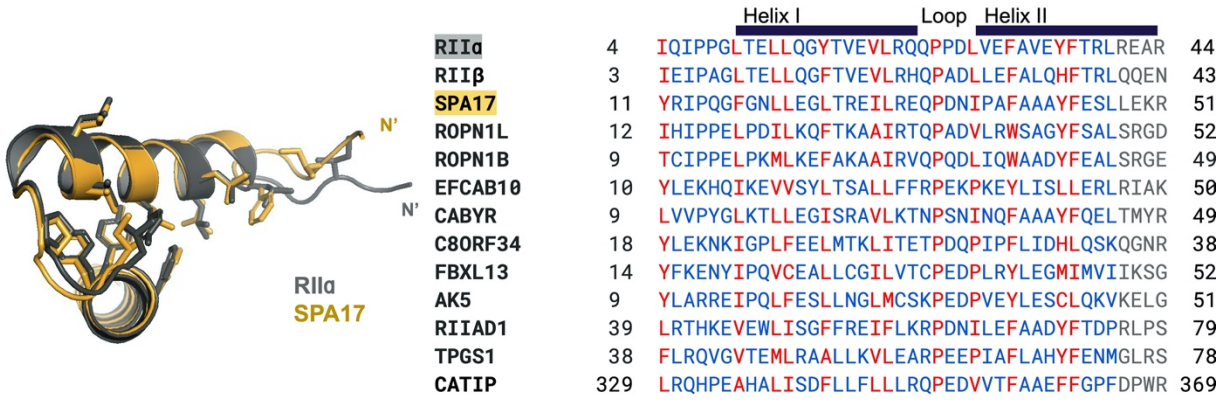

Figure 2.8. Sequences of RIIα proteins and SPA17.

A. Structural alignment of the helices from SPA17 and RIIα monomers. RMSD = 0.528 Å. B. Sequence alignment of selected RIIα superfamily DD domains. PDB: 2IZX

and published in the literature in the year 1994 by Richardson and colleagues studying sperm proteins (see Chapter 3). They identified Sperm SPA17 as a protein enriched in testis and sperm with an N-terminal domain highly homologous to that of type II PKA (Richardson et al., 1994). The next major study did not come until six years later when the Narumiya group in Japan discovered Ropporin-1 as a RhoA interacting protein in testis (Fujita et al., 2000). This protein also contains a highly conserved RIIα-type helical sequence. Subsequently, Carr and colleagues published numerous studies significantly expanding knowledge of the R2D2 proteins ROPN1, ROPN1L (sometimes known as AKAP-associated sperm protein (ASP)), SPA17, and CABYR (Fiedler et al., 2013). They also coined the term R2D2 protein for this family as it is the RII docking and dimerization (DD) domain (RIID2/ R2D2) family (Figure 2.8). All four of these proteins bind AKAP helices with differing specificities (Newell et al., 2008).

Table 2.4. Human R2D2 Proteins: Chromosome and Knockout Phenotype.

Protein (Abbr.)	Aliases	Chr.	Knockout Phenotype	Taxonomy Span	Domains
Ropporin 1 (ROPN1)	Rhophilin Associated Tail Protein 1A (ROPN1A), Cancer/Testis Antigen 91 (CT91), Outer Dense Fiber of Sperm Tails 6 (ODF6)	3	Reduced sperm motility; Male subfertility; Abnormal fibrous sheath with ROPN1L DKO	Tetrapod Vertebrates, coincident with acquisition of fibrous sheath	71 AA DD Domain; Unknown CTD, PHYRE2 predicts homology to EF- Hands
Ropporin 1B (ROPN1B)	AKAP-Binding Sperm Protein Ropporin	3	N/A	Primates	71 AA DD Domain; Unknown CTD, PHYRE2 predicts homology to EF- Hands
Ropporin 1-Like (ROPN1L)	Rhophilin Associated Tail Protein 1-like (ROPN1L); Radial Spoke Head 11 Homolog (RSPH11); AKAP-Associated Sperm Protein (ASP)	5	Reduced ciliary motility; Abnormal snout morphology; Abnormal spine curvature/ kyphosis; Abnormal tooth morphology	Metazoa Chaonoflagellates Chytrids Green Algae Green Plants Diplomonads Fungi Ciliates Kinetoplastids Dinoflagellates Oomycetes Brown Algae Haptophytes	71 AA DD Domain; Unknown CTD, PHYRE2 predicts homology to EF- Hands
Sperm Autoantigenic Protein 17 (SPA17)	Sperm Protein 17 (SP17); Sperm Surface Protein 17 (SP17); Cancer/Testis Antigen 22 (CT22)	11	N/A	Metazoa	75 AA DD Domain; IQ motif
Calcium Binding Tyrosine	Fibrousheathin 2 (FSP2); Cancer/Testis	18	Male subfertility; Abnormal	Tetrapod Vertebrates, coincident with	75AA DD Domain; EF-Hand-like

Protein (Abbr.)	Aliases	Chr.	Knockout Phenotype	Taxonomy Span	Domains
Phosphorylation Regulated Protein (CABYR)	Antigen 88 (CT88); Testis-Specific Calcium-Binding Protein (CBP86)		fibrous sheath; Abnormal capacitation; Reduced activated motility	acquisition of fibrous sheath	calcium binding domain; Tandem PxxP motifs
RIIα Domain Containing Protein 1 (RIIAD1)	C1ORF230	1	Absent whiskers; Increased bone mineral content; Abnormal grasping; Preweaning lethality	Metazoa Eukaryotes Slime Nets Chytrids Haptophytes Oomycetes Blastomycoses Kinetoplastids	85 AA DD Domain
Ciliogenesis Associated TTC17 Interacting Protein (CATIP)	C2ORF62	2	Male infertility	Opisthokonts	Unknown; 75 AA C-terminal DD Domain
Adenylate Kinase 8 (AK8)	ATP-AMP Transphosphorylase 8	9	Hydrocephaly; Dilated lateral ventricles; Small hippocampus	Metazoa Choanoflagellates Haptophytes Chytrids Apicomplexans Diplomonads Ciliates	60 AA DD Domain; Adenylate Kinase Domain
Adenylate Kinase 5 (AK5)	ATP-AMP Transphosphorylase 5	1	N/A	Metazoa Chytrids (Opisthokonts)	66AA DD Domain; Adenylate Kinase Domain
F-Box and Leucine-Rich Repeat Protein 13 (FBXL13)	Dynein Regulatory Complex Subunit 6 (DRC6); Cilia and Flagella Associated 169 (CFAP169)	7	Abnormal bone structure; Abnormal bone mineral content	Metazoa	70 AA DD Domain; Leucine-rich repeats

Protein (Abbr.)	Aliases	Chr.	Knockout Phenotype	Taxonomy Span	Domains
EF-Hand Domain Containing 10 (EFCAB10)		7	N/A	Metazoa Eukaryotes Green Algae Green Plants Ciliates Fungi Chytrids Oomycetes Dinoflagellates Haptophytes	60AA DD Domain; EF-Hand
Tubulin Polyglutamylase Complex Subunit 1 (TPGSI)	C19ORF20	19	Abnormal sperm axoneme; Abnormal spermio-genesis; Absent flagellum; Male infertility; Decreased body fat; Increased submissive behavior	Metazoa Chytrids Cryptomonads Ciliates Green Algae Eukaryotes Oomycetes	45AA DD Domain; CTD involved in tubulin modifications
Chromosome 8 Open Reading Frame 34 (C8ORF34)	Vestibule-1 (VEST1)	8	N/A	Metazoa	70 AA DD Domain; DUF5586
Testis Expressed 55 (TEX55)	C3ORF30; Testis-Specific Conserved cAMP-Dependent Type II PK Anchoring Protein (TSCPA)	3	N/A	Metazoa	34 AA DD Domain; DUF5582

The last eukaryotic common ancestor likely contained both type II PKA and R2D2 proteins. The most ancestral R2D2 protein appears to be ROPN1L/ RSP11. All major clades of eukaryotic life contain RIIα protein representatives. Eukaryotic unicellular species in the Excavata

and Harosa supergroups, and plant lineages commonly contain RSP7 and RSP11. Furthermore, only land plants which still utilize sperm for reproduction still contain R2D2 proteins. When spores are utilized instead of sperm, species lose R2D2 proteins, which is also why they are not well represented in fungi (Figure 2.9).

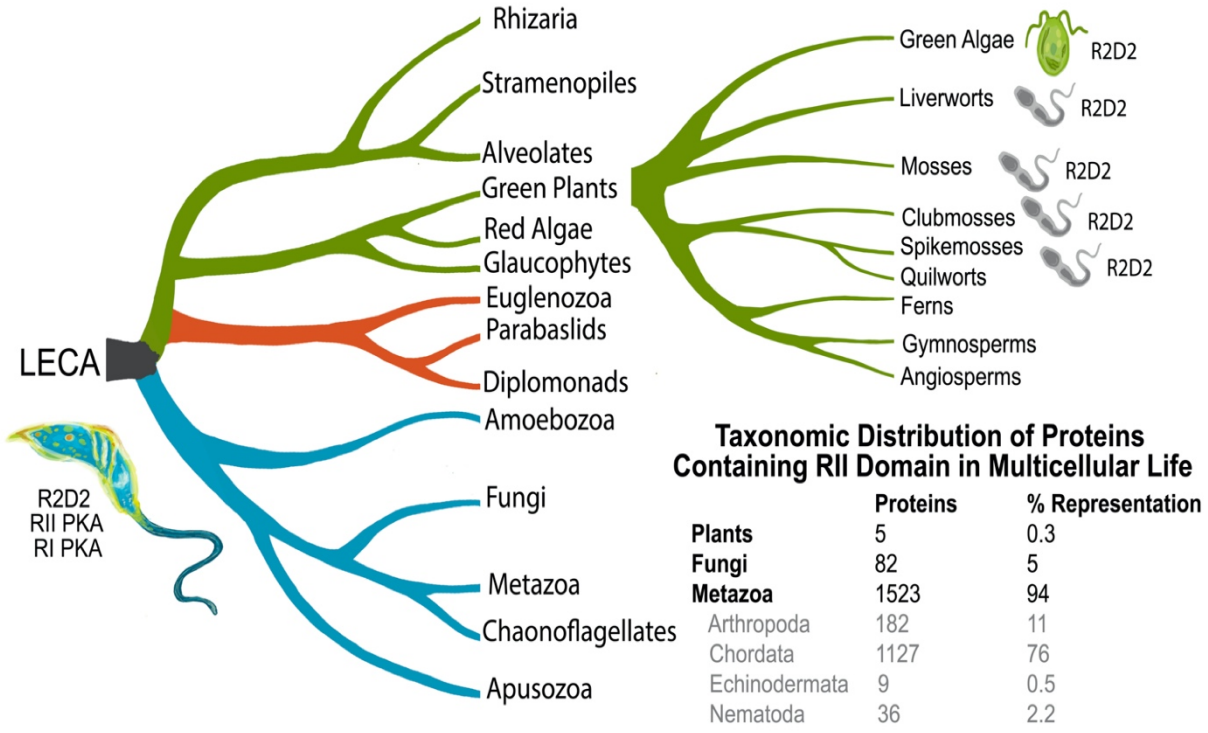

Taxonomic Distribution of Proteins Containing RII Domain in Multicellular Life

	Proteins	% Representation
Plants	5	0.3
Fungi	82	5
Metazoa	1523	94
Arthropoda	182	11
Chordata	1127	76
Echinodermata	9	0.5
Nematoda	36	2.2

Figure 2.9. Distribution of RIIα proteins among eukaryotic clades.
R2D2 proteins are present in all major clades but are lost in species which lack cilia. Metazoa has an over-representation of these proteins due to cilia specialization and reliance on PKA signaling. Data reproduced from SMART.

Human R2D2 proteins, chromosomal location, phylogenetic origin and consequences of knockout (Bult et al., 2019) are shown in Table 2.4. All R2D2 proteins are ubiquitously and predominantly expressed in ciliated tissues and sperm flagella, however they can display limited expression in all tissues if they function in primary cilia. The four most well-studied R2D2 proteins, ROPN1, ROPN1L, SPA17, and CABYR bind to AKAP110 and are known components of the sperm fibrous

sheath (Lehti & Sironen, 2017). This fibrous, elastic structure surrounding the axoneme possess circumferential ribs and longitudinal columns that are structurally comprised of AKAP110 and AKAP82. Furthermore, ROPN1L/ RSP11 is a known component of the radial spoke (a macromolecular complex necessary for ciliary motility). Knockout of ROPN1L in mice and RSP11 in *Chlamydomonas* results in motility defects, and knockout of both ROPN1L and ROPN1 results in subfertility and impaired flagellar motility (Fiedler et al., 2013). Knockout of CABYR also results in subfertility in mice but is not reported to impact ciliary motility (Young et al., 2016). The algal flagellar protein RSP7 appears homologous to the N-terminal domain of SPA17 as the two proteins share a conserved length of this domain (70-75 amino acids) and both have flanking strands on N and C-terminal regions of the DD with conserved aromatic amino acids (Figure 2.10). SPA17 has yet to be knocked out and so its function in sperm motility is unproven.

```
RSP7   1 MSARYQKT-FTIPEGFPQLLKAFTREILRNQPDNIYEFGAKYFEDLIEENKRAAERESSPEVAADEGGGVEAGWWN 75
         MS  +  T + IP+GF  LL+  TREILR QPDNI  F A YFE L+E      +RE +    A+ G  VE  ++N
SPA17  1 MSIPFSNTHYRIPQGFGNLLEGLTREILREQPDNIPAFAAAYFESLLE------KREKTNFDPAEWGSKVEDRFYN 70
```

Figure 2.10. Alignment of RSP7 NTD (Green Algae) with SPA17 NTD (Human).

The R2D2 proteins share a conserved core of hydrophobic residues with the R-subunit for dimerization and AKAP binding, and R2D2 proteins are reported to interact with a diverse repertoire of AKAP helices with differing specificity. In an illuminating review, Burton and McKnight (2007) describe the effects of knockout of different PKA isoforms, (Cα, Cb, RIα, and RIIα) and while AKAPs appear to have a functional role in fertility, this is not dependent upon RIIα, and excess PKA activity is associated with subfertility. The AKAP peptide derived from human thyroid, Ht31, disrupts AKAP complexes *in vitro* and its application has a profound negative effect on flagellar motility, while H-89 and PKI, both kinase inhibitors, have a limited impact (Vijayarghavan et al. 1996; Carr et al. 2001). All these results suggest that AKAPs have PKA-independent functions enriched within motile cilia and flagella. Interestingly, R2D2 proteins may be essential for proper assembly or activity of select PKA: AKAP complexes as ROPN1L knockout mice have decreased phosphorylation of specific PKA substrates. Some AKAPs like AKAP82 and AKAP110 have multiple binding helices on a single strand.

In addition to AKAP binding, R2D2 proteins contain C-terminal regions with affinity towards other macromolecules (Table 2.3). The CTD of ROPN1 is known to interact with the PDZ domain of RhoA, an actin binding protein. ROPN1L binds the Armadillo domain containing protein RSP14. The CTD of SPA17 is an IQ-motif, which binds calmodulin in a calcium regulated manner. Of note is that the calmodulin spoke complex lies at the base of the radial spoke. During sperm capacitation, the CTD of CABYR is phosphorylated on its calcium binding domain (Naaby-Hansen et al., 2002). Adenylate Kinase 5 (AK5) and Adenylate Kinase 8 (AK8) are phosphotransferases that catalyze the conversion of ATP and AMP to two ADP. The CTD of EFCAB10 has high homology to calcium binding EF Hands, hence its designation. Tubulin polyglutamylase 1 (TPGS1) is involved in sperm development and post-translationally modifies axonemal tubulin. VEST1, RIIAD1, Ropporin family, and CABYR are essentially dark outside of their region of homology with RIIα, meaning that structure and mechanisms of action are not well understood.

Figure 2.11 shows staining for select R2D2 proteins in the fallopian tube and expression patterns of R2D2 in humans. These proteins are expressed in ciliated epithelial tissue and in ependymal rich brain tissues. The distribution of the R2D2 protein SPA17 is discussed in detail in the next chapter. Despite the known interaction between R2D2 and AKAP proteins and homology with the PKA R-subunit, the structure of the R2D2 N-terminal domain and its specificity determinants have not been well evaluated. My study reports the structure of SPA17 with novel N and C-terminal strands that likely mediate the observed decreased affinity for AKAPs in the absence of ROPN1L heterodimerization (Chapter 4). This study also reports that ROPN1L and SPA17 form a heterodimer. The Narumiya group also found that ROPN1 and SPA17 heterodimerize (unpublished data). SPA17 contains a C-terminal IQ-motif and RSP7 contains C-terminal EF hand domains, and as such both SPA17 and RSP7 may be responsible for localizing calcium signaling with ROPN1L and RSP11 respectively.

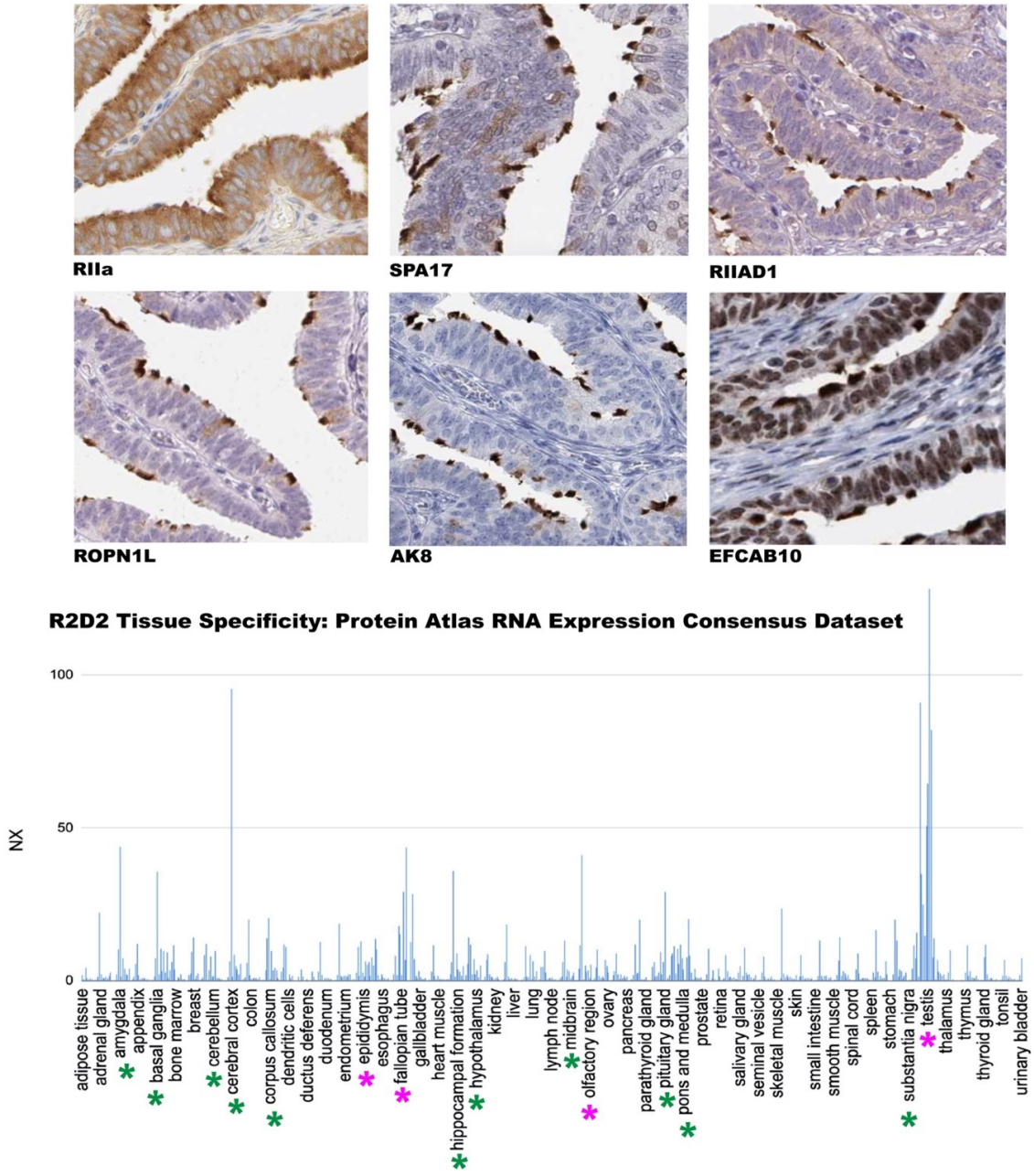

Figure 2.11. RIIα and R2D2 protein and RNA localization.

Top) Immunohistochemistry in fallopian tube tissue as shown in the Human Protein Atlas. RIIα is diffusely distributed in the cytosol whereas R2D2 proteins are localized to cilia (all) or cilia and nucleus (EFCAB10). Bottom) Comparison of RNA expression pattern of all R2D2 proteins from the Human Protein Atlas consensus dataset. R2D2 proteins are upregulated in ciliated tissues. Ciliated epithelium has a pink asterisk and ependymal rich brain tissues have a green asterisk.

2.7 SUMMARY AND CONCLUSION

Eukaryotic cells have membrane bound organelles called cilia or flagella which contain an axoneme comprised of nine microtubule doublets. Motile cilia and sperm flagella have a central pair of microtubules linked to the outer doublets by the radial spokes. The central pair and radial spokes control the action of the inner dynein arm to produce rigid and relaxed opposite pairs to give rise to ciliary bending. The central stalk of the radial spoke is nucleated by an AKAP called RSP3. AKAPs are a diverse family of molecules united by their ability to bind PKA through an amphipathic helix, however not all AKAPs which interact with PKA in biochemical assays do so in a physiologically relevant context. One example is RSP3, as PKA is not known to be a component of the radial spoke complex. The RIIα domain of PKA is present on at least thirteen other proteins as labelled in the superfamily database which includes the radial spoke protein RSP11/ ROPN1L. Further, the sperm fibrous sheath that surrounds the flagellar axoneme is almost entirely comprised of AKAP110 (AKAP3) and AKAP82 (AKAP4), and the R2D2 proteins ROPN1L, ROPN1, SPA17, and CABYR.

R2D2 proteins are upregulated in ciliated tissues, were likely present in the last eukaryotic common ancestor, and are present in all eukaryotes with cilia or flagella. Evolutionary loss of cilia and flagella is correlated with a loss of R2D2 and AKAP proteins. Relatedly, ciliary specialization in metazoans is positively associated with RII, R2D2 and AKAP expansion and utilization. Humans rely on motile cilia for left-right patterning during development, mucous clearance, and fertility and as such understanding of the cilia is necessary for human health. Moreover, an emerging paradigm describes domains of cAMP dependent kinase activity as ‘signaling islands’ which constrain PKA action within a range less than 50 nanometers (Smith et al., 2017). It is therefore essential to understand how AKAP anchored enzyme activity is regulated when effectors like calcium and cAMP are theoretically highly mobile and diffusible. Signaling islands allow cellular compartmentalization of effectors. The radial spoke and other cilia associated AKAP complexes may be an optimal model to understand these processes as they have well defined structures and components and are putatively regulated by calcium and cyclic nucleotides. Ciliary motility requires the nine radial spoke units to take disparate actions despite close proximity. Thus, the fine structure of the radial spoke may provide more answers to the mechanism of action of

AKAP: RII complexes. In Chapter 3, we will examine the sequence of the RIIα domain of SPA17 and explore its role in physiology.

Chapter 3. SEQUENCE AND SIGNIFICANCE OF SPA17

3.1 SPA17: SURPRISING FINDINGS

O'Rand and colleagues (1984; 1994) discovered, sequenced and named SPA17 while studying rabbit sperm autoantigens involved in fertilization. Initial Northern blot analysis indicated the protein was not present in "any of the mouse somatic tissues examined (mouse heart, brain, spleen, lung, liver, skeletal muscle, and kidney)" and so they characterized it as a "sperm specific protein" (Kong et al., 1995). The sequence of mouse SPA17 was obtained from a mouse testis library using a cDNA probe; the mRNA sequence is 82% identical to rabbit. The SPA17 protein is 74% identical with the n-terminal AA 100% identical. This region was noted to share 45% identity to human PKA-RIIα. A C-terminal calmodulin binding site, 43% identical to human neuromodulin was also discovered (Kong et al., 1995). These sequences subsequently proved to be a marker for SPA17 as no other protein has an N-terminal PKA-RIIα domain and a C terminal calmodulin binding domain (Buchli et al., 2002). SPA17 functions in fertilization in part through its central, third domain which binds heparin/dextran (Richardson et al., 1994). This domain enables spermatozoa to adhere to the extracellular matrix of the oocyte. Despite failure of early research to localize SPA17 outside the testis, the presence of an IQ-motif and a PKA-RIIα domain suggests the protein might function in a calcium regulated pathway when expressed in somatic tissues. The central polysaccharide binding domain might facilitate cell-cell and cell-matrix adhesion, as it does during fertilization. Of the three domains, the central domain shows the most sequence divergence (Wen et al., 2001).

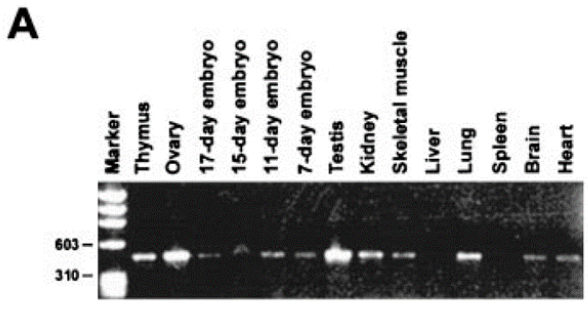

Figure 3.1. PCR of Tissue and embryonic expression of SPA17 (Wen et.al., 2001)

Seventeen years after the initial discovery of the protein, O'Rand's group published a more complete characterization of mouse SPA17 (Wen et al., 2001). Using PCR performed on a Mouse Multiple Tissue cDNA Panel I, and on ovary and thymus cDNA they showed the previous characterization of SPA17 as confined to the testis was incorrect.

The Northern blot method used previously was not sensitive enough to detect expression of the protein in various tissues. SPA17 is expressed in ciliated epithelial, muscle, reproductive and immune system tissue as indicated by its presence in the thymus, ovary, kidney, skeletal muscle, lung, brain and heart (Figure 3.1) (Wen et al., 2001). Brain and heart expression is 40% the testis level, eye, liver, kidney, skeletal muscle, thyroid, and uterus is 20% of the testis level (Wen et al., 2001). There is also differential expression across embryonic development with peak expression in the mouse 11-day embryo. Coincidentally in ED11-ED12 the XY gonad differentiates and ceases to be bi-potential (Munger et al., 2013). Furthermore, migrating coelomic epithelial cells became Sertoli cells ED11 (Karl & Capel, 1998).

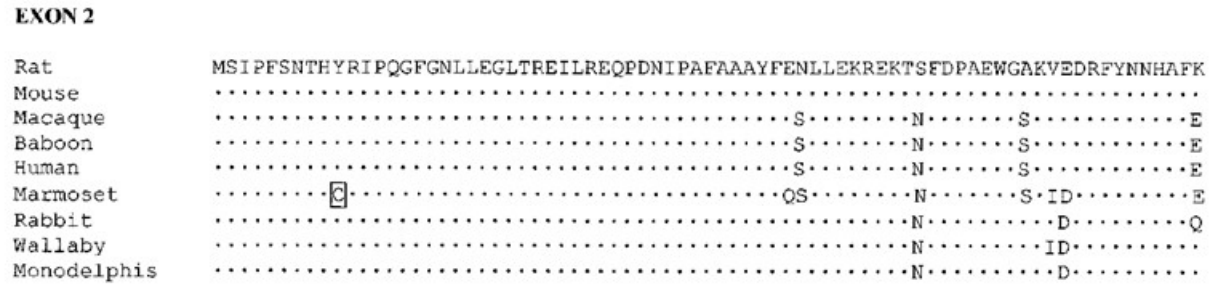

Figure 3.2. Sequence of SPA17 RIIα in select mammals (Wen et.al., 2000).

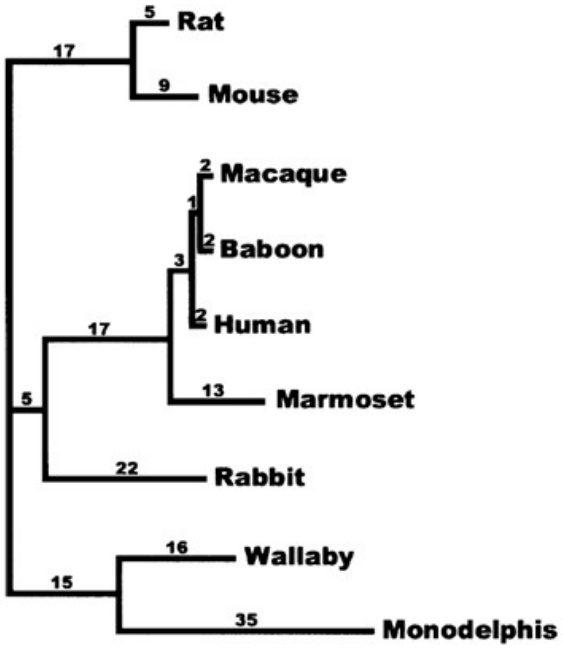

Figure 3.3. Phylogeny of Mammalian SPA17 (Wen et al., 2001)

The unique characteristics of SPA17 motivated Buchli, De Jong, and Robbins (2002) to investigate the structure of the protein's gene. The human gene is on chromosome 11 (11q24). Gene architecture is conserved between

L zX rodents and primates and the gene has multiple transcription start sites. Such complex gene regulation is associated with gene products that show tissue or cell specific expression, temporal developmental stage specific expression or respond to particular cellular or metabolic conditions (Buchli et al.,

2002). Phylogenic analysis confirmed initial findings that the N-terminal RIIα domain is highly conserved (Figure 3.2). Phylogenetic analysis of the anthropoid primate line reveals that the gene sequence has changed little over the last 40 million years (Wen et al., 2001). There is only a 2-base pair difference among apes and a 2-base pair difference between baboons and macaques. The difference between Old World and New World monkeys is larger (Figure 3.3).

3.1 SPA17 AS A MODEL FOR NON-PKA AKAP TARGETING

Human SPA17 primary sequence of 151 aa has a calculated molecular weight of 14.41kD. The N-terminal domain aa 1-51, encoded by exon 2, is homologous to PKA-RIIα docking and dimerization domain. This domain binds the amphipathic helix of AKAP110 (Lea et al., 2004). The central domain, aa 76-104 binds heparin, and is conserved in primates but is the least conserved of the three domains. The C-terminal domain aa 108-137 binds calmodulin.

Figure 3.4. Human SPA17 Domain Architecture

SPA17 is modular and organized in a manner similar to PKA. The calmodulin binding domain is analogous to the PKA catalytic domain but is on the same protein and instead participates in Ca^{+2} signaling (Figure 3.4). The N-terminal RIIα-like domain of SPA17 is responsible for dimerization to create quaternary structure and docking with AKAPs. Presumably, AKAPs target the protein to cilia and flagella. AKAP110 is the only AKAP that was known to bind SPA17 (Lea et al., 2004). It is not found outside the sperm flagellum so other AKAPs likely also bind SPA17 to target the protein to cilia and other sites of action. In addition to features shared with PKA, SPA17 has a carbohydrate binding module that enables the protein to bind to the cell matrix. The function of the carbohydrate binding domain in cilia and flagella is not known. It is also significant that the carbohydrate binding domain is the least conserved of the three modules. SPA17 may be the first well-described signaling molecule other than PKA that is targeted to its place of action by AKAPs. As previously stated, other non-PKA signaling molecules with homology to the DD domain of PKA likely are similarly targeted by AKAPs. There may be others in the RIIα Superfamily in addition to the R2D2 proteins described herein.

3.2 DETAILS OF SPA17 EXPRESSION AND FUNCTION

Table 3.5. SPA17 expression in Cancer Cell Lines

Reference	Cell Line	Findings
(Lim et al., 2001)	Multiple Myeloma	Sp17 is detectable in tumor cells from 12 of 47 (26%) myeloma patients.
(Lacy & Sanderson, 2001)	ARH-77, plasma cell leukemia; ARP-1, ARK, and MER, myeloma; Daudi and Raji, Burkitt lymphoma; Jurkat, T-cell lymphoma	mRNA detected in all cell lines. ARH-77 cells express relatively high levels of Sp17 on their surface.
(De Jong et al., 2002)	Basal cell carcinoma, lung cancer, prostate cancer, adenocarcinoma and osteocarcinoma cancer cell lines.	mRNA detected; no protein
(Coutinho-Camillo et al., 2006)	Prostate cancer cell line LNCaP	mRNA detected after androgen treatment.
(Kausar et al., 2010)	Esophageal squamous cell carcinoma cell line TE13	SPA17 intracellular levels decreased with cisplatin application
(Yamada et al., 2013)	LHK2 lung adenocarcinoma cells, SW480 colon adenocarcinoma cells and MCF7 breast adenocarcinoma cells with stem cell properties	Expression of SPA17 mRNA
(Mirandola et al., 2015)	Non-small cell lung cancer cell lines	mRNA and protein detected

Gaines et al. (2005) used immunocytochemistry and immunofluorescence to investigate the cellular and tissue distribution of SPA17. Sperm flagella and ciliated cells of the bronchus and fallopian tube ciliated epithelia stained strongly. SPA17 was also detected in the basal bodies of sperm and of cells from the renal tubule cell line mCCD, and in centrosomes from immortalized cells. SPA17 localized to the nucleus in tumor cell lines; human SPA17 N-terminal residues 46-53 are conserved and may indicate a nuclear localizing sequence (Gaines, 2006). Another immunofluorescent study found SPA17 with acetylated tubulin in mouse olfactory epithelial cells but only SPA17 was seen in cell nuclei (McClintock et al., 2008). SPA17 is also expressed in human olfactory epithelium and in tumors arising from this tissue (Bumm et al., 2005). These findings indicate the protein functions in both motile and primary cilia and perhaps gene regulation. SPA17 mRNA is expressed in multiple cancer cell lines and is accompanied by variable staining for the protein (Table 3.5).

3.3 CLINICAL SIGNIFICANCE OF SPA17

Table 3.6. Studies of SPA17 in Malignancy.

Reference	Cancer Type	Findings
(Straughn et al., 2004)	Ovarian Cancer	SPA17 detected in 8 of 19 ovarian tumor samples.
(Xia et al., 2013)	Hepatocellular carcinoma	SPA17 detected in 80% of specimen
(Grizzi et al., 2006)	Nervous system tumors	Neuroectodermal (21%) and meningeal tumours (4%) were found heterogeneously immunopositive for SPA17.
(Nakazato et al., 2007)	Clear cell adenocarcinoma of the ovary	SPA17 gene expression related to chemoresistance and poor prognosis.
(Li et al., 2009)	Epithelial ovarian carcinoma	43% (30/70) of the patients with primary epithelial ovarian carcinomas, and in all of the metastatic cancer cells of ascites from 8 patients.
(Li et al., 2010)	Endometrial and cervical cancer	SPA17 was found in 66% (33/50) of the patients with endometrial cancer and 61% (19/31) of those with cervical cancer.
(Gjerstorff et al., 2013)	Non-small cell lung cancer	SPA17 immunocytochemisty in 4.7% of patient biopsies.
(Singh et al., 2015)	Pancreatic periampullary carcinoma	SPA17 expressed in cancer cells and detected in serum.
(Dasgeb et al., 2019)	Merkel cell carcinoma (MCC)	Twelve of 14 (86%) MCC cases showed crisp nuclear staining for SPA17, with 2.06% of cells staining positive.

The structure and expression patterns of SPA17 indicate it likely functions in intracellular regulation, cell signaling and cell-cell/cell-matrix adhesion. It may also function during cellular differentiation. The protein is autoantigenic meaning that it evokes a strong immune response when injected even though it is a component of "self." The central heparin binding domain is the source of antigenicity and is responsible for evoking this immune response (Wen et al., 2001). The discovery of autoantigenic properties spurred research into the possibility of using the protein in a vaccine contraceptive. SPA17 contraceptive vaccines have been developed for rodents and *Macaca radiata* (O'Rand et al., 2004).

Interest in SPA17 by oncology researchers and clinical application to oncology has grown in the last 30 years. SPA17 is a Cancer Testis antigen and is detectable in serum and in malignant cells (Lim et al., 2001). Malignancies of multiple tissue types express SPA17 mRNA and the protein is often detected by immunohistochemistry (Table 3.6). It is also detected in the serum of cancer patients who may possess antibodies to the protein (Singh et al., 2015). The expression of SPA17 correlates with poor prognosis, de-differentiation, and metastases. The immunogenicity of the protein has spurred research into its use in cancer vaccines and immunotherapies (Chiriva-Internati et al., 2002, 2014; Xiang et al., 2015).

Chapter 4. STRUCTURE AND BIOCHEMISTRY OF SPA17

4.1 INTRODUCTION

Phosphorylation by cAMP-dependent kinase is a ubiquitous and well researched mechanism of reversible enzyme activation. The PKA holoenzyme is composed of two regulatory and two catalytic subunits and is compartmentalized through the association of the DD domain on the N-terminal region of the R-subunit to an amphipathic helix on an AKAP protein. However, the DD domain is modular and annotated as present on thirteen other proteins in the human genome. (see Chapter 2, Table 2.4). These proteins all have unique C-terminal domains with functions not directly associated with cAMP-dependent kinase activity.

The R2D2 proteins share a conserved core of hydrophobic residues with the R-subunit for dimerization and AKAP binding, and R2D2 proteins are reported to interact with a diverse repertoire of AKAP helices with differing specificity. In an illuminating review, Burton and McKnight (2007) describe the effects of knockout of different PKA isoforms, (Ca, Cb, RIα, and RIIα). While AKAPs appear to have a functional role in fertility, this is not dependent upon RIIα, and excess PKA activity is associated with subfertility. The AKAP peptide derived from human thyroid, Ht31, disrupts AKAP complexes *in vitro* and its application has a profound negative effect on flagellar motility, while H-89, a kinase inhibitor, has a limited impact. All these results demonstrate that AKAPs have PKA-independent functions enriched within motile cilia and flagella.

Further, SPA17 and ROPN1L likely have functions outside of the radial spoke and cilia that have not been fully explored. SPA17 and ROPN1L are expressed in a wide variety of tissues (see Chapter 3). Both proteins appear to interact with AKAP18 in large scale screening studies, but this interaction was not validated. AKAP18 is not known to localize to cilia, and interestingly is involved in calcium regulated pathways (Fraser et al., 2008). While my study is the first to examine a potential R2D2:AKAP interaction outside of cilia, the complex also serves as a prototype for how AKAP:ROPN1L:SPA17 interactions occur generally and could be organized in the radial spoke. Despite the known interaction between R2D2 and AKAP proteins and homology with the R-subunit (Figure 4.1), the structure of the R2D2 N-terminal domain and its specificity determinants have not been well evaluated.

Multiple sequence alignment is a key method to investigate protein similarity, model structures, and analyze phylogenetics. Multiple sequence alignments are constructed by organizing residues with putative common origin and structural and functional equivalence in the same column position. One can compare both orthologs and paralogs. This method was key to this study and drove many of the hypotheses. First, it identified proteins with homology to the R-subunit docking and dimerization domain. In this chapter, multiple sequence alignment analysis of orthologs indicated that SPA17 and ROPN1L likely have an extended domain with unique biochemical functions (Figure 4.1). This study reports the structure of SPA17 to 1.72 Å with novel N and C-terminal strands that likely mediate the observed decreased affinity for AKAPs and heterodimerization with ROPN1L.

4.2 SPA17 AND ROPPORIN PROTEINS HAVE AN EXTENDED RIIALPHA DOMAIN

Figure 4.1. Alignment of RIIα, SPA17, and ROPN1L orthologs.

Black arrows beneath RIIα indicate conserved -5 and -3 hydrophobic residues necessary for high affinity AKAP binding. (Gold et al., 2006) Red arrows beneath SPA17 and ROPN1L indicate conserved hydrophobic positions. In the SPA17 apo structure, these residues occlude the AKAP binding site. *Hs: Homo sapiens, Mm: Mus musculus, Dr: Danio rerio, Ta: Trichoplax adhaerens*.

The docking and dimerization domain of RIIα consists of a conserved core sequence of forty-one amino acids from residue four to forty-five in the human ortholog. There are five amino acids on the extreme N-terminus which lie on a strand that is disordered in the apo form, and asymmetrically ordered in the AKAP-bound form due to two highly conserved hydrophobic amino acids in the -5 and -3 positions relative to the core helix which are necessary for high affinity AKAP binding (Gold et al., 2006). The loop immediately adjacent to the C-terminus of the DD domain is not conserved (Figure 4.1) and is not resolved in any structures of PKA. In contrast, SPA17 and ROPN1L contain extended conserved cores comprising seventy-five amino acids in

SPA17 and seventy-one amino acids in ROPN1L by sequence alignment. In the structure of SPA17 NTD, amino acids 7-69 are resolved (Figure 4.2).

Table 4.1. Data and Refinement Statistics

Property	**Value**	**Source**
Space group	P 32	Depositor
Cell constants a, b, c, α, β, γ	60.96Å 60.96Å 89.02Å 90.00° 90.00° 120.00°	Depositor
Resolution (Å)	34.03 – 1.72 45.41 – 1.72	Depositor EDS
% Data completeness (in resolution range)	98.5 (34.03-1.72) 98.5 (45.41-1.72)	Depositor EDS
Wavelength	0.99996 Å	HKL2000
R_{meas}	0.098	Depositor
Rpim	0.035	Depositor
Rmerge (1.72-1.75 Å)	0.91 (0.269)	Depositor
Data redundancy (1.72-1.75 Å)	7.6 (5.6)	Depositor
$CC_{1/2}$	0.993	Depositor
$< I/\sigma(I) >$	1.02 (at 1.72 Å)	Xtriage
Refinement program	phenix.refine 1.18.2_3874, PHENIX 1.18.2_3874	Depositor
R, R_{free}	0.154 , 0.165 0.154 , 0.166	Depositor DCC
RMS (angles), RMS (bonds)	0.92, 0.008	Depositor
Ramachandran favored	100%	wwPDB-VP
R_{free} test set	1995 reflections (5.11%)	wwPDB-VP
Wilson B-factor ($Å^2$)	11.8	Xtriage
Anisotropy	0.632	Xtriage
Bulk solvent $k_{sol}(e/Å^3)$, $B_{sol}(Å^2)$	0.42, 34.0	EDS
L-test for twinning	$< \|L\| > = 0.51$, $< L^2 > =$ 0.34	Xtriage
Estimated twinning fraction	0.479 for -h,-k,l 0.480 for h,-h-k,-l 0.479 for -k,-h,-l	Xtriage
F_o,F_c correlation	0.96	EDS
Total number of atoms	4799	wwPDB-VP
Average B, all atoms ($Å^2$)	17.0	wwPDB-VP

4.3 Overall Structure of SPA17 N-Terminal Domain

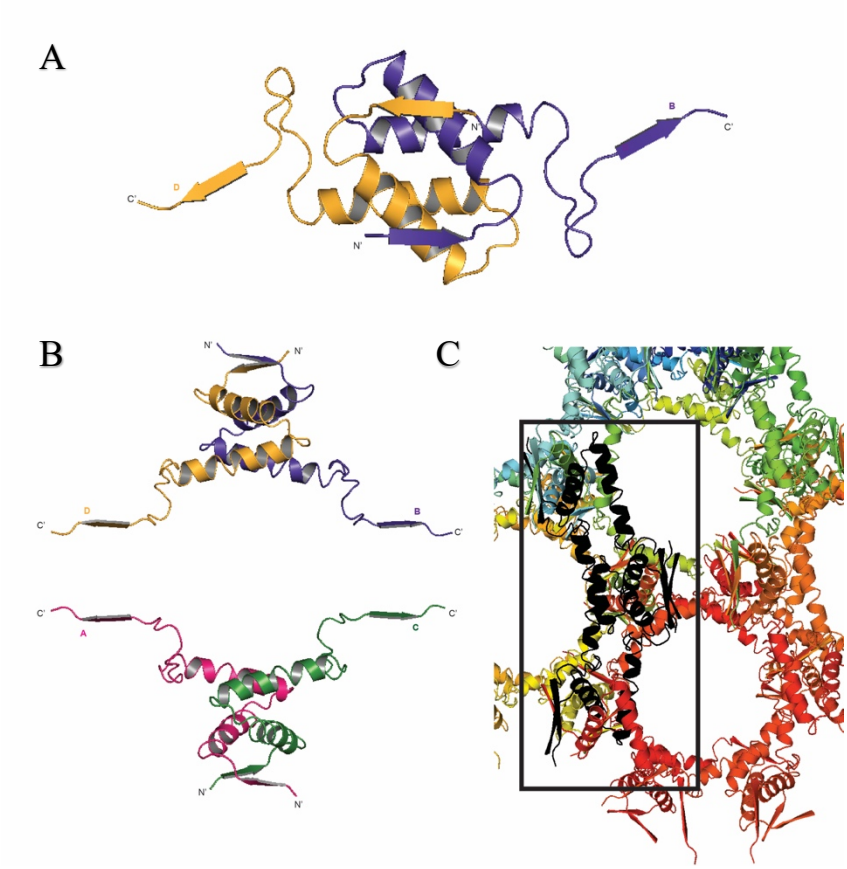

Figure 4.2. SPA17 NTD asymmetric unit.

A. Asymmetric unit dimer. B. Asymmetric unit. C. Tetramer formation within the crystal lattice. A single tetrameric unit is marked in black.

Amino acids 1-75 of SPA17 from *D. rerio* were expressed in *Escherichia coli* and purified with a three-step protocol beginning with affinity chromatography, followed by anion exchange chromatography, and ending with gel filtration chromatography. The crystallized zebrafish ortholog is 72% identical to the human ortholog (Figure 4.1). The crystals diffracted to 1.72 Å and structure was determined by molecular replacement using the DD domain of PKA RIIα as a search model (PDB ID: 2IZX), and subsequently refined to an R_{work} of 0.154 and R_{free} of 0.165 (Table 4.1). The point group can be defined as P 32 or P 622, with four molecules or one molecule in the

asymmetric unit respectively. P 32 was chosen as the point group for the final refinement because dimers and tetramers are the functional biological units for SPA17, (Figure 4.4) and thus each monomer has a slightly different conformation in the larger asymmetric unit, resulting in lower *R* values for the P32 group (R_{free} of 0.165 for P 32 vs R_{free} of 0.172 for P 622). Each monomer in the P 32 structure can be aligned to the monomers of the P 622 asymmetric unit with an RMSD of 0.03 Å.

The asymmetric unit is defined as a dimer with a single axis of translational symmetry (Figure 4.2). The minimal hexagon is comprised entirely of dimers, and tetramers are assembled as the strands pack against the core helix and the loops make contacts with each other and the core helix (Figure 4.2 and Figure 4.3). These contacts correspond primarily to conserved hydrophobic positions on the N-terminal and C-terminal regions adjacent to the core helices (Figure 4.1 and Figure 4.3). It is interesting to note that in addition to core hydrophobic positions, these loop regions contain conserved secondary structure breaking amino acids, glycine and proline, and are interspersed with charged amino acids: arginine, lysine, glutamate and aspartate (Figure 4.1). This indicates that conformational entropy likely underlies protein function. The secondary structure breaking and charged amino acids increase the flexibility of these regions and likelihood they will come into contact with solvent. However, when contact with solvent occurs, the highly conserved hydrophobic positions induce ordering of water imparting a high entropic cost to increased flexibility. As such, inter-subunit and protein-protein interactions involving these regions are thermodynamically favorable because ordered cages of solvent have a higher entropic cost than tertiary and quaternary arrangements. Thus, these regions are likely dynamic protein-protein interaction (PPI) sites that underlie the observed biochemical activity of the SPA17 NTD. It is worth noting that RIIβ lacks a proline at position 8 (Fig 2.8) (Hausken et al., 1994) and has a six-fold lower affinity for AKAPs as compared to RIIα (13 nM for RIIβ vs 2.2 nM for RIIα) (Burns-Hamuro et al., 2003), illustrating the importance of conformational entropy in RII domain PPIs.

Size exclusion chromatography with multi-angle light scattering analysis (SEC-MALS) was conducted to investigate the putative higher order oligomeric structures observed in the crystal structure. This dataset shows that full length SPA17 has absolute molecular masses of 72 kDa and 36 kDa, and SPA17 NTD has absolute molecular masses of 35 kDa and 17 kDa. Thus, unlike RIIα higher order homo-oligomeric complexes may be functionally relevant for SPA17, as the protein is observed in both tetrameric and dimeric species in the crystal and in solution.

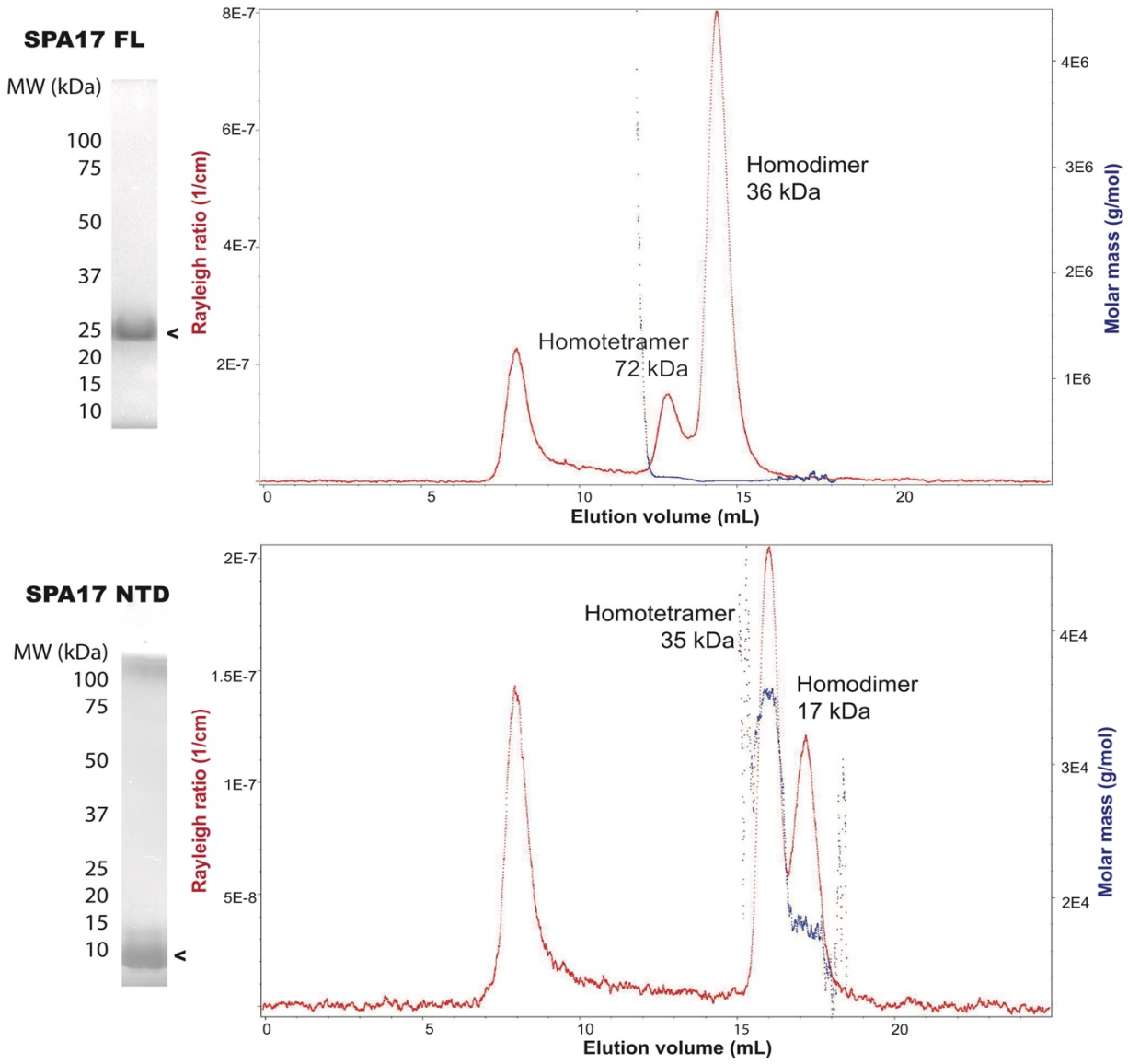

Figure 4.3. SEC-MALS analysis of SPA17 and SPA17 NTD.

There are both tetramers and dimers.

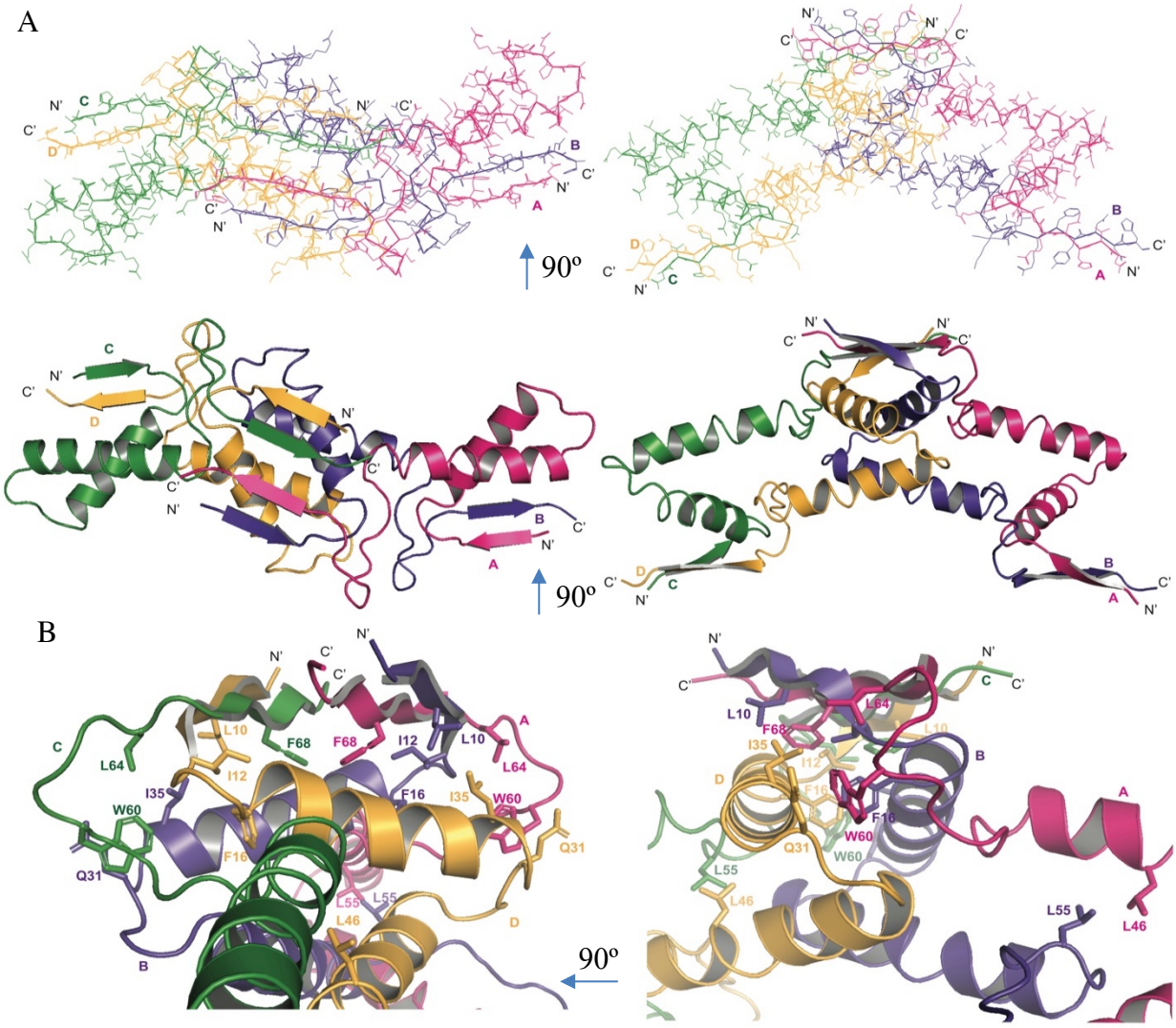

Figure 4.4. Overall structure of SPA17 NTD.

A. Top view and side view of SPA17 NTD in ribbon and cartoon representations. B. The tetramer is assembled by adjacent NT and CT strands assembling across a central dimer, mediated by extensive hydrophobic contacts between the strands and core helices.

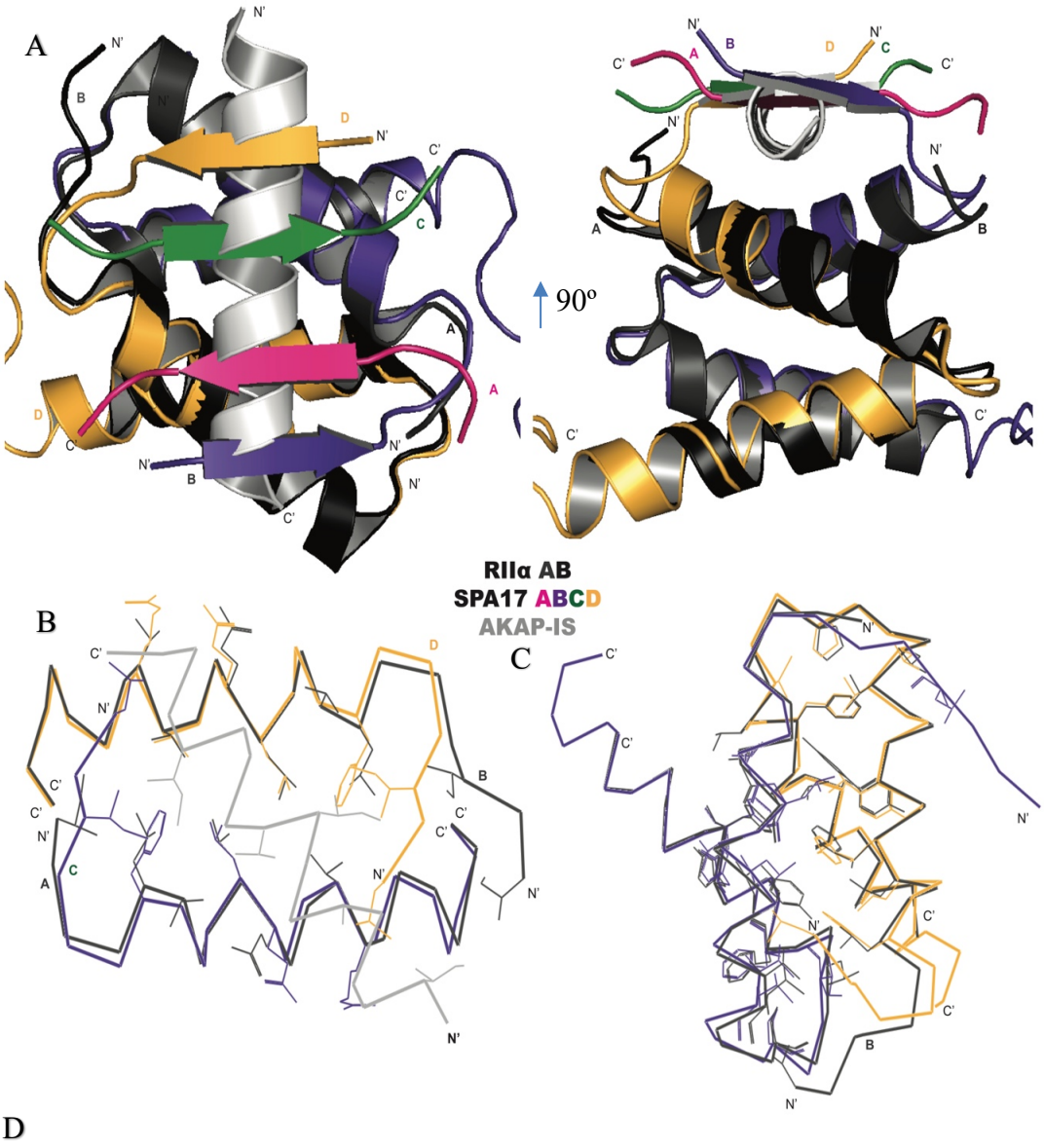


```
RIIα    2   SHIQIPAGLTELLQGYTVEVLRQQPPDLVDFAVEYFTRLREARRQES  48
            +H++IP G+  LL+G+T EVLR+QP D+  FA  YFT L +AR +
SPA17   8   THLRIPRGFGNLLEGLTREVLREQPEDIATFAAVYFTELLKAREESG  54
```

Figure 4.5. Structural alignment of RIIα bound to AKAP-IS and Apo SPA17. A. Alignment of RIIα DD domain bound to AKAP-IS and SPA17 NTD (RMSD = 0.528). NT and CT strands of SPA17 block the AKAP binding site. B. Hydrophobic positions for AKAP binding are conserved. C. Hydrophobic positions for dimer formation are conserved. D. Sequence alignment of murine RIIα and zebrafish SPA17. AKAP binding hydrophobic residues highlighted.

4.4 Comparison of APO SPA17 with AKAP-IS:RIIA Complex

The DD domain of RIIα bound to AKAP-IS superimposes over the apo structure of SPA17 NTD with an RMSD of 0.528 Å from residues 10 to 41 in RIIα (Figure 4.5). The N-terminal and C-terminal strands on the SPA17 NTD appear to block the AKAP binding site (Figure 4.5A). Strikingly however, the -5 and -3 and helical hydrophobic positions essential for AKAP binding are structurally and sequentially conserved (Figure 4.5B and D). Thus, it is likely any differences in AKAP are due to the presence of the N-terminal and C-terminal extensions present on SPA17. As expected by sequence, key hydrophobic residues necessary for dimerization are also strictly conserved in the structure (Figure 4.5C).

4.5 Homomeric SPA17 Binds AKAP18 with a Low Affinity

After building the structural model, it was not clear how SPA17 is able to interact with AKAPs, as there are strands that appear to block the AKAP binding site in the crystal structure(Figure 4.5). Others report that CABYR and SPA17 exhibit limited interactions with AKAPs (Newell et al., 2008). The Biological General Repository for Interaction Datasets (BioGRID) contains curated protein-protein interaction data from large scale screening analyses. AKAP18 is identified as an interactor with SPA17 in three studies reported in the BioGRID: two yeast two-hybrid screens (Luck et al., 2019; Rolland et al., 2014) and one affinity mass-spectrometry (MS) study (Huttlin et al., 2015). SPA17 is expressed in all tissues (Wen et al., 2001) so AKAP18 is likely a physiologically relevant interactor outside of cilia. Interestingly, RIIβ is a reported interactor by affinity-MS suggesting higher order complex formation as SPA17 does not bind to RII (Figure 4.6).

In order to characterize the interaction between SPA17 and AKAPs, pulldown experiments utilizing full length SPA17 and SPA17 NTD were conducted (Figure 4.6A). GST-AKAP18α was expressed in bacteria and purified with affinity chromatography. Subsequently SPA17 or SPA17 NTD were applied and the column thoroughly washed. Binding is observed between AKAP18α and SPA17 full length, human SPA17 NTD, and zebrafish SPA17 NTD, but not between GST-RIIα and human SPA17 NTD. As further validation of interaction, GST-AKAP18α and SPA17 comigrate on the gel filtration column (Figure 4.6B and C). However, SPA17 and AKAP18 appear weakly associated in these assays and the stoichiometry is not clear.

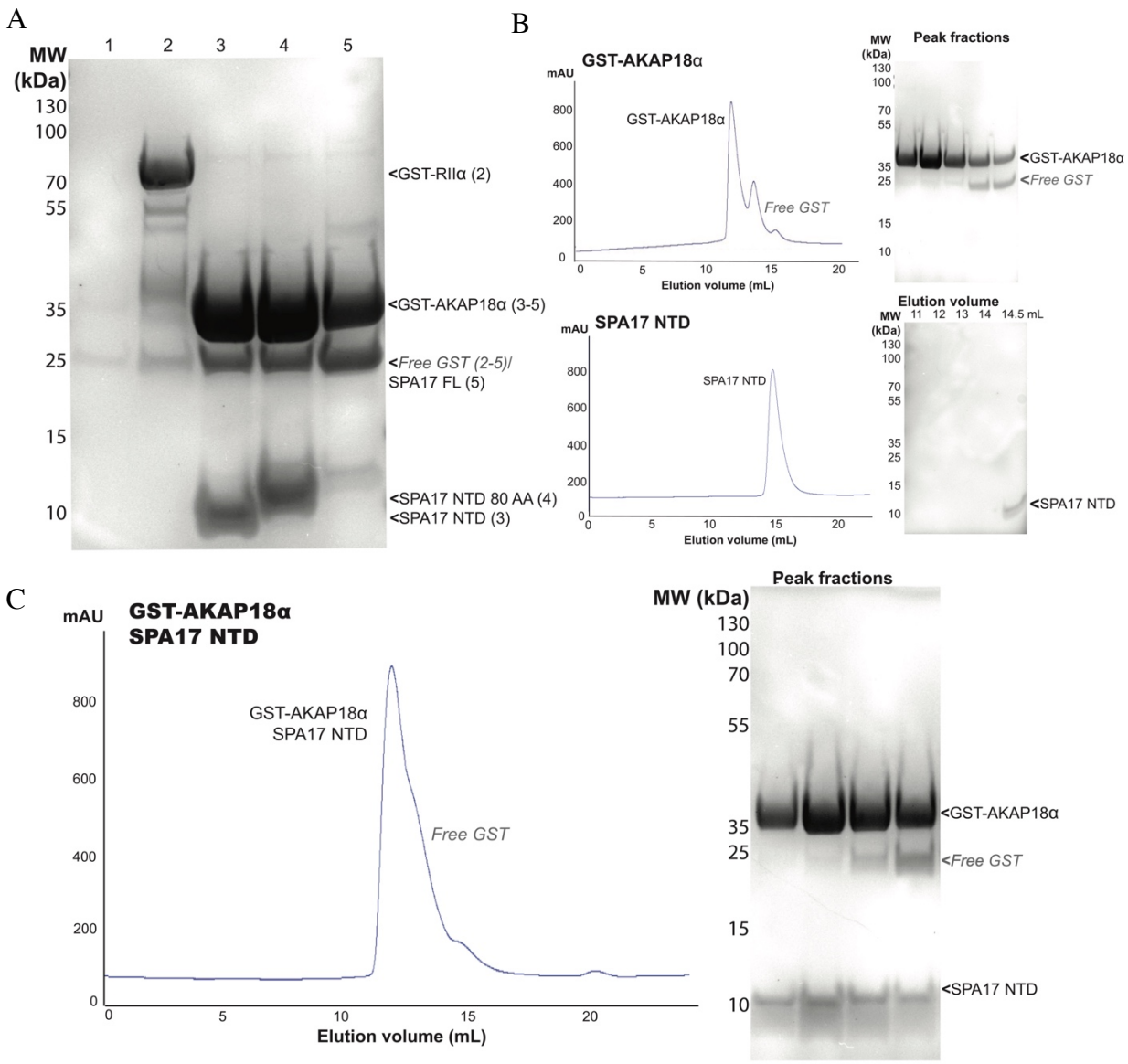

Figure 4.6. Interaction between AKAP18α and SPA17.

A. Pulldown showing interaction between GST-AKAP18α bound to the column (lanes 3-5) and SPA17 (1-75) (lane 3), SPA17 (1-80) (lane 4), and SPA17 full length (lane 5). SPA17 (1-75) did not bind either controls, beads only (lane 1) or GST-RIIα (lane 2). B. GST-AKAP18α and SPA17 (1-75) do not elute in the same fractions when run individually over a gel filtration column. C. GST-AKAP18α and SPA17 (1-75) form a complex and co-elute during gel filtration chromatography.

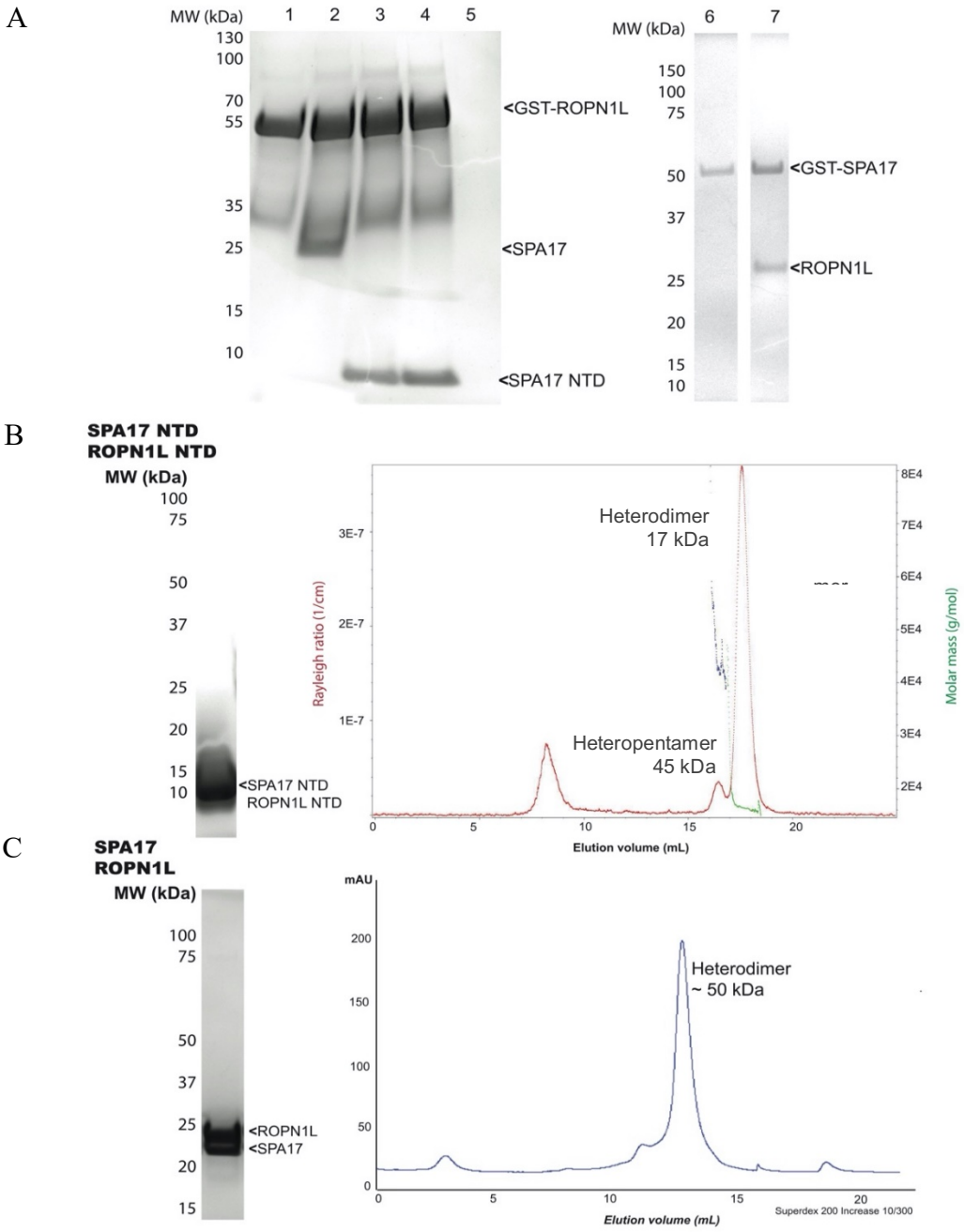

Figure 4.7. Interaction between SPA17 and ROPN1L.

A. Tandem GST pulldown experiments. The left panel shows GST-ROPN1L bound to the column (lane 1). SPA17 full length (lane 2), human SPA17 NTD (lane 3) and zebrafish SPA17 NTD (lane 4) bind GST-ROPN1L but not beads only (lane 5). The reciprocal is also true with ROPN1L binding GST-SPA17 (lane 7). B. Both NTD and full length SPA17 and ROPN1L comigrate with a similar pattern during SEC-MALS and SEC.

4.6 SPA17 HETERODIMERIZES WITH ROPN1L

The BioGRID further lists that SPA17 binds ROPN1L by yeast-two-hybrid (Luck et al., 2020) and affinity MS (Huttlin et al., 2015, 2017) analyses. In the initial report designating a Rho-interacting protein in the testis as Ropporin-1 (oppo is Japanese for tail and the protein is named for the C-terminal Rho interaction), the authors mention that they have observed ROPN1 and SPA17 heterodimerize (Fujita et al., 2000, unpublished data). Interestingly, in Li et al. (2010) report CABYR forms oligomers and binds to AKAPs and ROPN1 through its RIIa domain as demonstrated by yeast-two-hybrid screening. In order to further investigate the interaction between ROPN1L and SPA17, tandem GST pulldowns were conducted. Full length SPA17 and SPA17 NTD bind GST-ROPN1L, and ROPN1L binds GST-SPA17 even after thorough washing (Figure 4.7A). Further, SPA17 and ROPN1L NTD comigrate during SEC-MALs, and full length SPA17 and ROPN1L comigrate during SEC (SEC-MALS was not conducted), and both forms appear to have a pentameric peak (45 kDa by SEC-MALS of NTDs) not present with ROPN1L NTD alone (Figure 4.8).

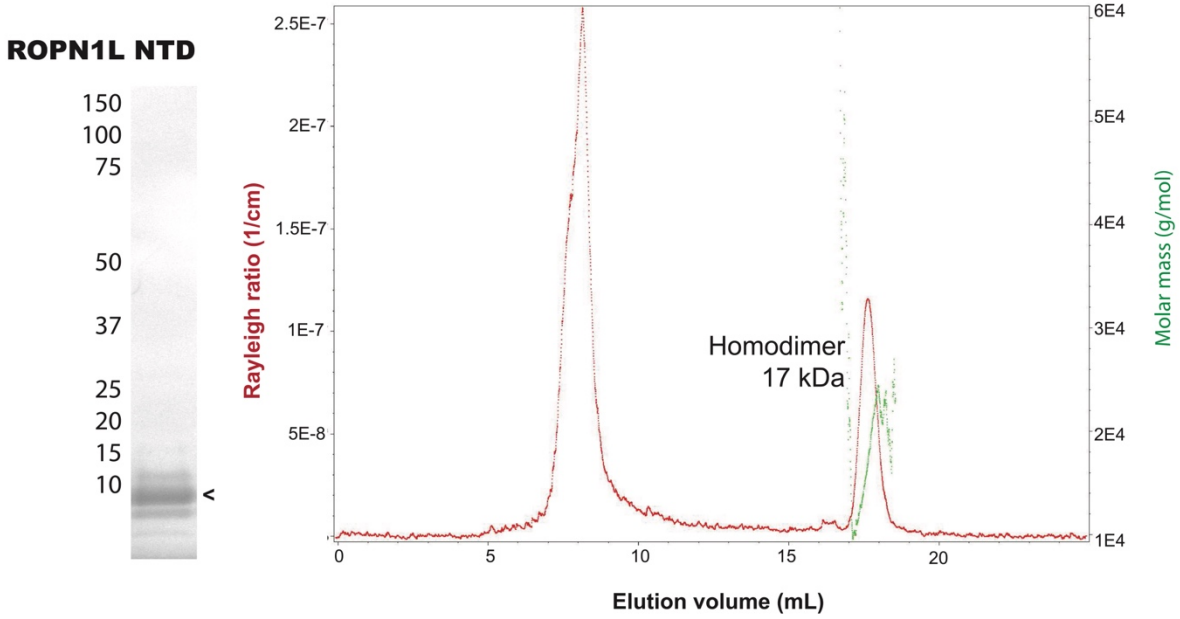

Figure 4.8. SEC-MALS of ROPN1L NTD. ROPN1L NTD is a 17 kDa homodimer.

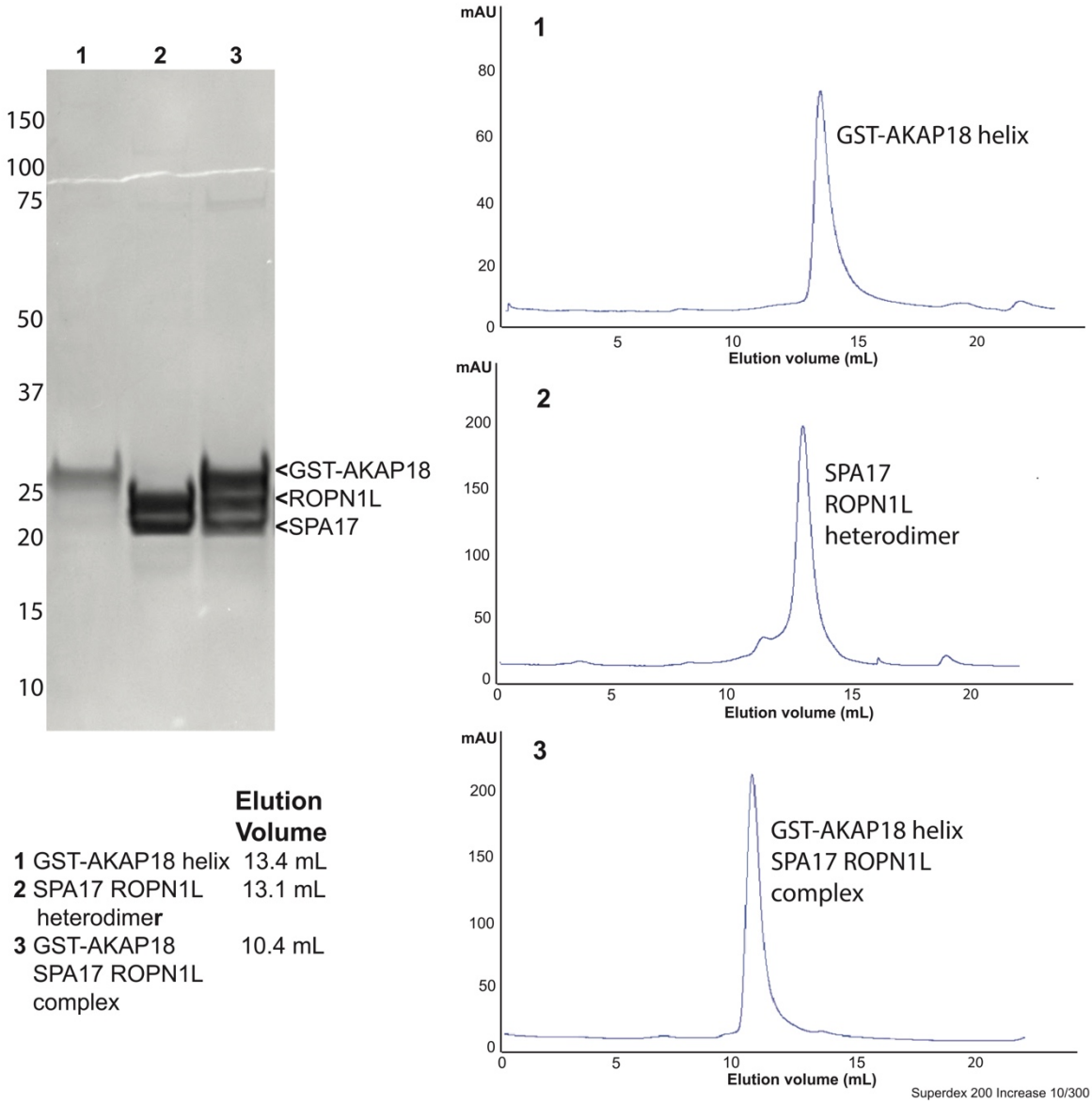

	Elution Volume
1 GST-AKAP18 helix	13.4 mL
2 SPA17 ROPN1L heterodimer	13.1 mL
3 GST-AKAP18 SPA17 ROPN1L complex	10.4 mL

Figure 4.9. Size exclusion chromatography analysis of SPA17: ROPN1L:AKAP18 helix macromolecular complex.

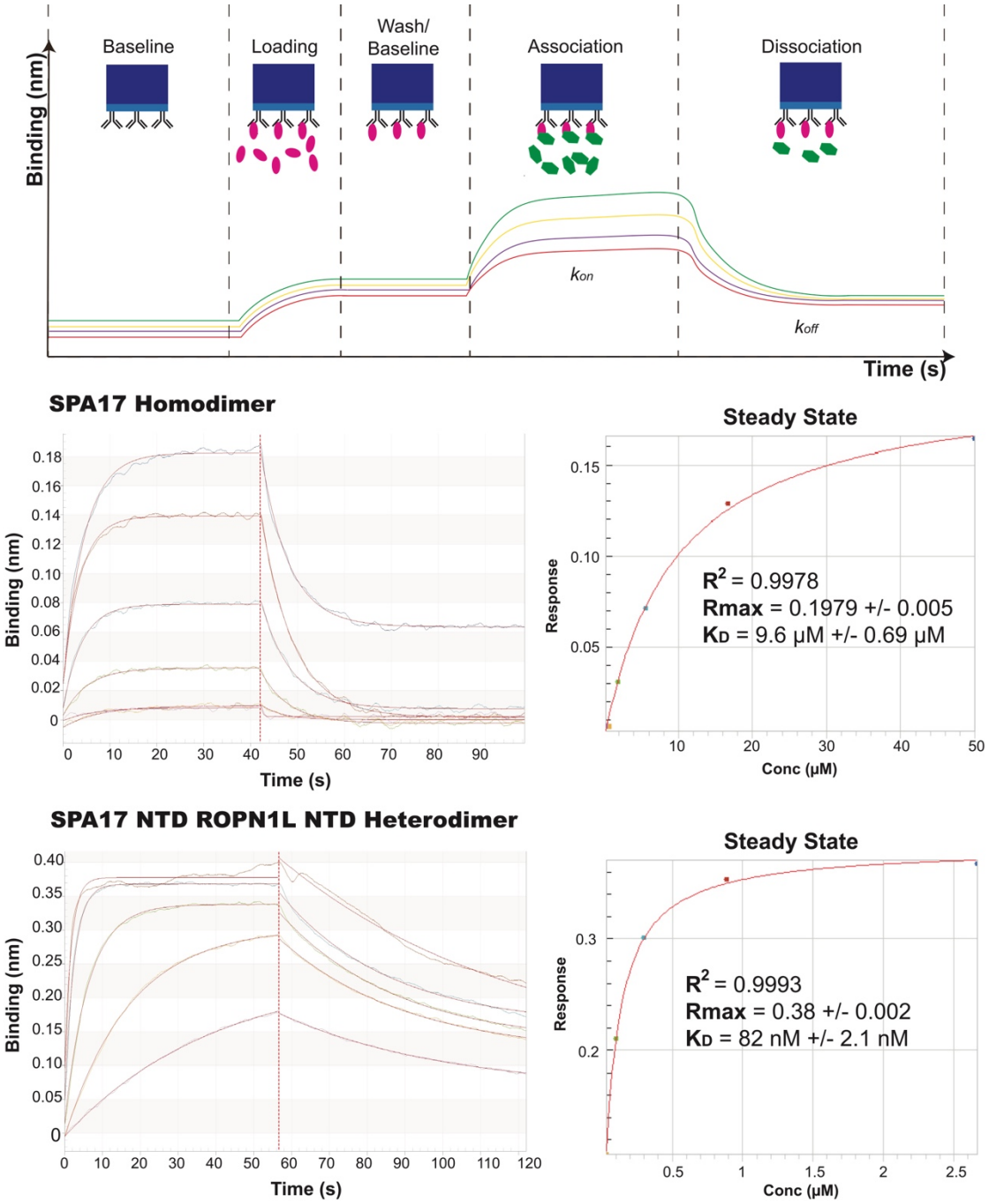

Figure 4.10. Octet analysis of the affinity of the SPA17 homodimer or SPA17 NTD: ROPN1L NTD heterodimer for the AKAP18 helix.

SPA17 alone has a 9.6 micromolar affinity while the SPA17:ROPN1L heterodimer has a physiologically relevant 82 nanomolar affinity.

4.7 SPA17:ROPN1L HETERODIMER IS THE FUNCTIONAL AKAP BINDING MODULE

After it was determined that the N-terminal domains of SPA17 and ROPN1L interact, the functional significance of heterodimerization was investigated. First, SEC analysis was conducted utilizing full length SPA17 and ROPN1L and the long form of the AKAP18 helix identical in length to that crystallized by Götz et al. (2016). Surprisingly, all three proteins comigrate in what appears to be a 1:1 stoichiometry at a very high molecular weight estimated at about 330 kDa by calibration of the Superdex 200 column (Figure 4.9). Further studies are needed to investigate if this is related to the SEC-MALS observed apo SPA17 NTD: ROPN1L NTD heteropentamer (Fig 4.7B). It is possible the strands form an extended interface accommodating two helices like S100B (Newlon et al., 2001).

Finally, affinity and kinetic characterization was performed using the Octet system. Briefly, a probe containing anti-GST antibodies is loaded with GST-AKAP18 helix, washed, and then incubated with a range of concentrations of R2D2 protein complexes, and washed again with buffer. The amount of protein bound to the probe is equivalent to an observed change in refractive index on the detection surface (response/binding (nm)) and thus the affinity can be calculated over the association and dissociation steps. The steady state affinity is calculated with the following equation: Response = (Rmax*concentration)/(K_D+concentration). As expected by the structure, SPA17 bound to the AKAP18 helix with an affinity of 9.6 +/- 0.69 micromolar, which may not result in physiologically relevant complexes. Surprisingly, despite the fact that both ROPN1L and SPA17 have extended DD domains, they bind to the AKAP18 helix with an affinity of 82 +/- 2.1 nanomolar (Figure 4.10). RII has a reported affinities for AKAP18 between 0.4 and 31 nanomolar (Götz et al., 2016; Hundsrucker et al., 2006).

4.8 SUMMARY AND CONCLUSIONS

Thus far, we have seen that SPA17 and ROPN1L have a high homology to the docking and dimerization domain of RII. However, their N-terminal and C-terminal regions appear to be extended relative to RII by sequence alignment. In the crystal structure of SPA17, these strands mediate the higher order structure of SPA17 and block the AKAP binding site. Functionally, SPA17 forms a heterodimer with ROPN1L and has a reduced affinity for AKAPs in the

homodimeric state. These characteristics are likely mediated by the strands on the N-terminal and C-terminal parts of the SPA17 DD domain.

4.9 METHODS

4.9.1 *Molecular Biology and Protein Purification*

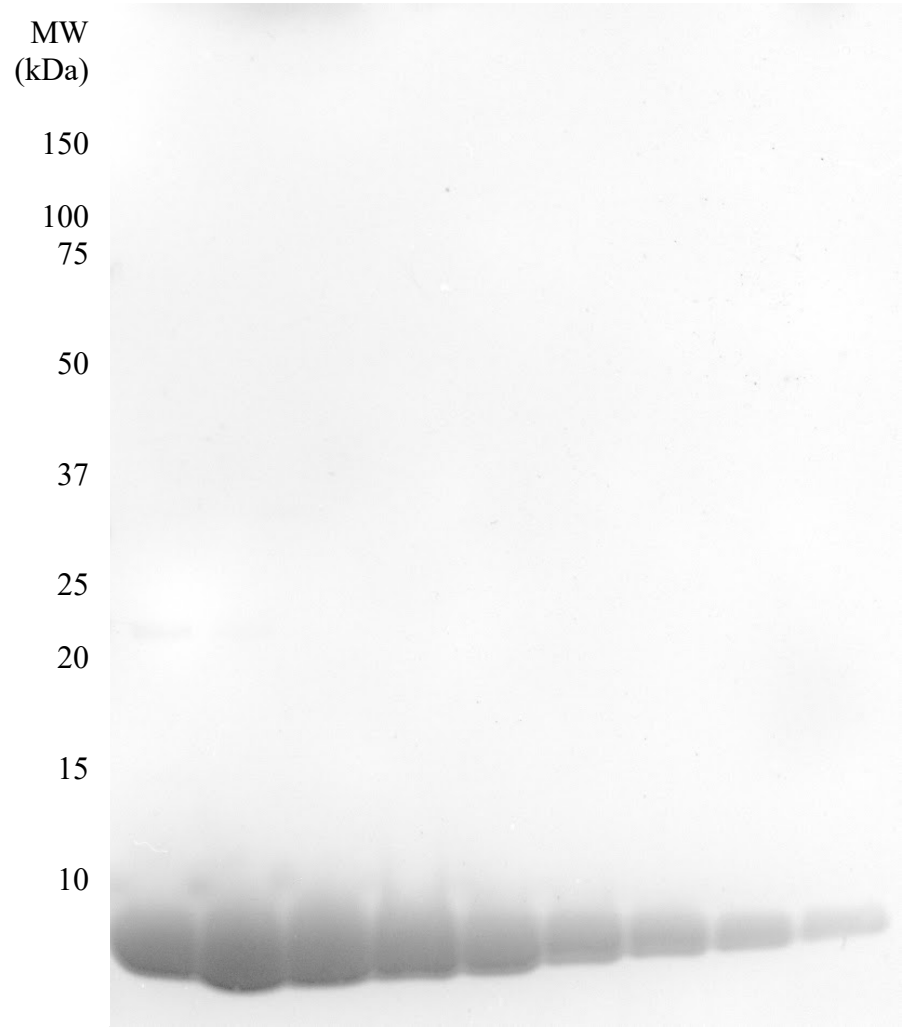

Figure 4.11 Gel of SPA17 NTD *Danio* eluted from the Superdex 200 Gel Filtration column.
This sample was used for crystallization.

Human ROPN1L, ROPN1L (1-75), SPA17, SPA17 NTD (1-75), SPA17 NTD (1-80), AKAP18α (48-90), and zebrafish SPA17 (1-75) were cloned into pGEX-6P-1 using the BamHI and XhoI restriction sites. These plasmids were then transformed into BL21 cells from Invitrogen for protein expression. Induction was performed at 16 degrees overnight and cells were lysed in a buffer containing 50 mM Tris pH 8, 200 mM NaCl and 5 mM DTT. Lysates were clarified via centrifugation at 40,000g. The clarified lysate was first purified using a glutathione affinity column (GE Healthcare) pre-equilibrated in the lysis buffer. Protein was eluted from the column by overnight on-column cleavage of the GST-tag by 3C-HRV protease produced in house at 4°C. Eluted material was further purified using the AKTA system with a 5 mL HiTrap Q-HP column (GE Healthcare), followed by a Superdex 200 gel filtration column (GE Healthcare) in a final buffer containing 10 mM Tris pH 8, 200 mM NaCl, 5 mM DTT. Proteins were concentrated to 15-20 mg/mL, flash frozen in liquid nitrogen and stored in -80 ºC.

4.9.2 *Crystallization*

SPA17 NTD (1-75) from *Danio rerio* was mixed in a 1:1 ratio using 150 nL of each component using the Mosquito onto hanging drop seals. They were then placed at 4 ºC. The crystals used for analysis grew in 0.1 M HEPES pH 7.5 and 0.5 M magnesium formate dihydrate from the Index Screen by Hampton Research. Crystals appeared after 2-3 days and reached their final size in 1-2 weeks. Crystals were directly transferred to a cryobuffer containing 50% glycerol and 50% mother liquor and frozen in liquid nitrogen for synchrotron data collection.

iii. X-ray Data Collection and Structure Determination

X-ray diffraction data was collected at the Advanced Light Source at Berkeley. Diffraction data were indexed, integrated, and scaled with the HKL2000 package (Otwinowski and Minor, 1997). Resolution cutoffs were determined using completeness (> 80%) and $I/\sigma > 1$ as primary criteria.

Initial phases were determined using PKA RIIα (PDB ID: 2IZX) as a search model. Density modification was subsequently performed using cycles of autobuild and phase and build in PHENIX (Adams et al., 2010). Some building was done manually in Coot (Emsley and Cowtan, 2004). Refinement was also conducted in PHENIX and the final model had an R_{work}/R_{free} of 0.154/0.165. All structural figures used for data analysis were visualized in Pymol, and structural analysis and modeling was based on superposition.

4.9.3 *Protein Pulldown*

GST-AKAP18α and GST-RIIα were transformed into BL21 cells and purified using GST purification and anion exchange chromatography as just described. About 1 microgram of purified GST proteins, GST-AKAP18α, GST-SPA17, GST-ROPN1L and GST-RIIα were loaded onto a GST purification column (GE Healthcare) in a bed volume of 200 microliters. Solutions containing 1 microgram of SPA17 NTD, SPA17 or ROPN1L were then applied to the column and it was washed with three times with ten column volumes of lysis buffer (50 mM Tris pH 8, 200mM NaCl, 5mM DTT). Samples were eluted with 10 mM glutathione in lysis buffer, mixed with SDS page loading buffer, and visualized by Coomassie staining.

4.9.4 *Gel Filtration Chromatography and MALS analysis*

Gel Filtration chromatography was performed using an AKTA system with a Superdex 200 Increase 10/300 Gel Filtration column in 20 mM Tris 8, 200 mM NaCl, and 5mM DTT at a flow rate of 0.5 mL/min. MALS analysis was conducted using a Wyatt system attached to a Superdex 200 Increase 10/300 gel filtration column in the same buffer with the same flow rate.

4.9.5 *Octet BioLayer Interferometry Measurement*

Binding affinity was measured using purified GST-AKAP18α on the Octet Red 96 (ForteBio, Pall Life Sciences). The reaction was carried out in black 96 well plates. The reaction volume was 200 μL in each well and the reaction was carried out at room temperature. The optical probes contained anti-GST to capture GST-AKAP18α which was loaded at a concentration of 200 nM. The binding buffer contained 50 mM Tris-HCl, 200 mM NaCl, 5 mM DTT and 0.1% BSA, pH 8.0. Concentrations of 50, 16.7, 5.56, 1.85, 0.617, and 0.2058 micromolar SPA17 homodimer, and 9, 2.67, 0.889, 0.2963, 0.0988, and 0.329 micromolar SPA17 NTD ROPN1L NTD heterodimer were loaded onto the probes. The analyte did not bind to the unloaded probes or a probe containing GST-His alone at the same 200 nanomolar concentration. Binding kinetics for all concentrations were measured at the same time using default instrument settings. Data analysis was conducted with Octet data analysis software. The association and dissociation curves were locally fit over the entire step time with a 1:1 ligand model. Steady state analysis was used to determines the

affinity constant K_D from the calculated equilibrium response with the following equation: Response = (Rmax*concentration)/(K_D+concentration).

4.9.6 *Protein Quantitation*

Protein Quantitation was conducted using a NanoDrop with A280 extinction coefficients calculated for each protein using Expasy ProtParam.

Chapter 5. BEYOND PKA

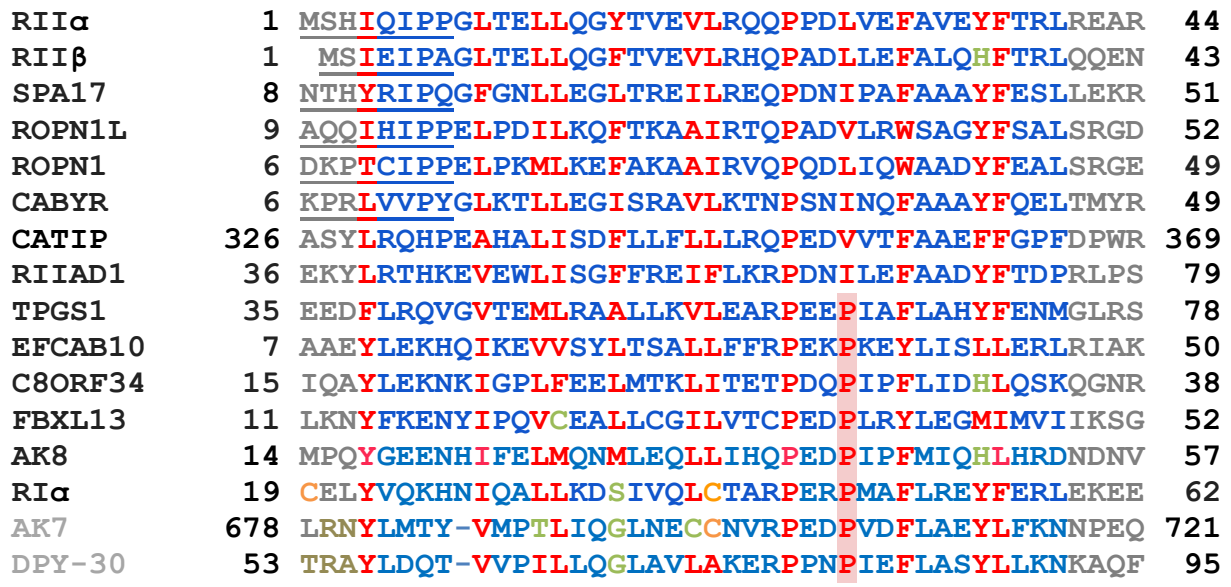

Figure 4.1. Alignment of RIIα Clan members.

RII-like defining strands are underlined. All core residues not strictly conserved are blue and conserved hydrophobic positions are red. Cysteines related to RI type DD domains are in orange, and divergent residues from conserved hydrophobic positions are green.

My work unambiguously demonstrates that the DD domain of PKA is modular. ROPN1L and SPA17 form a complex with a nanomolar affinity for AKAP helices. Prior work demonstrates that CABYR, SPA17, ROPN1L and ROPN1 are like RII and bind to AKAPs in the cilium and sperm flagellum. This study goes further and identifies nine other proteins with a domain analogous to the R-subunit DD domain. The four proteins initially identified have unambiguous homology to type II PKA R subunits. The DD domain of the RII-subunit can be distinguished from the RI-subunit in two major regions, the distal N-terminal region, and the loop between the two core helices. In type I, the N-terminal region forms a helix and is defined hydrophobic amino acids. It excludes flexible residues like glycine and proline, and in the core helices, the loop has a core sequence of PxxP. In contrast, type II DD domains have a proline rich N-terminal sequence which forms a strand and in the core helices the loop has a sequence Pxx[L,I,V] (Figure 4.1). Further analysis of the RIIa family DD domains by NCBI BLAST indicates that they form two groups. SPA17, ROPN1L, ROPN1, ROPN1B, CABYR, CATIP, and RIIAD1 group with RII and TPGS1,

FXCAK8, AK5, EFCAB10, C8ORF34, and FBXL13 group with RI (Fig 5.1 and 5.2). Testis-specific expressed 55 (TEX55) was also identified by BLAST search as an additional family member (See PhyML tree in supplemental information for relationship) containing an extreme C-terminal DD domain with homology to type-I PKA, but it has a shortened second helix as the protein ends at the eighth helical residue of the second core helix.

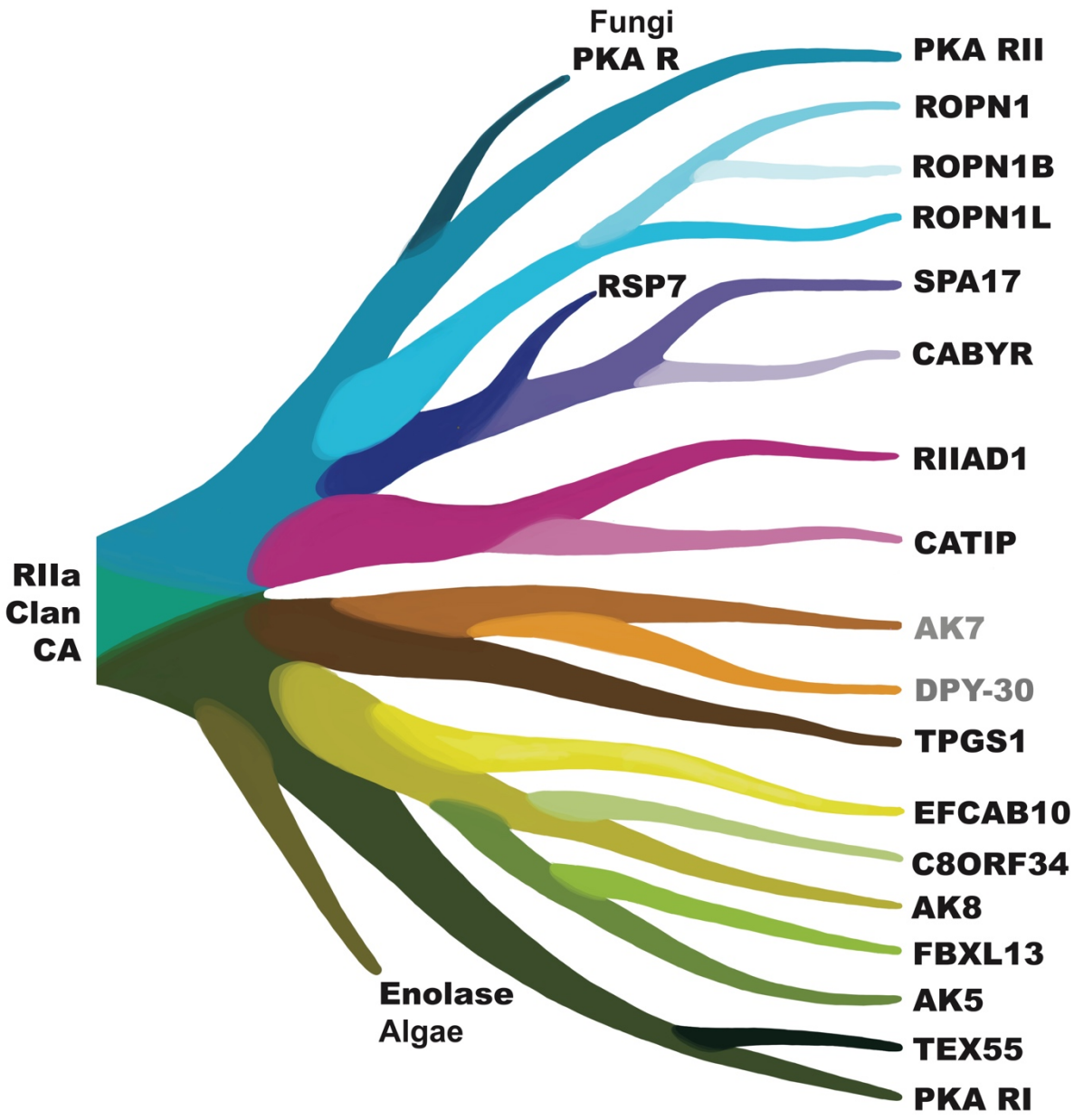

Figure 5.2. Phylogeny of RIIa Clan Proteins.

CA: Common Ancestor

BLAST combined with distance of tree analysis of species orthologs and phylogenetic dating can be used to construct an inferred family tree of the RIIa Clan and Superfamily. The distance trees used to infer the family member relationships are included in the supplementary information. Representative proteins from divergent clades were selected from a BLAST search against each protein using the human or *T. adhaerens* orthologs (highlighted proteins in the supplementary information). This analysis recapitulates the groupings defined by the alignment.

```
Blastocladiella R 6   IPSELPPILKDLSREVLRHQPADLVQFCHDYFAKL  40
                      IP ELP +LK+ ++  +R QP DL+Q+  DYF  L
Human ROPN1L     10   IPPELPKMLKEFAKAAIRAQPQDLIQWGADYFEAL  44
```

Figure 5.3. Comparison of human ROPN1L with a fungal R-subunit from *Blastocladiella emersonii*.

Finally, these results were validated with maximum likelihood analysis by PhyML (Anisimova et al., 2006, Dereeper at al., 2006, Guindon et al., 2008). The last eukaryotic common ancestor contained both RI and RII PKA, and a variety of R2D2 proteins: ROPN1L/RSP11, RSP7, TPGS1, EFCAB10, AK8, and RIIAD1. This is inferred from the fact that these proteins are contained in divergent kingdoms (Table 2.4). Fungal PKA groups with RII based on the N-terminal beta strand and absence of a second proline in the loop region (Figure 5.3). This is surprising given that the solved structure of the cAMP binding domains from fungal PKA indicate a higher homology to RI (Rinaldi et al., 2010).

The two primary ancient prototypes for the RIIa Clan appear to be DPY-30/ RI module and RSP11/ROPN1L/ RII module. Due to the presence of all these proteins in the last eukaryotic common ancestor, it is difficult to determine exactly how and the order in which DPY-30, RSP11/ROPN1L, RI PKA, and RII PKA evolved, but it is clear that the R-subunit unites both halves of the tree. A BLAST search of DPY-30 itself brings up DPY-30, Nucleoside Diphosphate Kinase 5 (NDK5) and AK7 as most similar to DPY-30 and indeed these are the only human proteins in the NCBI database annotated as part of the DPY-30 superfamily. The primary differences between RIIa superfamily and the DPY-30 superfamily are the replacement of a conserved hydrophobic amino acid in the middle of the helix with a glycine reside, and the length of the N-terminal helix; RI and RII helices are a single residue longer than DPY-30 (Figure 2.5

and Figure 4.1). The difference in length makes the cleft between the distal N-terminal helices slightly wider in RI as compared to DPY-30. TPGS1 is the only member of the RI half of the tree

```
Hs      35  EDFLRQVGVTEMLRAALLKVLEARPEEPIAFLAHYFENMGLRSP  79
Mm      35  EDFLRQLGVTEMLRAALLKVLEIRPEEPIAFLAHYFENMGLRSP  79
Dr      25  QEFVSRSGVSALLAGALLRLLDCRSGDPLGFLAEHFAHLSAEAE  67
Ta      12  NEYLDRAGVASNLQSALLLVLENKPDDPIYFLSQFFRNACTENA  56
```

Figure 5.4. Alignment of TPGS1 helix orthologs. *Hs: H. sapiens, Mm: M. musculus, Dr: D. rerio, Ta: T. adhaerens*

apart from RI itself that aligns with RII in BLAST analysis (Supplementary Information). It appears to have an N-terminal helix and loop like RI, but the sequence has some similarities to RII (Figure 4.1 and Figure 5.4), for example a glycine in the first residue of the first helix. Surprisingly it also aligns with DPY-30 and AK7, and AK7 shares one of the conserved cysteine residues characteristic of RI (Figure 4.1). It is also interesting that RIIAD1 has an N-terminal region similar to RI and a loop similar to RII (Figure 4.1). This indicates that the first DD domain was likely present on R and then specialized and diverged through evolution, as these ancient R2D2 proteins present in the LECA contain characteristics of both RI and RII.

Further research will be needed to determine how RIIa Superfamily complexes are organized and distinguished. It is unclear exactly how AKAP:SPA17:ROPN1L complexes are assembled and the stoichiometry of the components. Given the stoichiometry observed by gel filtration, is likely that further research will reveal novel binding modes for these components. It is possible that more RIIa Clan members heterodimerize. Yeast two hybrid screening indicates that AK8 binds to DPY-30 (Luck et al., 2020), and this is likely to be via heterodimerization given the small size of the DPY-30 protein and lack of additional functional domains. Given the similarity of all proteins within the RIIa Clan, proper assembly of complexes is probably not mediated by determinants within the helices themselves, but by localization/ additional domain interactions outside of the DD, and RNA co-translation. The existence of dual specific AKAPs further supports this hypothesis. Although RI was originally thought to be unanchored due to its presence in the cytosol, its similarity with proteins like AK8, which is clearly localized to cilia (Figure 2.9) solidify the importance of anchoring even among type I-like DD modules.

In conclusion, my work represents a breakthrough in understanding AKAPs and the evolution of scaffolded domains. It was originally believed that any protein that binds PKA in an

RII overlay is an AKAP that interacts with PKA *in vivo*. This study shows that even RII specific AKAPs like AKAP18 can bind to molecules other than PKA through a DD:amphipathic helix interface. The DD domain is modular, and mediates a large variety of PPIs, and careful research is necessary to demonstrate the physiologically relevant interactions of amphipathic helices with their target DD domain containing protein.

5.1 SUPPLEMENTARY INFORMATION PHYML AND BLAST TREES

```
oooooooooooooooooooooooooooooooooooooooooooooooooooooooooooooooooooo

                        ---  PhyML v3.0  ---

  A simple, fast, and accurate algorithm to estimate large
              phylogenies by maximum likelihood
             Stephane Guindon & Olivier Gascuel

                    http://atgc.lirmm.fr/phyml

          Copyright CNRS - Universite Montpellier II


oooooooooooooooooooooooooooooooooooooooooooooooooooooooooooooooooooo


. Sequence file : phymlao5RZ7iz/input.phy
. Data set : #1
. Tree search : NNIs. Initial tree : BIONJ
. Model of amino acids substitution : WAG
. Number of taxa : 195
. Log-likelihood : -16424.24652
. Discrete gamma model : Yes
  - Number of categories : 4
  - Gamma shape parameter : 2.704
. Proportion of invariant : 0.009
. Time used 0h53m35s
. -> 3215 seconds

oooooooooooooooooooooooooooooooooooooooooooooooooooooooooooooooooooo

--------2-------
```

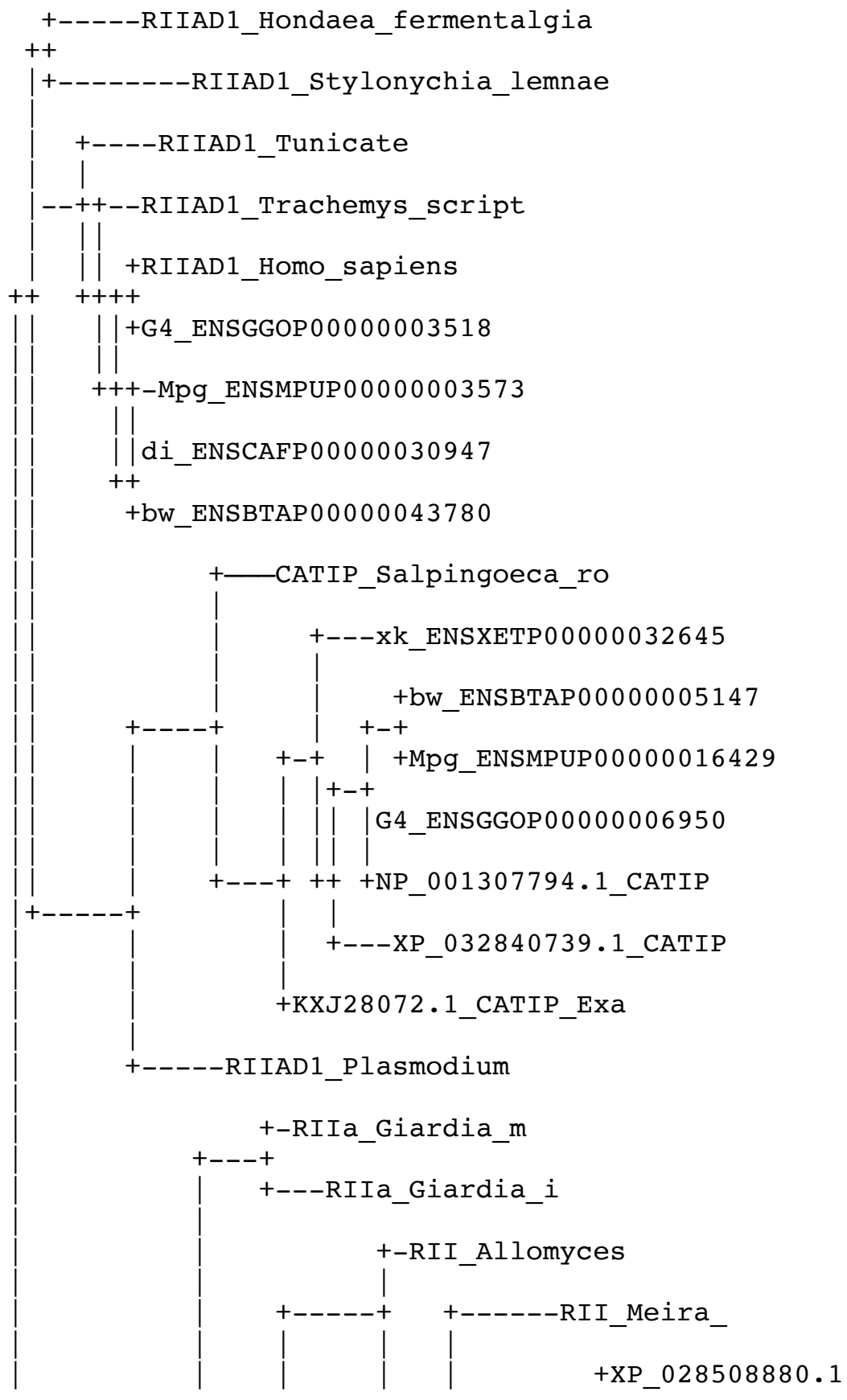
RIIAD1_Hondaea_fermentalgia
RIIAD1_Stylonychia_lemnae
RIIAD1_Tunicate
RIIAD1_Trachemys_script
RIIAD1_Homo_sapiens
G4_ENSGGOP00000003518
Mpg_ENSMPUP00000003573
di_ENSCAFP00000030947
bw_ENSBTAP00000043780
CATIP_Salpingoeca_ro
xk_ENSXETP00000032645
bw_ENSBTAP00000005147
Mpg_ENSMPUP00000016429
G4_ENSGGOP00000006950
NP_001307794.1_CATIP
XP_032840739.1_CATIP
KXJ28072.1_CATIP_Exa
RIIAD1_Plasmodium
RIIa_Giardia_m
RIIa_Giardia_i
RII_Allomyces
RII_Meira_
XP_028508880.1

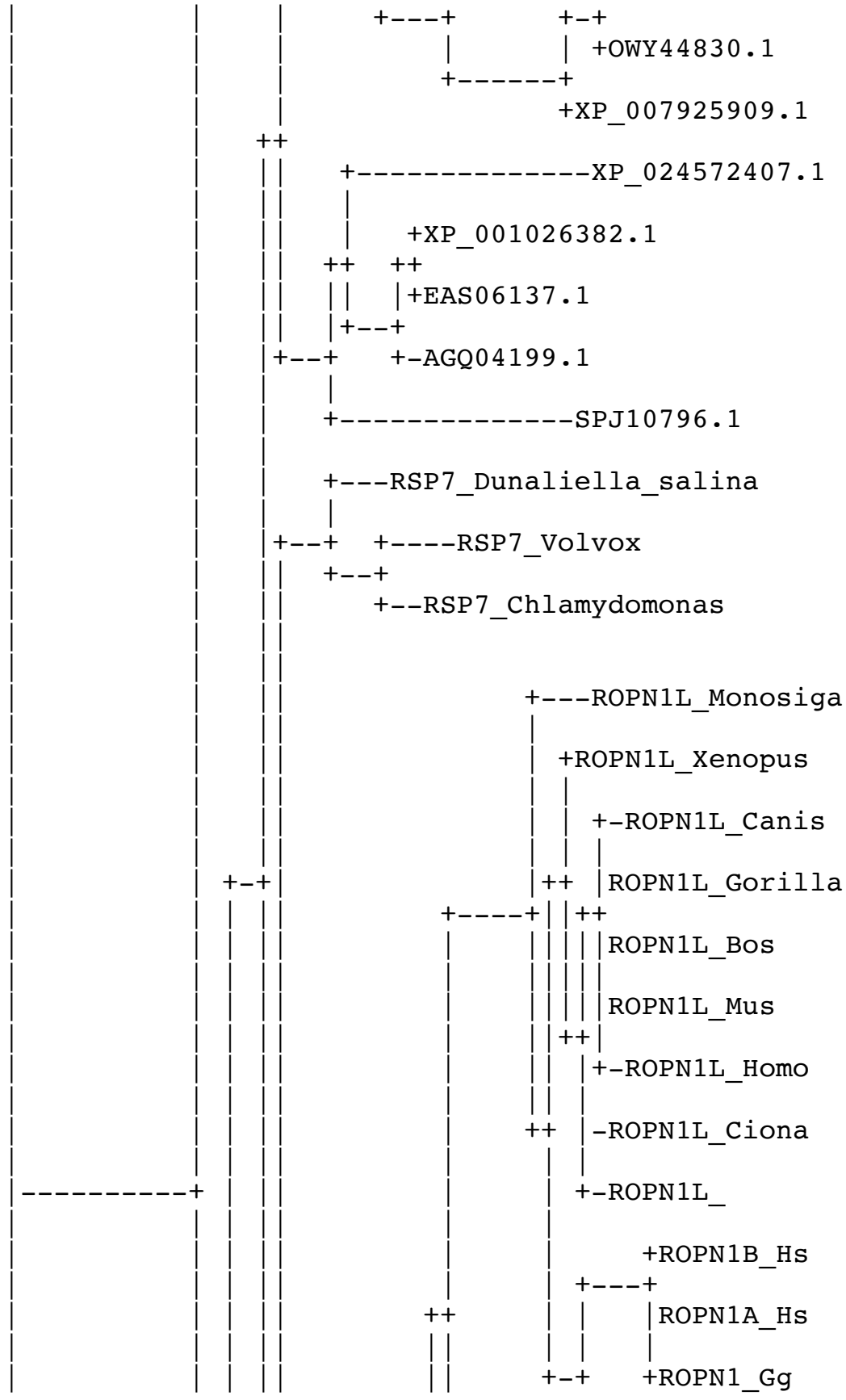
OWY44830.1
XP_007925909.1
XP_024572407.1
XP_001026382.1
EAS06137.1
AGQ04199.1
SPJ10796.1
RSP7_Dunaliella_salina
RSP7_Volvox
RSP7_Chlamydomonas
ROPN1L_Monosiga
ROPN1L_Xenopus
ROPN1L_Canis
ROPN1L_Gorilla
ROPN1L_Bos
ROPN1L_Mus
ROPN1L_Homo
ROPN1L_Ciona
ROPN1L_
ROPN1B_Hs
ROPN1A_Hs
ROPN1_Gg


ROPN1_Bt
ROPN1_Mm
ROPN1_Cl
RSP11_Micromonas
RSP11_Haematococcus
RSP11_Chlamydomonas
RSP11_Giardia
ROPN1L_Selaginella
RSP11_Marchantia
xk_ENSXETP00000020557
NP_004148.1_RIIa
ENSGGOP00000008988
ENSCAFP00000017836
ENSBTAP00000018886
d1r2aa
gh_ENSGALP00000011344
RIIa_trichoplax
ENSXETP00000013024
ENSBTAP00000019916
ENSCAFP00000005888
Prkar2b_Mus
ENSGGOP00000003850

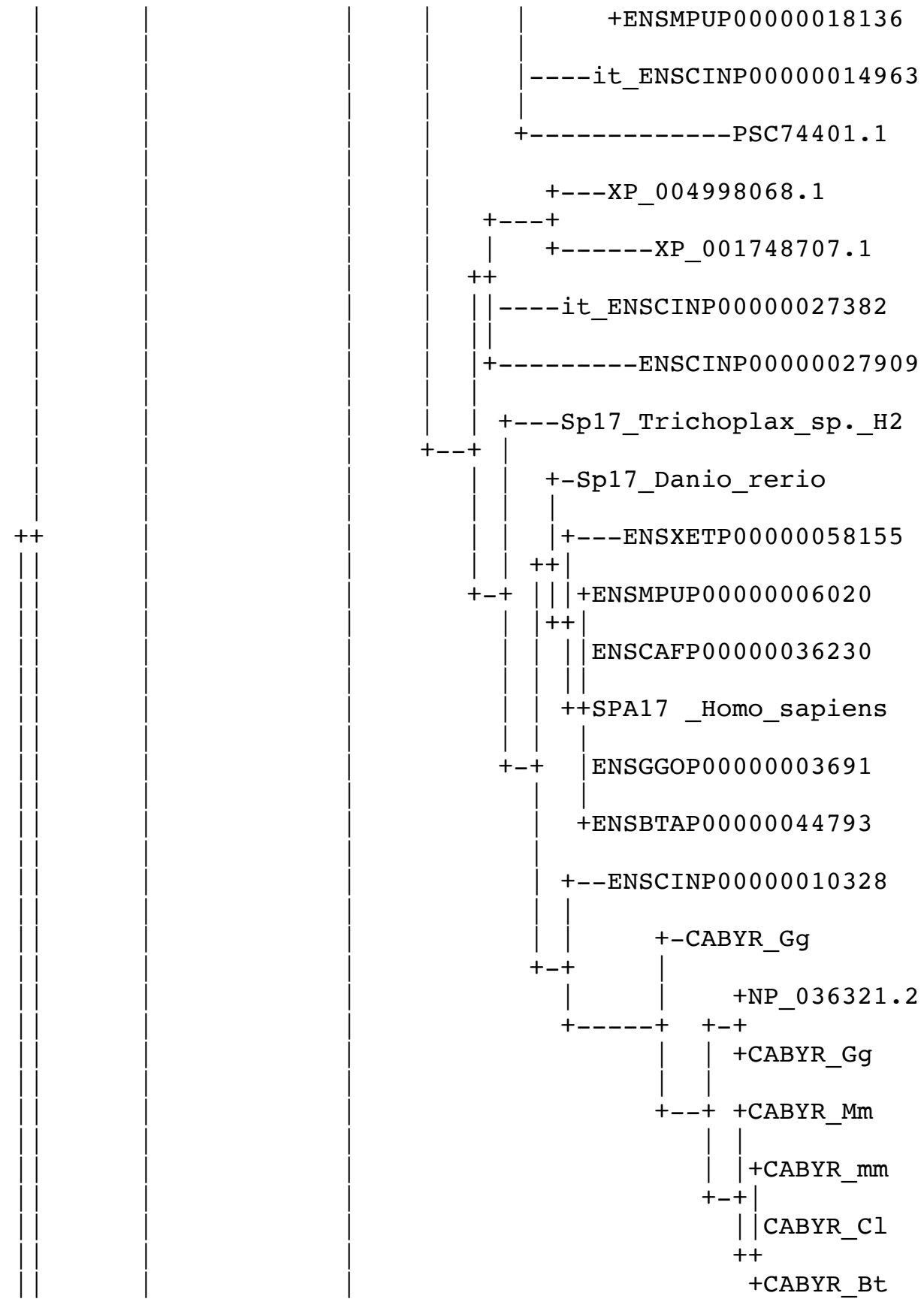
+ENSMPUP00000018136
it_ENSCINP00000014963
PSC74401.1
XP_004998068.1
XP_001748707.1
it_ENSCINP00000027382
ENSCINP00000027909
Sp17_Trichoplax_sp._H2
Sp17_Danio_rerio
ENSXETP00000058155
ENSMPUP00000006020
ENSCAFP00000036230
SPA17 _Homo_sapiens
ENSGGOP00000003691
ENSBTAP00000044793
ENSCINP00000010328
CABYR_Gg
NP_036321.2
CABYR_Gg
CABYR_Mm
CABYR_mm
CABYR_Cl
CABYR_Bt

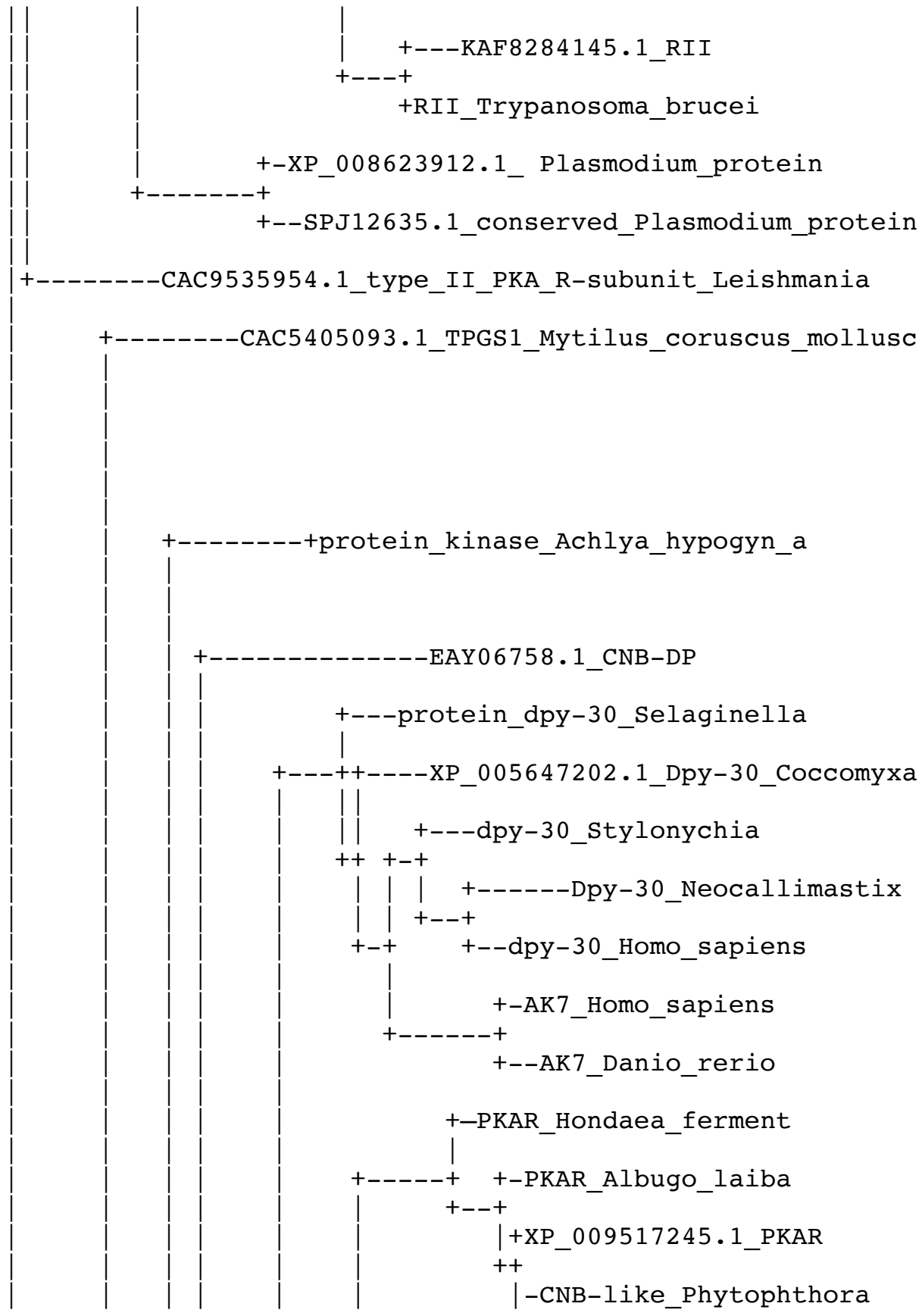
KAF8284145.1_RII
RII_Trypanosoma_brucei
XP_008623912.1_ Plasmodium_protein
SPJ12635.1_conserved_Plasmodium_protein
CAC9535954.1_type_II_PKA_R-subunit_Leishmania
CAC5405093.1_TPGS1_Mytilus_coruscus_mollusc
protein_kinase_Achlya_hypogyn_a
EAY06758.1_CNB-DP
protein_dpy-30_Selaginella
XP_005647202.1_Dpy-30_Coccomyxa
dpy-30_Stylonychia
Dpy-30_Neocallimastix
dpy-30_Homo_sapiens
AK7_Homo_sapiens
AK7_Danio_rerio
PKAR_Hondaea_ferment
PKAR_Albugo_laiba
XP_009517245.1_PKAR
CNB-like_Phytophthora

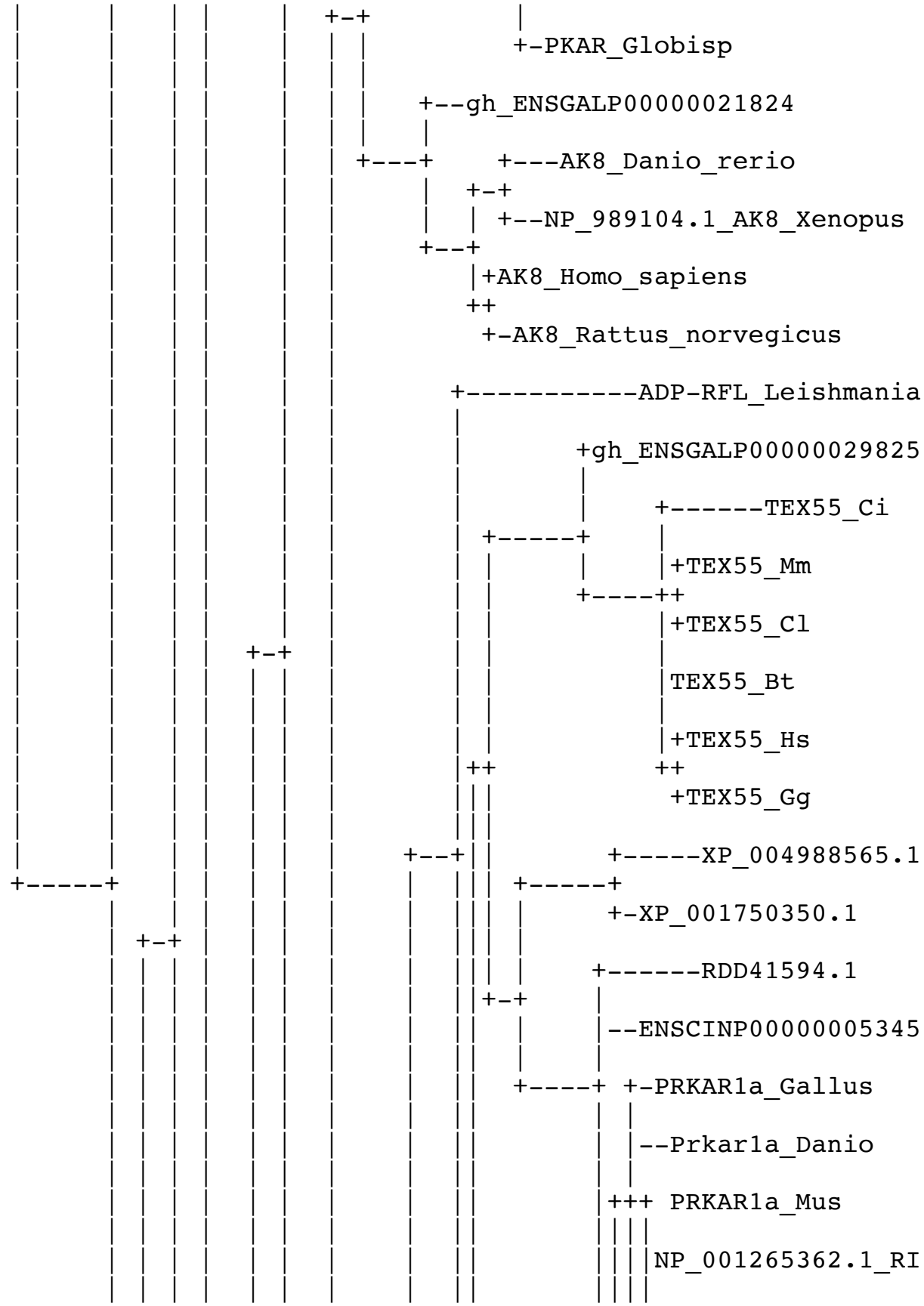
PKAR_Globisp
gh_ENSGALP00000021824
AK8_Danio_rerio
NP_989104.1_AK8_Xenopus
AK8_Homo_sapiens
AK8_Rattus_norvegicus
ADP-RFL_Leishmania
gh_ENSGALP00000029825
TEX55_Ci
TEX55_Mm
TEX55_Cl
TEX55_Bt
TEX55_Hs
TEX55_Gg
XP_004988565.1
XP_001750350.1
RDD41594.1
ENSCINP00000005345
PRKAR1a_Gallus
Prkar1a_Danio
PRKAR1a_Mus
NP_001265362.1_RI

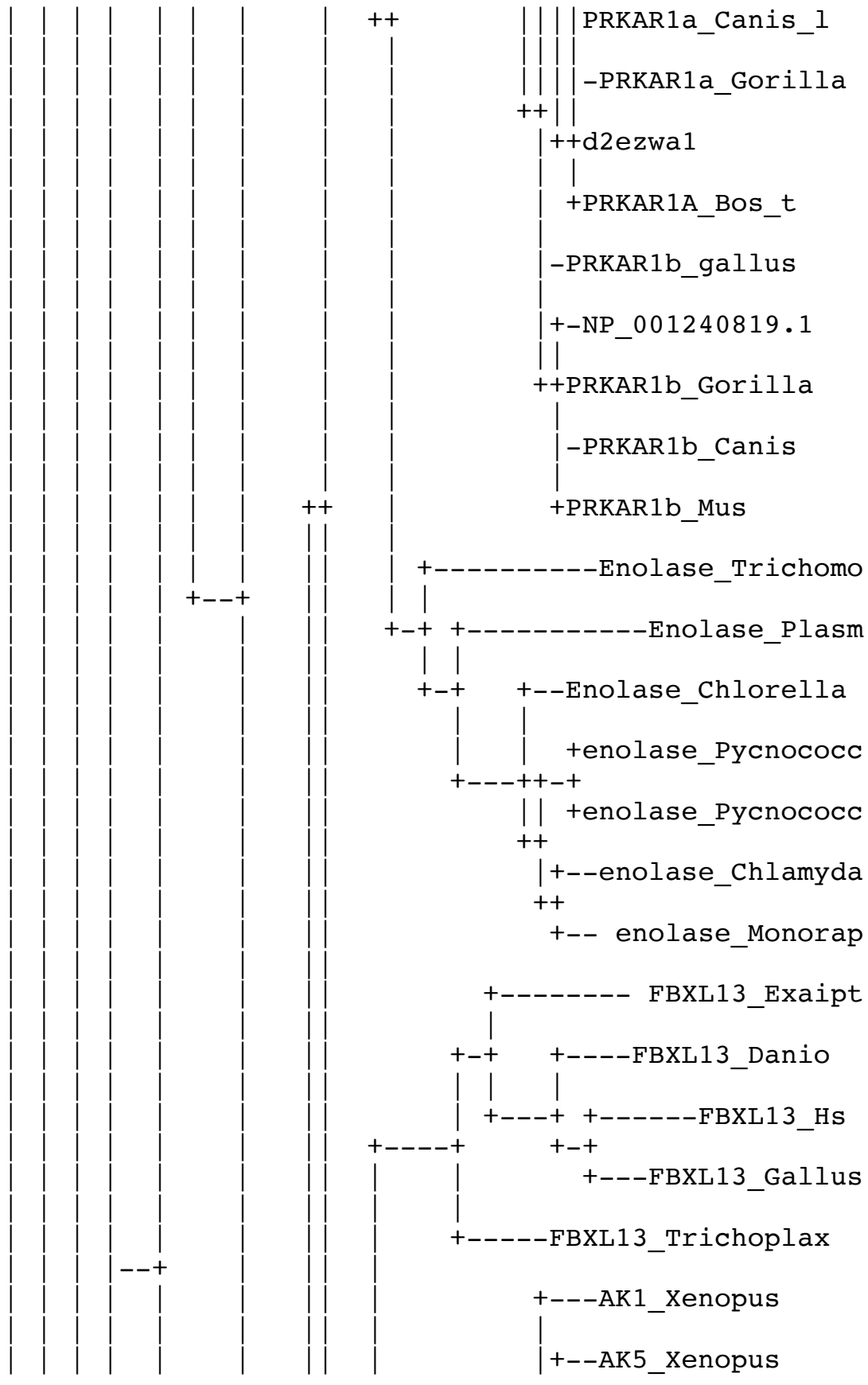
PRKAR1a_Canis_l
-PRKAR1a_Gorilla
d2ezwa1
PRKAR1A_Bos_t
-PRKAR1b_gallus
-NP_001240819.1
PRKAR1b_Gorilla
-PRKAR1b_Canis
PRKAR1b_Mus
Enolase_Trichomo
Enolase_Plasm
Enolase_Chlorella
enolase_Pycnococc
enolase_Pycnococc
--enolase_Chlamyda
enolase_Monorap
FBXL13_Exaipt
FBXL13_Danio
FBXL13_Hs
FBXL13_Gallus
FBXL13_Trichoplax
AK1_Xenopus
AK5_Xenopus

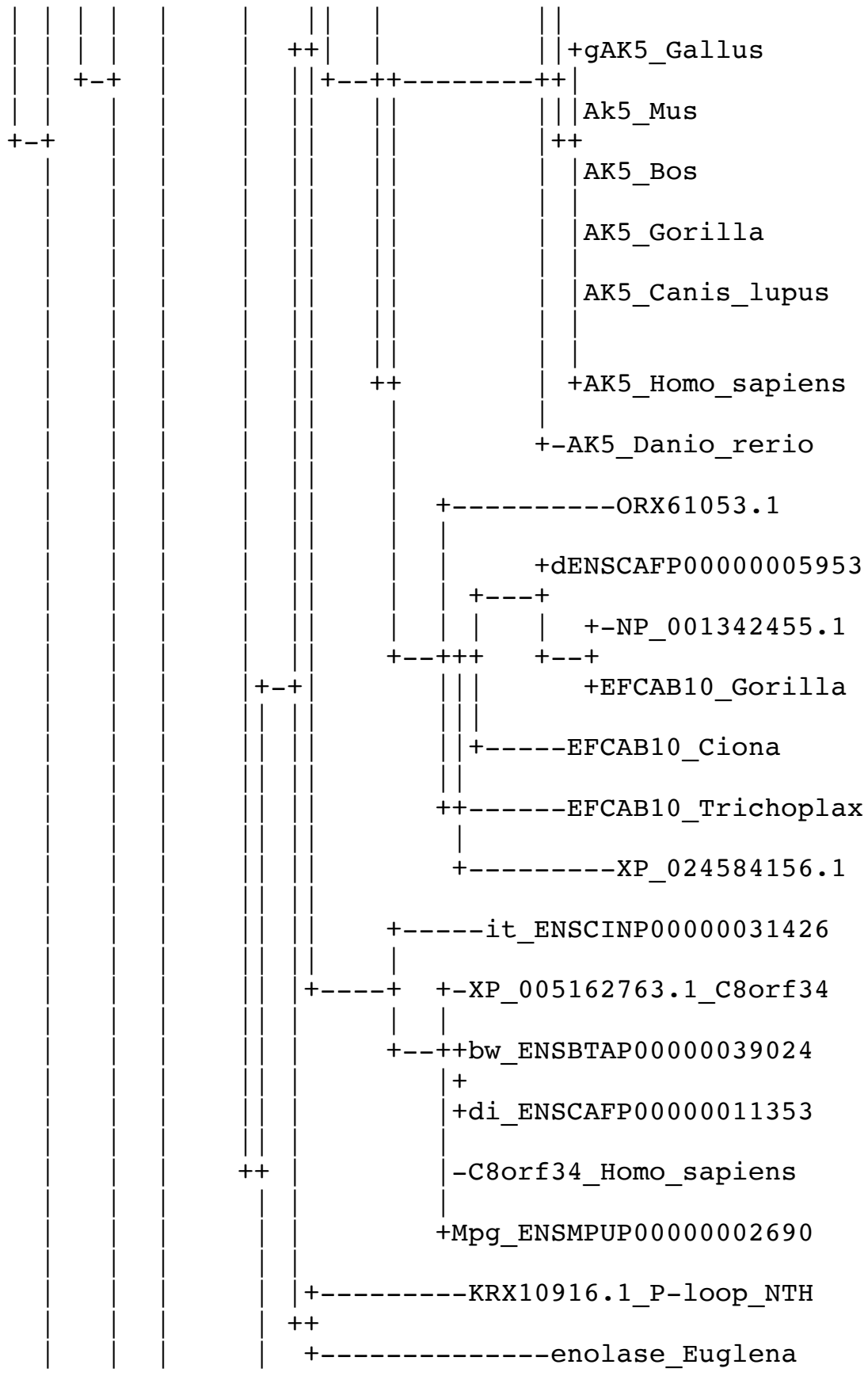
gAK5_Gallus
Ak5_Mus
AK5_Bos
AK5_Gorilla
AK5_Canis_lupus
AK5_Homo_sapiens
AK5_Danio_rerio
ORX61053.1
dENSCAFP00000005953
NP_001342455.1
EFCAB10_Gorilla
EFCAB10_Ciona
EFCAB10_Trichoplax
XP_024584156.1
it_ENSCINP00000031426
XP_005162763.1_C8orf34
bw_ENSBTAP00000039024
di_ENSCAFP00000011353
C8orf34_Homo_sapiens
Mpg_ENSMPUP00000002690
KRX10916.1_P-loop_NTH
enolase_Euglena

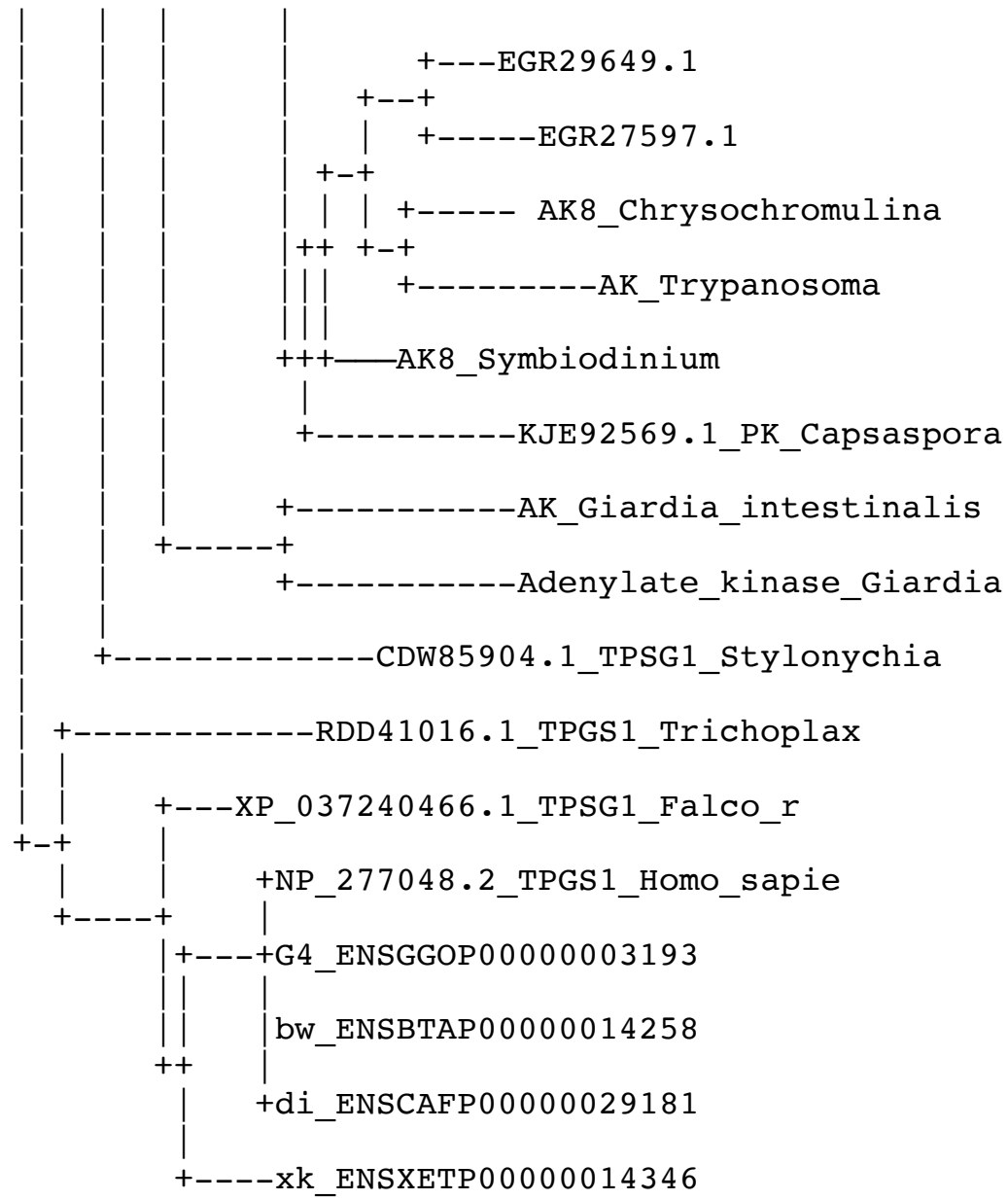
EGR29649.1
EGR27597.1
AK8_Chrysochromulina
AK_Trypanosoma
AK8_Symbiodinium
KJE92569.1_PK_Capsaspora
AK_Giardia_intestinalis
Adenylate_kinase_Giardia
CDW85904.1_TPSG1_Stylonychia
RDD41016.1_TPGS1_Trichoplax
XP_037240466.1_TPSG1_Falco_r
NP_277048.2_TPGS1_Homo_sapie
G4_ENSGGOP00000003193
bw_ENSBTAP00000014258
di_ENSCAFP00000029181
xk_ENSXETP00000014346

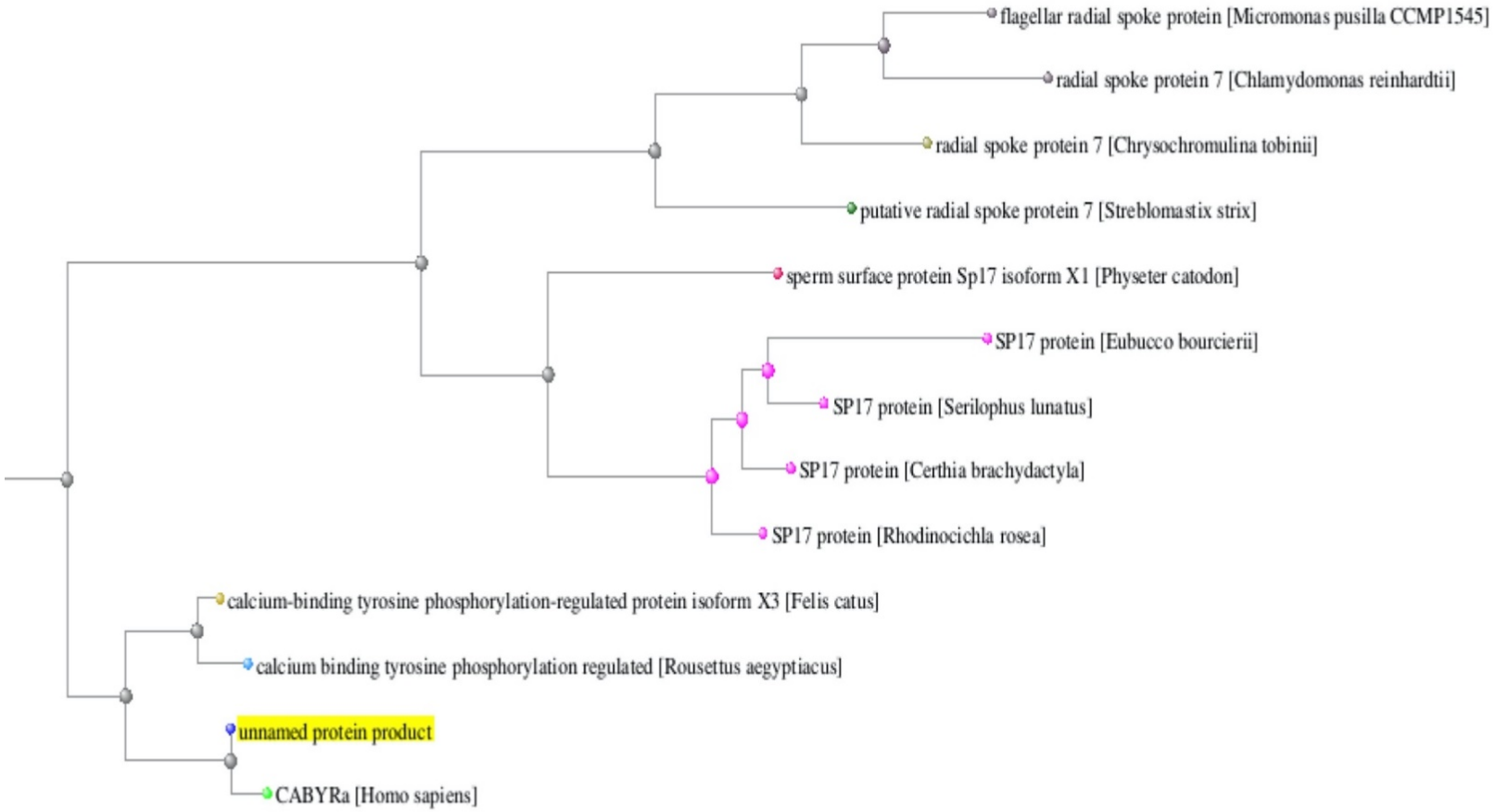
flagellar radial spoke protein [Micromonas pusilla CCMP1545]
radial spoke protein 7 [Chlamydomonas reinhardtii]
radial spoke protein 7 [Chrysochromulina tobinii]
putative radial spoke protein 7 [Streblomastix strix]
sperm surface protein Sp17 isoform X1 [Physeter catodon]
SP17 protein [Eubucco bourcierii]
SP17 protein [Serilophus lunatus]
SP17 protein [Certhia brachydactyla]
SP17 protein [Rhodinocichla rosea]
calcium-binding tyrosine phosphorylation-regulated protein isoform X3 [Felis catus]
calcium binding tyrosine phosphorylation regulated [Rousettus aegyptiacus]
unnamed protein product
CABYRa [Homo sapiens]

cAMP-dependent protein kinase type II regulatory subunit isoform X1 [Athalia rosae]
cAMP-dependent protein kinase type II regulatory subunit [Trichoplax sp. H2]
radial spoke protein 11 [Chlamydomonas reinhardtii]
radial spoke protein 11 [Micromonas commoda]
flagellar radial spoke protein [Micromonas pusilla CCMP1545]
CAMP-dependent protein kinase/ dimerization/docking domain protein [Giardia intestinalis assemblage E
ropporin-1-like protein [Selaginella moellendorffii]
ropporin-1A [Alligator sinensis]
ropporin-1 [Mus musculus]
ropporin-1A [Pteropus alecto]
ROPN1L [Cervus elaphus hippelaphus]
Ropporin-1-like protein [Collichthys lucidus]
ropporin-1-like protein [Cynoglossus semilaevis]
radial spoke protein 7 [Volvox carteri f. nagariensis]
putative radial spoke protein 7 [Strebloma stix strix]
Flagellar radial spoke protein [Spironucleus salmonicida]
radial spoke protein 7 [Dunaliella salina]
SP17 protein [Hemiprocne comata]
sperm surface protein Sp17 [Calypte anna]
Sperm surface protein Sp17 [Trichoplax sp. H2]
sperm surface protein Sp17 [Lacerta agilis]
sperm surface protein Sp17 [Enhydra lutris kenyoni]
cAMP-dependent protein kinase type II-beta regulatory subunit isoform X1 [Orcinus orca]
protein kinase, cAMP-dependent, regulatory, type II, alpha A [Danio rerio]
cAMP-dependent protein kinase type II-alpha regulatory subunit [Protobothrops mucrosquamatus]
Chain A, cAMP-dependent protein kinase Type II-alpha regulatory chain [Mus musculus]
unnamed protein product
cAMP-dependent protein kinase [Homo sapiens]

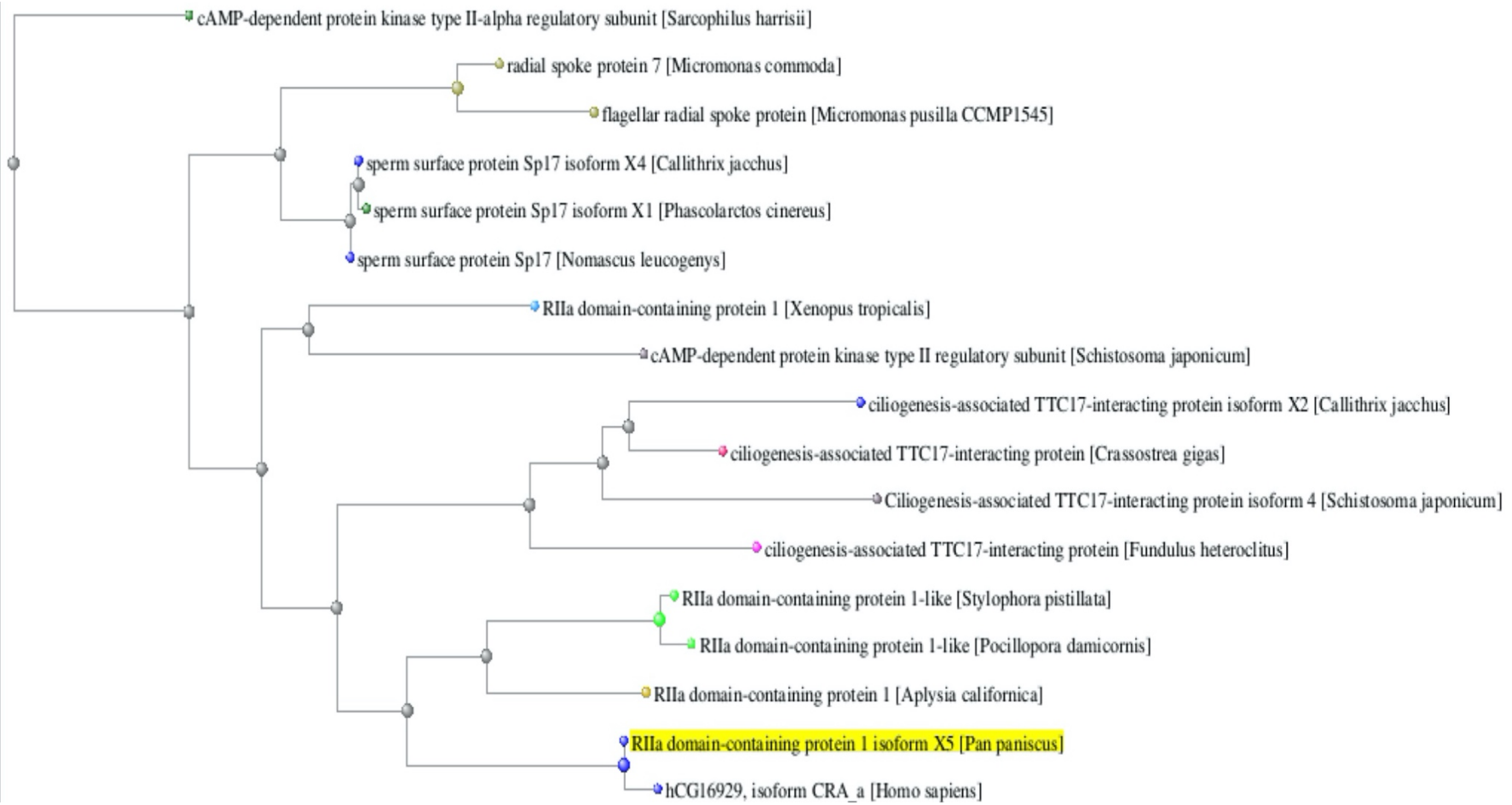
cAMP-dependent protein kinase type II-alpha regulatory subunit [Sarcophilus harrisii]
radial spoke protein 7 [Micromonas commoda]
flagellar radial spoke protein [Micromonas pusilla CCMP1545]
sperm surface protein Sp17 isoform X4 [Callithrix jacchus]
sperm surface protein Sp17 isoform X1 [Phascolarctos cinereus]
sperm surface protein Sp17 [Nomascus leucogenys]
RIIa domain-containing protein 1 [Xenopus tropicalis]
cAMP-dependent protein kinase type II regulatory subunit [Schistosoma japonicum]
ciliogenesis-associated TTC17-interacting protein isoform X2 [Callithrix jacchus]
ciliogenesis-associated TTC17-interacting protein [Crassostrea gigas]
Ciliogenesis-associated TTC17-interacting protein isoform 4 [Schistosoma japonicum]
ciliogenesis-associated TTC17-interacting protein [Fundulus heteroclitus]
RIIa domain-containing protein 1-like [Stylophora pistillata]
RIIa domain-containing protein 1-like [Pocillopora damicornis]
RIIa domain-containing protein 1 [Aplysia californica]
RIIa domain-containing protein 1 isoform X5 [Pan paniscus]
hCG16929, isoform CRA_a [Homo sapiens]

cAMP-dependent protein kinase type II-beta regulatory subunit [Petromyzon marinus]
cAMP-dependent protein kinase type II-alpha regulatory subunit-like [Petromyzon marinus]
cAMP-dependent protein kinase type II-alpha regulatory subunit [Coturnix japonica]
cAMP-dependent protein kinase type II-alpha regulatory subunit [Podarcis muralis]
cAMP-dependent protein kinase type II-alpha regulatory subunit [Lacerta agilis]
cAMP-dependent protein kinase type I-alpha regulatory subunit [Trichinella pseudospiralis]
cAMP-dependent protein kinase type I-alpha regulatory subunit [Trichinella murrelli]
cAMP-dependent protein kinase type I-alpha regulatory subunit [Trichinella patagoniensis]
cAMP-dependent protein kinase type I-alpha regulatory subunit-like [Anarrhichthys ocellatus]
cAMP-dependent protein kinase type I-alpha regulatory subunit-like isoform X1 [Scleropages formosus]
cAMP-dependent protein kinase type I-beta regulatory subunit-like [Petromyzon marinus]
cAMP-dependent protein kinase type I-beta regulatory subunit [Fasciola hepatica]
cAMP-dependent protein kinase regulatory subunit [Schistosoma japonicum]
tubulin polyglutamylase complex subunit 1 [Nematostella vectensis]
Tubulin polyglutamylase complex subunit 1 [Trichoplax sp. H2]
DPY30 domain-containing protein 2 [Colius striatus]
DPY30 domain-containing protein 1 [Calypte anna]
DPY30 domain-containing protein 2 [Apaloderma vittatum]
DPY30 domain-containing protein 1 [Taeniopygia guttata]
DYDC1 protein [Eulacestoma nigropectus]
DPY30 domain-containing protein 2 [Chlamydotis macqueenii]
DPY30 domain-containing protein 1 isoform X1 [Oxyura jamaicensis]
DPY30 domain-containing protein 2 [Trichoplax sp. H2]
protein dpy-30 homolog [Eurytemora affinis]
adenylate kinase 7-like isoform X2 [Pseudomyrmex gracilis]
Putative adenylate kinase 7 [Atta colombica]
adenylate kinase 7-like [Danaus plexippus plexippus]
adenylate kinase 7-like [Vanessa tameamea]
adenylate kinase 7-like [Bicyclus anynana]
Tubulin polyglutamylase complex subunit 1 [Larimichthys crocea]
tubulin polyglutamylase complex subunit 1 isoform X1 [Ornithorhynchus anatinus]
tubulin polyglutamylase complex subunit 1 [Corapipo altera]
TPGS1 polyglutamylase [Cepphus grylle]
TPGS1 polyglutamylase [Calonectris borealis]
tubulin polyglutamylase complex subunit 1 [Onychomys torridus]
unnamed protein product
tubulin polyglutamylase complex subunit 1 [Homo sapiens]
tubulin polyglutamylase complex subunit 1 [Nomascus leucogenys]

EF-hand calcium-binding domain-containing protein 10-like [Dendronephthya gigantea]
EF-hand calcium-binding domain-containing protein 10-like [Stylophora pistillata]
EF-hand calcium-binding domain-containing protein 10 [Archocentrus centrarchus]
Dimerization-anchoring domain of cAMP-dependent protein kinase, regulatory subunit [Pseudocohnilembus persalinus]
adenylate kinase 8 isoform X1 [Sander lucioperca]
adenylate kinase 8 [Larimichthys crocea]
uncharacterized protein C8orf34-like isoform X1 [Dendronephthya gigantea]
vestibule 1 [Molossus molossus]
uncharacterized protein C8orf34 homolog isoform X1 [Mus pahari]
vestibule 1 [Pipistrellus kuhlii]
cAMP-dependent protein kinase, regulatory subunit, type I/II alpha/beta containing protein [Cricetulus griseus]
uncharacterized protein C8orf34 homolog isoform X3 [Molothrus ater]
uncharacterized protein C8orf34 homolog isoform X2 [Corapipo altera]
uncharacterized protein C8orf34 homolog isoform X3 [Trachypithecus francoisi]
vestibule 1 [Myotis myotis]
FBXL13 [Mytilus coruscus]
F-box/LRR-repeat protein 13 isoform X1 [Microcebus murinus]
dynein regulatory complex subunit 6 isoform X4 [Hylobates moloch]
dynein regulatory complex subunit 6 isoform X3 [Papio anubis]
dynein regulatory complex subunit 6 isoform X19 [Callithrix jacchus]
adenylate kinase 5, like [Danio rerio]
adenylate kinase 5, like isoform X2 [Electrophorus electricus]
adenylate kinase isoenzyme 5 isoform X3 [Camelus dromedarius]
adenylate kinase isoenzyme 5 isoform X3 [Heterocephalus glaber]
adenylate kinase isoenzyme 5 [Zootoca vivipara]
adenylate kinase isoenzyme 5 isoform X2 [Sarcophilus harrisii]
adenylate kinase isoenzyme 5 [Aythya fuligula]
adenylate kinase isoenzyme 5-like [Oncorhynchus nerka]
adenylate kinase isoenzyme 5 isoform X2 [Takifugu rubripes]
Adenylate kinase isoenzyme 5 [Larimichthys crocea]
unnamed protein product
hypothetical protein TRIADDRAFT_55288 [Trichoplax adhaerens]

cAMP-dependent protein kinase regulatory subunit, dimerization-anchoring domain [Phytophthora cactorum]
EF-hand calcium-binding domain-containing protein 10 [Trachemys scripta elegans]
EF-hand calcium-binding domain-containing protein 10 [Rhinatrema bivittatum]
EF-hand calcium-binding domain-containing protein 10 [Scophthalmus maximus]
EF-hand calcium-binding domain-containing protein 10 [Notolabrus celidotus]
EF-hand calcium-binding domain-containing protein 10 [Maylandia zebra]
EF-hand calcium-binding domain-containing protein 10 [Anguilla anguilla]
EF-hand calcium-binding domain-containing protein 10 [Nematostella vectensis]
adenylate kinase 8 isoform X2 [Esox lucius]
adenylate kinase 8 isoform X4 [Salmo trutta]
adenylate kinase 8 isoform X3 [Tachysurus fulvidraco]
adenylate kinase 8 [Pangasianodon hypophthalmus]
adenylate kinase 8 isoform X1 [Tachysurus fulvidraco]
adenylate kinase 8 isoform X2 [Paramormyrops kingsleyae]
adenylate kinase 8 [Chanos chanos]
adenylate kinase 8 isoform X1 [Scleropages formosus]
PREDICTED: adenylate kinase 8 [Cyprinodon variegatus]
Adenylate kinase 8 [Oryzias melastigma]
cAMP-dependent protein kinase type I-alpha regulatory subunit-like isoform X1 [Mastacembelus armatus]
cAMP-dependent protein kinase type I-alpha regulatory subunit-like isoform X2 [Mastacembelus armatus]
cAMP-dependent protein kinase type I-alpha regulatory subunit [Acipenser ruthenus]
cAMP-dependent protein kinase type I-alpha regulatory subunit isoform X2 [Petromyzon marinus]
cAMP-dependent protein kinase type I-alpha regulatory subunit isoform X1 [Petromyzon marinus]
cAMP-dependent protein kinase type I-alpha regulatory subunit [Rhincodon typus]
cAMP-dependent protein kinase type I-alpha regulatory subunit isoform X2 [Amblyraja radiata]
regulatory subunit of type II PKA R-subunit [Ancylostoma caninum]
regulatory subunit of type II PKA R-subunit [Ancylostoma duodenale]
EF-hand calcium-binding domain-containing protein 10 [Onychomys torridus]
unnamed protein product
EF-hand calcium-binding domain-containing protein 10 isoform 1 [Homo sapiens]

REFERENCES

Anisimova M., Gascuel O. *Approximate likelihood ratio test for branches: A fast, accurate and powerful alternative*. Syst Biol. 2006, Aug;55(4):539-52.

Brown, S. H. J., Cheng, C. Y., Saldanha, S. A., Wu, J., Cottam, H. B., Sankaran, B., & Taylor, S. S. (2013). Implementing Fluorescence Anisotropy Screening and Crystallographic Analysis to Define PKA Isoform-Selective Activation by cAMP Analogs. *ACS Chemical Biology*, *8*(10). https://doi.org/10.1021/cb400247t

Brown, S. H. J., Wu, J., Kim, C., Alberto, K., & Taylor, S. S. (2009). Novel Isoform-specific Interfaces Revealed by PKA RIIβ Holoenzyme Structures. *Journal of Molecular Biology*, *393*(5), 1070–1082. https://doi.org/10.1016/j.jmb.2009.09.014

Buchli, R., De Jong, A., & Robbins, D. L. (2002). Genomic organization of an intron-containing sperm protein 17 gene (Sp17-1) and an intronless pseudogene (Sp17-2) in humans: A new model. *Biochimica et Biophysica Acta (BBA) - Gene Structure and Expression*, *1578*(1), 29–42. https://doi.org/10.1016/S0167-4781(02)00478-5

Bult, C. J., Blake, J. A., Smith, C. L., Kadin, J. A., Richardson, J. E., & Mouse Genome Database Group. (2019). Mouse Genome Database (MGD) 2019. *Nucleic Acids Research*, *47*(D1), D801–D806. https://doi.org/10.1093/nar/gky1056

Bumm, K., Grizzi, F., Franceschini, B., Koch, M., Iro, H., Wurm, J., Ceva-Grimaldi, G., Dimmler, A., Cobos, E., Dioguardi, N., Sinha, U. K., Kast, W. M., & Chiriva-Internati, M. (2005). Sperm protein 17 expression defines 2 subsets of primary esthesioneuroblastoma. *Human Pathology*, *36*(12), 1289–1293. https://doi.org/10.1016/j.humpath.2005.08.023

Burns-Hamuro, L. L., Ma, Y., Kammerer, S., Reineke, U., Self, C., Cook, C., Olson, G. L., Cantor, C. R., Braun, A., & Taylor, S. S. (2003). Designing isoform-specific peptide disruptors of protein kinase A localization. *Proceedings of the National Academy of Sciences*, *100*(7), 4072–4077.

Burton, K. A., & McKnight, G. S. (2007). PKA, germ cells, and fertility. *Physiology*, *22*(1), 40–46.

Cao, B., Lu, T.-W., Martinez Fiesco, J. A., Tomasini, M., Fan, L., Simon, S. M., Taylor, S. S., & Zhang, P. (2019). Structures of the PKA RIα Holoenzyme with the FLHCC Driver J-PKAcα or Wild-Type PKAcα. *Structure*, *27*(5), 816-828.e4. https://doi.org/10.1016/j.str.2019.03.001

Carr, D. W., Stofko-Hahn, R. E., Fraser, I. D., Bishop, S. M., Acott, T. S., Brennan, R. G., & Scott, J. D. (1991). Interaction of the regulatory subunit (RII) of cAMP-dependent protein kinase with RII-anchoring proteins occurs through an amphipathic helix binding motif. *Journal of Biological Chemistry*, *266*(22), 14188–14192.

Carvalho-Santos, Z., Azimzadeh, J., Pereira-Leal, J. B., & Bettencourt-Dias, M. (2011). Tracing the origins of centrioles, cilia, and flagella. *The Journal of Cell Biology*, *194*(2), 165–175. https://doi.org/10.1083/jcb.201011152

Chiriva-Internati, M., Mirandola, L., Figueroa, J. A., Yu, Y., Grizzi, F., Kim, M., Jenkins, M., Cobos, E., Jumper, C., & Alalawi, R. (2014). Selective expression and immunogenicity of the cancer/testis antigens SP17, AKAP4 and PTTG1 in non-small cell lung cancer: New candidates for active immunotherapy. *Chest*. https://doi.org/10.1378/chest.13-0770

Chiriva-Internati, M., Wang, Z., Salati, E., Bumm, K., Barlogie, B., & Lim, S. H. (2002). Sperm protein 17 (Sp17) is a suitable target for immunotherapy of multiple myeloma. *Blood*, *100*(3), 961–965. https://doi.org/10.1182/blood-2002-02-0408

Coutinho-Camillo, C. M., Salaorni, S., Sarkis, A. S., & Nagai, M. A. (2006). Differentially expressed genes in the prostate cancer cell line LNCaP after exposure to androgen and anti-androgen. *Cancer Genetics and Cytogenetics*, *166*(2), 130–138. https://doi.org/10.1016/j.cancergencyto.2005.09.012

Dasgeb, B., Mehregan, D., Ring, C., Nartker, N., & Brownell, I. (2019). Cancer-testis antigens as biomarkers for Merkel cell carcinoma: Pitfalls and opportunities. *Journal of Cutaneous Pathology*, *46*(10), 748–752. https://doi.org/10.1111/cup.13528

De Jong, A., Buchli, R., & Robbins, D. (2002). Characterization of sperm protein 17 in human somatic and neoplastic tissue. *Cancer Letters*, *186*(2), 201–209. https://doi.org/10.1016/s0304-3835(02)00350-6

Dereeper A.*, Guignon V.*, Blanc G., Audic S., Buffet S., Chevenet F., Dufayard J.F., Guindon S., Lefort V., Lescot M., Claverie J.M., Gascuel O. *Phylogeny.fr: robust phylogenetic analysis for the non-specialist*. Nucleic Acids Res. 2008 Jul 1;36(Web Server issue):W465-9. Epub 2008 Apr 19. *: joint first authors

Diller, T. C., Madhusudan, Xuong, N.-H., & Taylor, S. S. (2001). Molecular Basis for Regulatory Subunit Diversity in cAMP-Dependent Protein Kinase: Crystal Structure of the Type IIβ Regulatory Subunit. *Structure*, *9*(1), 73–82. https://doi.org/10.1016/S0969-2126(00)00556-6

Dutcher, S. K. (2020). Asymmetries in the cilia of Chlamydomonas. *Philosophical Transactions of the Royal Society B*, *375*(1792), 20190153.

Eddy, E. M., Toshimori, K., & O'Brien, D. A. (2003). Fibrous sheath of mammalian spermatozoa. *Microscopy Research and Technique*, *61*(1), 103–115. https://doi.org/10.1002/jemt.10320

Fiedler, S. E., Dudiki, T., Vijayaraghavan, S., & Carr, D. W. (2013). Loss of R2D2 Proteins ROPN1 and ROPN1L Causes Defects in Murine Sperm Motility, Phosphorylation, and Fibrous Sheath Integrity. *Biology of Reproduction*, *88*(2). https://doi.org/10.1095/biolreprod.112.105262

Finn, R. D., Bateman, A., Clements, J., Coggill, P., Eberhardt, R. Y., Eddy, S. R., Heger, A., Hetherington, K., Holm, L., Mistry, J., Sonnhammer, E. L. L., Tate, J., & Punta, M. (2014). Pfam: The protein families database. *Nucleic Acids Research*, *42*(Database issue), D222–D230. https://doi.org/10.1093/nar/gkt1223

Fujita, A., Nakamura, K., Kato, T., Watanabe, N., Ishizaki, T., Kimura, K., Mizoguchi, A., & Narumiya, S. (2000). Ropporin, a sperm-specific binding protein of rhophilin, that is localized in the fibrous sheath of sperm flagella. *Journal of Cell Science*, *113 (Pt 1)*, 103–112.

Gaines, J. P. (2006). *The role of sperm protein 17 (Sp17) in somatic cells and cancer*.

Gaines, J. P., Muminova, Z. E., Phillippi, M., Yoder, B. K., Shaw, D. R., & Strong, T. V. (2005). Immunolocalization of sperm protein 17 (Sp17) in normal and malignant cells. *Cancer Research*, *65*(9 Supplement), 1214–1215.

Gjerstorff, M. F., Pøhl, M., Olsen, K. E., & Ditzel, H. J. (2013). Analysis of GAGE, NY-ESO-1 and SP17 cancer/testis antigen expression in early stage non-small cell lung carcinoma. *BMC Cancer*, *13*, 466. https://doi.org/10.1186/1471-2407-13-466

Gold, M. G., Fowler, D. M., Means, C. K., Pawson, C. T., Stephany, J. J., Langeberg, L. K., ... & Scott, J. D. (2013). Engineering A-kinase anchoring protein (AKAP)-selective

regulatory subunits of protein kinase A (PKA) through structure-based phage selection. *Journal of Biological Chemistry*, *288*(24), 17111-17121.

Gold, M. G., Lygren, B., Dokurno, P., Hoshi, N., McConnachie, G., Taskén, K., Carlson, C. R., Scott, J. D., & Barford, D. (2006). Molecular basis of AKAP specificity for PKA regulatory subunits. *Molecular Cell*, *24*(3), 383–395. https://doi.org/10.1016/j.molcel.2006.09.006

Götz, F., Roske, Y., Schulz, M. S., Autenrieth, K., Bertinetti, D., Faelber, K., Zühlke, K., Kreuchwig, A., Kennedy, E. J., Krause, G., Daumke, O., Herberg, F. W., Heinemann, U., & Klussmann, E. (2016). AKAP18:PKA-RIIα structure reveals crucial anchor points for recognition of regulatory subunits of PKA. *The Biochemical Journal*, *473*(13), 1881–1894. https://doi.org/10.1042/BCJ20160242

Grizzi, F., Gaetani, P., Franceschini, B., Di Ieva, A., Colombo, P., Ceva-Grimaldi, G., Bollati, A., Frezza, E. E., Cobos, E., Rodriguez y Baena, R., Dioguardi, N., & Chiriva-Internati, M. (2006). Sperm protein 17 is expressed in human nervous system tumours. *BMC Cancer*, *6*, 23. https://doi.org/10.1186/1471-2407-6-23

Grosberg, R. K., & Strathmann, R. R. (2007). The Evolution of Multicellularity: A Minor Major Transition? *Annual Review of Ecology, Evolution, and Systematics*, *38*, 621–654. JSTOR.

Guindon S., Gascuel O. *A simple, fast, and accurate algorithm to estimate large phylogenies by maximum likelihood*. Syst Biol. 2003, Oct;52(5):696-704. (PubMed)

Hausken, Z. E., CoghlanS, V., Hastings O. S., Reimann O. E., & Scott, J.D. (1994). Type I1 Regulatory Subunit (RII) of the CAMP-dependent Protein Kinase Interaction with A-kinase Anchor Proteins Requires Isoleucines3 and 5. *Journal of Biological Chemistry*, *269*(39), 24245–24251.

Haddad, J. F., Yang, Y., Takahashi, Y. H., Joshi, M., Chaudhary, N., Woodfin, A. R., ... & Brand, M. (2018). Structural analysis of the Ash2L/Dpy-30 complex reveals a heterogeneity in H3K4 methylation. *Structure*, *26*(12), 1594-1603.

Herrgård, S., Jambeck, P., Taylor, S. S., & Subramaniam, S. (2000). Domain architecture of a Caenorhabditis elegans AKAP suggests a novel AKAP function. *FEBS Letters*, *486*(2), 107–111.

Hsu, P. L., Li, H., Lau, H. T., Leonen, C., Dhall, A., Ong, S. E., ... & Zheng, N. (2018). Crystal structure of the COMPASS H3K4 methyltransferase catalytic module. *Cell*, *174*(5), 1106-1116.

Hsu, D. R., & Meyer, B. J. (1994). The dpy-30 gene encodes an essential component of the Caenorhabditis elegans dosage compensation machinery. *Genetics*, *137*(4), 999-1018.

Hundsrucker, C, Rosenthal, W., & Klussmann, E. (2006). *Peptides for disruption of PKA anchoring*.

Hundsrucker, Christian, Skroblin, P., Christian, F., Zenn, H.-M., Popara, V., Joshi, M., Eichhorst, J., Wiesner, B., Herberg, F. W., Reif, B., Rosenthal, W., & Klussmann, E. (2010). Glycogen synthase kinase 3beta interaction protein functions as an A-kinase anchoring protein. *The Journal of Biological Chemistry*, *285*(8), 5507–5521. https://doi.org/10.1074/jbc.M109.047944

Huttlin, E. L., Bruckner, R. J., Paulo, J. A., Cannon, J. R., Ting, L., Baltier, K., Colby, G., Gebreab, F., Gygi, M. P., & Parzen, H. (2017). Architecture of the human interactome defines protein communities and disease networks. *Nature*, *545*(7655), 505–509.

Huttlin, E. L., Ting, L., Bruckner, R. J., Gebreab, F., Gygi, M. P., Szpyt, J., Tam, S., Zarraga, G., Colby, G., & Baltier, K. (2015). The BioPlex network: A systematic exploration of the human interactome. *Cell*, *162*(2), 425–440.

Ilouz, R., Bubis, J., Wu, J., Yim, Y. Y., Deal, M. S., Kornev, A. P., Ma, Y., Blumenthal, D. K., & Taylor, S. S. (2012). Localization and quaternary structure of the PKA RI holoenzyme. *Proceedings of the National Academy of Sciences*, *109*(31), 12443–12448. https://doi.org/10.1073/pnas.1209538109

Karl, J., & Capel, B. (1998). Sertoli Cells of the Mouse Testis Originate from the Coelomic Epithelium. *Developmental Biology*, *203*(2), 323–333. https://doi.org/10.1006/dbio.1998.9068

Kausar, T., Ahsan, A., Hasan, M. R., Lin, L., Beer, D. G., & Ralhan, R. (2010). Sperm protein 17 is a novel marker for predicting cisplatin response in esophageal squamous cancer cell lines. *International Journal of Cancer*, *126*(6), 1494–1503. https://doi.org/10.1002/ijc.24828

Kim, C., Cheng, C. Y., Saldanha, S. A., & Taylor, S. S. (2007). PKA-I Holoenzyme Structure Reveals a Mechanism for cAMP-Dependent Activation. *Cell*, *130*(6), 1032–1043. https://doi.org/10.1016/j.cell.2007.07.018

Kim, C., Xuong, N.-H., & Taylor, S. S. (2005). Crystal Structure of a Complex Between the Catalytic and Regulatory (RIα) Subunits of PKA. *Science*, *307*(5710), 690–696. https://doi.org/10.1126/science.1104607

Kinderman, F. S., Kim, C., von Daake, S., Ma, Y., Pham, B. Q., Spraggon, G., Xuong, N.-H., Jennings, P. A., & Taylor, S. S. (2006). A Dynamic Mechanism for AKAP Binding to

RII Isoforms of cAMP-Dependent Protein Kinase. *Molecular Cell*, *24*(3), 397–408. https://doi.org/10.1016/j.molcel.2006.09.015

Kong, M., Richardson, R. T., Widgren, E. E., & O'Rand, M. G. (1995). Sequence and Localization of the Mouse Sperm Autoantigenic Protein, Sp17. *Biology of Reproduction*, *53*(3), 579–590. https://doi.org/10.1095/biolreprod53.3.579

Lacy, H. M., & Sanderson, R. D. (2001). Sperm protein 17 is expressed on normal and malignant lymphocytes and promotes heparan sulfate-mediated cell-cell adhesion. *Blood*, *98*(7), 2160–2165. https://doi.org/10.1182/blood.v98.7.2160

Langeberg, L. K., & Scott, J. D. (2015). Signalling scaffolds and local organization of cellular behaviour. *Nature Reviews Molecular Cell Biology*, *16*(4), 232–244. https://doi.org/10.1038/nrm3966

Lea, I. A., Widgren, E. E., & O'Rand, M. G. (2004). Association of sperm protein 17 with A-kinase anchoring protein 3 in flagella. *Reproductive Biology and Endocrinology*, *2*(1), 57. https://doi.org/10.1186/1477-7827-2-57

Lehti, M. S., & Sironen, A. (2017). Formation and function of sperm tail structures in association with sperm motility defects. *Biology of Reproduction*, *97*(4), 522–536. https://doi.org/10.1093/biolre/iox096

Li, F.-Q., Gangal, M., Jones, J. M., Deich, J., Lovett, K. E., Taylor, S. S., & Johnson, D. A. (2000). Consequences of cAMP and catalytic-subunit binding on the flexibility of the A-kinase regulatory subunit. *Biochemistry*, *39*(50), 15626–15632. https://doi.org/10.1021/bi0021961

Li, F.-Q., Han, Y.-L., Liu, Q., Wu, B., Huang, W.-B., & Zeng, S.-Y. (2009). Overexpression of human sperm protein 17 increases migration and decreases the chemosensitivity of

human epithelial ovarian cancer cells. *BMC Cancer*, *9*, 323. https://doi.org/10.1186/1471-2407-9-323

Li, F.-Q., Liu, Q., Han, Y.-L., Wu, B., & Yin, H.-L. (2010). Sperm protein 17 is highly expressed in endometrial and cervical cancers. *BMC Cancer*, *10*, 429. https://doi.org/10.1186/1471-2407-10-429

Lim, S. H., Wang, Z., Chiriva-Internati, M., & Xue, Y. (2001). Sperm protein 17 is a novel cancer-testis antigen in multiple myeloma. *Blood*, *97*(5), 1508–1510. https://doi.org/10.1182/blood.v97.5.1508

Littler, D. R., Bullen, H. E., Harvey, K. L., Beddoe, T., Crabb, B. S., Rossjohn, J., & Gilson, P. R. (2016). Disrupting the Allosteric Interaction between the *Plasmodium falciparum* cAMP-dependent Kinase and Its Regulatory Subunit. *Journal of Biological Chemistry*, *291*(49), 25375–25386. https://doi.org/10.1074/jbc.M116.750174

Lodish, H., Berk, A., Zipursky, S. L., Matsudaira, P., Baltimore, D., & Darnell, J. (2000). *Molecular and Cell Biology* (4th ed.). W. H. Freeman. http://www.ncbi.nlm.nih.gov/books/NBK21673/

Lohmann, S. M., DeCamilli, P., Einig, I., & Walter, U. (1984). High-affinity binding of the regulatory subunit (RII) of cAMP-dependent protein kinase to microtubule-associated and other cellular proteins. *Proceedings of the National Academy of Sciences*, *81*(21), 6723–6727.

Luck, K., Kim, D.-K., Lambourne, L., Spirohn, K., Begg, B., Bian, W., Brignall, R., Cafarelli, T., Campos-Laborie, F., & Charloteaux, B. (2019). *A reference map of the human protein interactome*.

Margulis, L. (1981). *Symbiosis in Cell Evolution: Life and Its Environment on the Early Earth*. W. H. Freeman. https://books.google.com/books?id=QYxwQgAACAAJ

McClintock, T. S., Glasser, C. E., Bose, S. C., & Bergman, D. A. (2008). Tissue expression patterns identify mouse cilia genes. *Physiological Genomics*, *32*(2), 198–206. https://doi.org/10.1152/physiolgenomics.00128.2007

Mirandola, L., Figueroa, J. A., Phan, T. T., Grizzi, F., Kim, M., Rahman, R. L., Jenkins, M. R., Cobos, E., Jumper, C., Alalawi, R., & Chiriva-Internati, M. (2015). Novel antigens in non-small cell lung cancer: SP17, AKAP4, and PTTG1 are potential immunotherapeutic targets. *Oncotarget*, *6*(5), 2812–2826. https://doi.org/10.18632/oncotarget.2802

Munger, S. C., Natarajan, A., Looger, L. L., Ohler, U., & Capel, B. (2013). Fine Time Course Expression Analysis Identifies Cascades of Activation and Repression and Maps a Putative Regulator of Mammalian Sex Determination. *PLOS Genetics*, *9*(7), e1003630. https://doi.org/10.1371/journal.pgen.1003630

Naaby-Hansen, S., Mandal, A., Wolkowicz, M. J., Sen, B., Westbrook, V. A., Shetty, J., Coonrod, S. A., Klotz, K. L., Kim, Y.-H., Bush, L. A., Flickinger, C. J., & Herr, J. C. (2002). CABYR, a novel calcium-binding tyrosine phosphorylation-regulated fibrous sheath protein involved in capacitation. *Developmental Biology*, *242*(2), 236–254. https://doi.org/10.1006/dbio.2001.0527

Nakazato, T., Kanuma, T., Tamura, T., Faried, L. S., Aoki, H., & Minegishi, T. (2007). Sperm protein 17 influences the tissue-specific malignancy of clear cell adenocarcinoma in human epithelial ovarian cancer. *International Journal of Gynecological Cancer: Official Journal of the International Gynecological Cancer Society*, *17*(2), 426–432. https://doi.org/10.1111/j.1525-1438.2007.00815.x

Newell, A. E. H., Fiedler, S. E., Ruan, J. M., Pan, J., Wang, P. J., Deininger, J., Corless, C. L., & Carr, D. W. (2008). Protein kinase A RII-like (R2D2) proteins exhibit differential localization and AKAP interaction. *Cell Motility*, *65*(7), 539–552. https://doi.org/10.1002/cm.20279

Newlon, M. G., Roy, M., Hausken, Z. E., Scott, J. D., & Jennings, P. A. (1997). The A-kinase anchoring domain of type IIalpha cAMP-dependent protein kinase is highly helical. *The Journal of Biological Chemistry*, *272*(38), 23637–23644. https://doi.org/10.1074/jbc.272.38.23637

Newlon, M. G., Roy, M., Morikis, D., Carr, D. W., Westphal, R., Scott, J. D., & Jennings, P. A. (2001). A novel mechanism of PKA anchoring revealed by solution structures of anchoring complexes. *The EMBO Journal*, *20*(7), 1651–1662. https://doi.org/10.1093/emboj/20.7.1651

Newlon, M. G., Roy, M., Morikis, D., Hausken, Z. E., Coghlan, V., Scott, J. D., & Jennings, P. A. (1999). The molecular basis for protein kinase A anchoring revealed by solution NMR. *Nature Structural Biology*, *6*(3), 222–227. https://doi.org/10.1038/6663

Niu, J., Vaiskunaite, R., Suzuki, N., Kozasa, T., Carr, D. W., Dulin, N., & Voyno-Yasenetskaya, T. A. (2001). Interaction of heterotrimeric G13 protein with an A-kinase-anchoring protein 110 (AKAP110) mediates cAMP-independent PKA activation. *Current Biology*, *11*(21), 1686–1690. https://doi.org/10.1016/S0960-9822(01)00530-9

O'Rand, M. G., Irons, G. P., & Porter, J. P. (1984). Monoclonal Antibodies to Rabbit Sperm Autoantigens. I. Inhibition of In Vitro Fertilization and Localization on the Egg. *Biology of Reproduction*, *30*(3), 721–729. https://doi.org/10.1095/biolreprod30.3.721

O'Rand, M., Widgren, E., Sivashanmugam, P., Richardson, R., Hall, S., French, F., VandeVoort, C., Ramachandra, S., Ramesh, V., & Rao, A. J. (2004). Reversible immunocontraception in male monkeys immunized with eppin. *Science*, *306*(5699), 1189–1190.

Osinka, A., Poprzeczko, M., Zielinska, M. M., Fabczak, H., Joachimiak, E., & Wloga, D. (2019). Ciliary proteins: Filling the gaps. Recent advances in deciphering the protein composition of motile ciliary complexes. *Cells*, *8*(7), 730.

Richardson, R. T., Yamasaki, N., & O'Rand, M. G. (1994). Sequence of a rabbit sperm zona pellucida binding protein and localization during the acrosome reaction. *Developmental Biology*, *165*(2), 688–701. https://doi.org/10.1006/dbio.1994.1285

Rolland, T., Taşan, M., Charloteaux, B., Pevzner, S. J., Zhong, Q., Sahni, N., Yi, S., Lemmens, I., Fontanillo, C., & Mosca, R. (2014). A proteome-scale map of the human interactome network. *Cell*, *159*(5), 1212–1226.

Satir, P., & Christensen, S. T. (2007). Overview of Structure and Function of Mammalian Cilia. *Annual Review of Physiology*, *69*(1), 377–400. https://doi.org/10.1146/annurev.physiol.69.040705.141236

Scott, J. D., & McCartney, S. (1994). Localization of A-kinase through anchoring proteins. *Molecular Endocrinology*, *8*(1), 5–11. https://doi.org/10.1210/mend.8.1.8152430

Shinohara, K., Chen, D., Nishida, T., Misaki, K., Yonemura, S., & Hamada, H. (2015). Absence of radial spokes in mouse node cilia is required for rotational movement but confers ultrastructural instability as a trade-off. *Developmental Cell*, *35*(2), 236–246.

Singh, S., Saraya, A., & Sharma, R. (2015). Increased levels of sperm protein 17 mRNA and circulating antibodies in periampullary carcinoma patients. *International Journal of Clinical Oncology*, *20*(4), 736–744. https://doi.org/10.1007/s10147-014-0762-7

Smith, F. D., Esseltine, J. L., Nygren, P. J., Veesler, D., Byrne, D. P., Vonderach, M., Strashnov, I., Eyers, C. E., Eyers, P. A., & Langeberg, L. K. (2017). Local protein kinase A action proceeds through intact holoenzymes. *Science*, *356*(6344), 1288–1293.

Stelzer, G., Rosen, N., Plaschkes, I., Zimmerman, S., Twik, M., Fishilevich, S., Stein, T. I., Nudel, R., Lieder, I., Mazor, Y., Kaplan, S., Dahary, D., Warshawsky, D., Guan-Golan, Y., Kohn, A., Rappaport, N., Safran, M., & Lancet, D. (2016). The GeneCards Suite: From Gene Data Mining to Disease Genome Sequence Analyses. *Current Protocols in Bioinformatics*, *54*(1), 1.30.1-1.30.33. https://doi.org/10.1002/cpbi.5

Straughn, J. M., Shaw, D. R., Guerrero, A., Bhoola, S. M., Racelis, A., Wang, Z., Chiriva-Internati, M., Grizzle, W. E., Alvarez, R. D., Lim, S. H., & Strong, T. V. (2004). Expression of sperm protein 17 (Sp17) in ovarian cancer. *International Journal of Cancer*, *108*(6), 805–811. https://doi.org/10.1002/ijc.11617

South, P. F., Fingerman, I. M., Mersman, D. P., Du, H. N., & Briggs, S. D. (2010). A conserved interaction between the SDI domain of Bre2 and the Dpy-30 domain of Sdc1 is required for histone methylation and gene expression. *Journal of Biological Chemistry*, *285*(1), 595-607.

Su, Y., Dostmann, W. R., Herberg, F. W., Durick, K., Xuong, N. H., Ten Eyck, L., Taylor, S. S., & Varughese, K. I. (1995). Regulatory subunit of protein kinase A: Structure of deletion mutant with cAMP binding domains. *Science (New York, N.Y.)*, *269*(5225), 807–813. https://doi.org/10.1126/science.7638597

Taylor, S., & Kornev, A. P. (2017). *PKA and the Structural Kinome*. https://doi.org/10.18054/PB.V118I4.4846

Taylor, S. S., Ilouz, R., Zhang, P., & Kornev, A. P. (2012). Assembly of allosteric macromolecular switches: Lessons from PKA. *Nature Reviews. Molecular Cell Biology*, *13*(10), 646–658. https://doi.org/10.1038/nrm3432

Theurkauf, W. E., & Vallee, R. (1982). Molecular characterization of the cAMP-dependent protein kinase bound to microtubule-associated protein 2. *Journal of Biological Chemistry*, *257*(6), 3284–3290.

Tremblay, V., Zhang, P., Chaturvedi, C. P., Thornton, J., Brunzelle, J. S., Skiniotis, G., ... & Couture, J. F. (2014). Molecular basis for DPY-30 association to COMPASS-like and NURF complexes. *Structure*, *22*(12), 1821-1830.

Turnham, R. E., & Scott, J. D. (2016). Protein kinase A catalytic subunit isoform PRKACA; history, function and physiology. *Gene*, *577*(2), 101–108. https://doi.org/10.1016/j.gene.2015.11.052

Vijayaraghavan, S., Goueli, S. A., Davey, M. P., & Carr, D. W. (1997). Protein kinase A-anchoring inhibitor peptides arrest mammalian sperm motility. *Journal of Biological Chemistry*, *272*(8), 4747-4752.

Walker-Gray, R., & Klussmann, E. (2020). The role of AKAP12 in coordination of VEGF-induced endothelial cell motility. *Acta Physiologica*, *228*(1), e13359. https://doi.org/10.1111/apha.13359

Walsh, D., Perkins, J. P., & Krebs, E. G. (1968). An adenosine 3', 5'-monophosphate-dependant protein kinase from rabbit skeletal muscle. *Journal of Biological Chemistry*, *243*(13), 3763–3765.

Wang, X., Lou, Z., Dong, X., Yang, W., Peng, Y., Yin, B., Gong, Y., Yuan, J., Zhou, W., Bartlam, M., Peng, X., & Rao, Z. (2009). Crystal Structure of the C-Terminal Domain of

Human DPY-30-Like Protein: A Component of the Histone ahs2transferase Complex. *Journal of Molecular Biology*, *390*(3), 530–537. https://doi.org/10.1016/j.jmb.2009.05.061

Wen, Y., Richardson, R. T., Widgern, E. E., & O'Rand, M. G. (2001). Characterization of Sp17: A ubiquitous three domain protein that binds heparin. *Biochemical Journal*, *357*(1), 25–31.

Wu, J., Brown, S. H. J., von Daake, S., & Taylor, S. S. (2007). PKA Type IIα Holoenzyme Reveals a Combinatorial Strategy for Isoform Diversity. *Science (New York, N.Y.)*, *318*(5848), 274–279. https://doi.org/10.1126/science.1146447

Xia, Q.-Y., Liu, S., Li, F.-Q., Huang, W.-B., Shi, L.-N., & Zhou, X.-J. (2013). Sperm protein 17, MAGE-C1 and NY-ESO-1 in hepatocellular carcinoma: Expression frequency and their correlation with clinical parameters. *International Journal of Clinical and Experimental Pathology*, *6*(8), 1610–1616.

Xiang, S. D., Gao, Q., Wilson, K. L., Heyerick, A., & Plebanski, M. (2015). Mapping T and B cell epitopes in sperm protein 17 to support the development of an ovarian cancer vaccine. *Vaccine*, *33*(44), 5950–5959. https://doi.org/10.1016/j.vaccine.2015.07.094

Yamada, R., Takahashi, A., Torigoe, T., Morita, R., Tamura, Y., Tsukahara, T., Kanaseki, T., Kubo, T., Watarai, K., Kondo, T., Hirohashi, Y., & Sato, N. (2013). Preferential expression of cancer/testis genes in cancer stem-like cells: Proposal of a novel sub-category, cancer/testis/stem gene. *Tissue Antigens*, *81*(6), 428–434. https://doi.org/10.1111/tan.12113

Yang, P., Diener, D. R., Yang, C., Kohno, T., Pazour, G. J., Dienes, J. M., Agrin, N. S., King, S. M., Sale, W. S., Kamiya, R., Rosenbaum, J. L., & Witman, G. B. (2006). Radial spoke

proteins of Chlamydomonas flagella. *Journal of Cell Science*, *119*(Pt 6), 1165–1174. https://doi.org/10.1242/jcs.02811

Yapo, C., Nair, A. G., Hellgren Kotaleski, J., Vincent, P., & Castro, L. R. V. (2018). Switch-like PKA responses in the nucleus of striatal neurons. *Journal of Cell Science*, *131*(14). https://doi.org/10.1242/jcs.216556

Young, S. A. M., Miyata, H., Satouh, Y., Aitken, R. J., Baker, M. A., & Ikawa, M. (2016). CABYR is essential for fibrous sheath integrity and progressive motility in mouse spermatozoa. *Journal of Cell Science*, *129*(23), 4379–4387. https://doi.org/10.1242/jcs.193151

Zhang, P., Knape, M. J., Ahuja, L. G., Keshwani, M. M., King, C. C., Sastri, M., Herberg, F. W., & Taylor, S. S. (2015). Single Turnover Autophosphorylation Cycle of the PKA RIIβ Holoenzyme. *PLOS Biology*, *13*(7), e1002192. https://doi.org/10.1371/journal.pbio.1002192

Zhang, P., Smith-Nguyen, E. V., Keshwani, M. M., Deal, M. S., Kornev, A. P., & Taylor, S. S. (2012). Structure and Allostery of the PKA RIIβ Tetrameric Holoenzyme. *Science*, *335*(6069), 712–716. https://doi.org/10.1126/science.1213979

Zhang, P., Ye, F., Bastidas, A. C., Kornev, A. P., Wu, J., Ginsberg, M. H., & Taylor, S. S. (2015). An Isoform-Specific Myristylation Switch Targets Type II PKA Holoenzymes to Membranes. *Structure*, *23*(9), 1563–1572. https://doi.org/10.1016/j.str.2015.07.007

Zhu, X., Liu, Y., & Yang, P. (2017). Radial Spokes-A Snapshot of the Motility Regulation, Assembly, and Evolution of Cilia and Flagella. *Cold Spring Harbor Perspectives in Biology*, *9*(5). https://doi.org/10.1101/cshperspect.a028126